

AWARD NUMBER: W81XWH-15-1-0389

TITLE: Theranostics Targeting Metastatic Breast Cancer

PRINCIPAL INVESTIGATOR: Kevin Burgess

CONTRACTING ORGANIZATION: Texas A&M University  
College Station, TX 77845

REPORT DATE: October 2018

TYPE OF REPORT: Annual Report

PREPARED FOR: U.S. Army Medical Research and Materiel Command  
Fort Detrick, Maryland 21702-5012

DISTRIBUTION STATEMENT: Approved for Public Release;  
Distribution Unlimited

The views, opinions and/or findings contained in this report are those of the author(s) and should not be construed as an official Department of the Army position, policy or decision unless so designated by other documentation.

<b>REPORT DOCUMENTATION PAGE</b>				<i>Form Approved</i> <i>OMB No. 0704-0188</i>	
Public reporting burden for this collection of information is estimated to average 1 hour per response, including the time for reviewing instructions, searching existing data sources, gathering and maintaining the data needed, and completing and reviewing this collection of information. Send comments regarding this burden estimate or any other aspect of this collection of information, including suggestions for reducing this burden to Department of Defense, Washington Headquarters Services, Directorate for Information Operations and Reports (0704-0188), 1215 Jefferson Davis Highway, Suite 1204, Arlington, VA 22202-4302. Respondents should be aware that notwithstanding any other provision of law, no person shall be subject to any penalty for failing to comply with a collection of information if it does not display a currently valid OMB control number. <b>PLEASE DO NOT RETURN YOUR FORM TO THE ABOVE ADDRESS.</b>					
<b>1. REPORT DATE</b> October 2018		<b>2. REPORT TYPE</b> Annual		<b>3. DATES COVERED</b> 30 Sep 2017 - 29 SEP 2018	
<b>4. TITLE AND SUBTITLE</b>  Theranostics Targeting Metastatic Breast Cancer				<b>5a. CONTRACT NUMBER</b>	
				<b>5b. GRANT NUMBER</b> W81XWH-15-1-0389	
				<b>5c. PROGRAM ELEMENT NUMBER</b>	
<b>6. AUTHOR(S)</b> Kevin Burgess  E-Mail: burgess@tamu.edu				<b>5d. PROJECT NUMBER</b>	
				<b>5e. TASK NUMBER</b>	
				<b>5f. WORK UNIT NUMBER</b>	
<b>7. PERFORMING ORGANIZATION NAME(S) AND ADDRESS(ES)</b>  Texas A&M University College Station, TX 77845				<b>8. PERFORMING ORGANIZATION REPORT NUMBER</b>	
<b>9. SPONSORING / MONITORING AGENCY NAME(S) AND ADDRESS(ES)</b>  U.S. Army Medical Research and Materiel Command Fort Detrick, Maryland 21702-5012				<b>10. SPONSOR/MONITOR'S ACRONYM(S)</b>	
				<b>11. SPONSOR/MONITOR'S REPORT NUMBER(S)</b>	
<b>12. DISTRIBUTION / AVAILABILITY STATEMENT</b>  Approved for Public Release; Distribution Unlimited					
<b>13. SUPPLEMENTARY NOTES</b>					
<b>14. ABSTRACT</b>  This application is designed to impact three of the overarching challenges identified for this award type: (i) revolutionary treatment regimes replacing drugs that have life-threatening toxicities with safe and effective interventions; (ii) elimination of mortality associated with metastatic breast cancer; and, (iii) distinguishing aggressive breast cancer from indolent forms, to avoid over-diagnosis and treatment. Overall, this work addresses issues that relate to: (i) revolutionary treatment regimes replacing drugs that have life-threatening toxicities with safe and effective interventions; (ii) elimination of mortality associated with metastatic breast cancer; and, (iii) distinguishing aggressive breast cancer from indolent forms, to avoid over-diagnosis and treatment.					
<b>15. SUBJECT TERMS</b>  Nothing listed					
<b>16. SECURITY CLASSIFICATION OF:</b>			<b>17. LIMITATION OF ABSTRACT</b>  UU	<b>18. NUMBER OF PAGES</b>  63	<b>19a. NAME OF RESPONSIBLE PERSON</b> USAMRMC
<b>a. REPORT</b>  Unclassified	<b>b. ABSTRACT</b>  Unclassified	<b>c. THIS PAGE</b>  Unclassified			<b>19b. TELEPHONE NUMBER</b> (include area code)

## Table of Contents

	<u>Page</u>
<b>1. Introduction.....</b>	<b>4</b>
<b>2. Keywords.....</b>	<b>4</b>
<b>3. Accomplishments.....</b>	<b>4</b>
<b>4. Impact.....</b>	<b>11</b>
<b>5. Changes/Problems.....</b>	<b>12</b>
<b>6. Products.....</b>	<b>12</b>
<b>7. Participants &amp; Other Collaborating Organizations.....</b>	<b>13</b>
<b>8. Special Reporting Requirements.....</b>	<b>13</b>
<b>9. Appendices.....</b>	<b>14</b>

# Theranostics Targeting Metastatic Breast Cancer

---

## A. Introduction (1 paragraph)

The overall goal of this proposal is to prepare TrkC<sup>+</sup>-targeted fluorescence/PET/PDT for breast cancer. For this we use a TrkC<sup>+</sup> targeting fragment (parts of structures colored in blue throughout this report) and compare them with isomeric compounds that do not target TrkC<sup>+</sup> (green). Last year we reported the synthesis aza-BODIPY **1**. This compound was designed for optical imaging of TrkC<sup>+</sup> tumors; this year we did that in a 4T1 mouse model, and published the results. Agent **1** accumulated well in tumors, but was not very bright perhaps due to insolubility aggregation effects. We had also proposed to make compound **2** for positron emission tomography (PET) and photodynamic therapy (PDT). After much effort, we made **2** then realized the reason that was so difficult was due to compound instability, specifically the compound loses iodine easily. Instability means **2** is not useful for imaging or therapy. Consequently, just as indicated as a back-up plan last year, we switched focus to the more water-soluble cyanine-based systems (here, **3** - **7**). These are more soluble, brighter, and less prone to aggregation. So far, dyes **3** and **4** have been tested *in vivo*, but they accumulated in the kidneys and cleared quickly with little imaging of the tumor. To address this issue, we have prepared other systems with more lipophilic cyanines (eg **5** - **7**), and plan to make other systems with albumin binders to increase retention (based on a literature precedent); all these compounds are ready to be tested *in vivo*. It is necessary to find cyanines that sensitize production of singlet oxygen to realize the overall goal of this study: fluorescent/PET/PDT theranostics. We discovered a brominated cyanine core that does indeed act as a singlet oxygen sensitizer, and compounds **5** - **7** are designed to exploit this. Finally, we prepared the targeted PET agent (**8**), and the targeted maytensin (**9**) mentioned in our previous report (also awaiting *in vivo* studies). The PET agent **8** was tested *in vivo* in a 4T1 mouse model; it had good stability (no 18-fluoride in bone) but cleared quickly. Modifications of this are suggested for year 3. Overall, we are extremely optimistic of reaching our goal for a TrkC<sup>+</sup>-targeted fluorescence/PET/PDT theranostic for breast cancer.

## B. Keywords (limit to 20 words)

reagents for histology of TrkC<sup>+</sup> tumors • photodynamic therapy (PDT) • positron emission tomography (PET)

## C. Accomplishments

### What were the major goals of the project?

- 1 Design and synthesis of second-generation fluorescent, PDT and PET/PDT agents *that absorb >700 nm*, bind TrkC, are localized in TrkC<sup>+</sup> cells, generate singlet oxygen under conditions for PDT, and have TrkC<sup>+</sup> selective photocytotoxicities.

begins in year 1 and continues throughout grant period (about 40 % of total work required achieved this year)

- 2 Validation of a fluorescent form of one of these agents in histochemistry for diagnosis of patients with TrkC<sup>+</sup>-expressing tumors.

year 2 and then continues throughout grant period

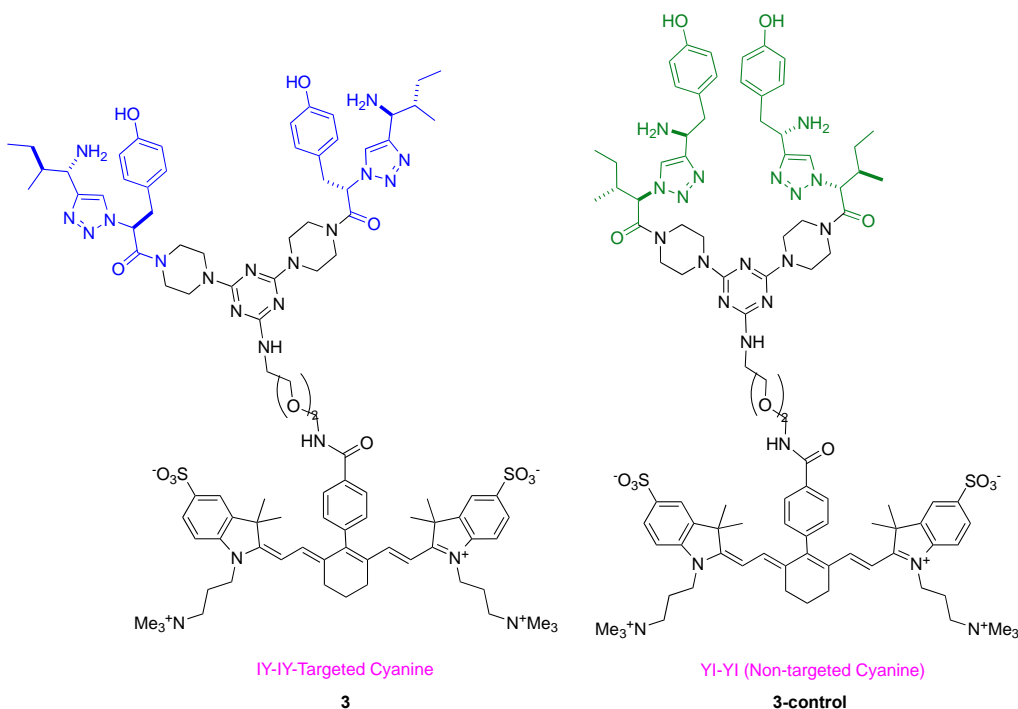
- 3 Validation of the iodinated second-generation agent PET imaging human breast cancer tumors in mice, and ablation of these tumors via PDT. This study will involve determination of toxicity *in vivo*, pharmacokinetics and -dynamics (using PET) to ascertain distribution and clearance of the labels.

only in years 2 and 3

## What was accomplished under these goals?

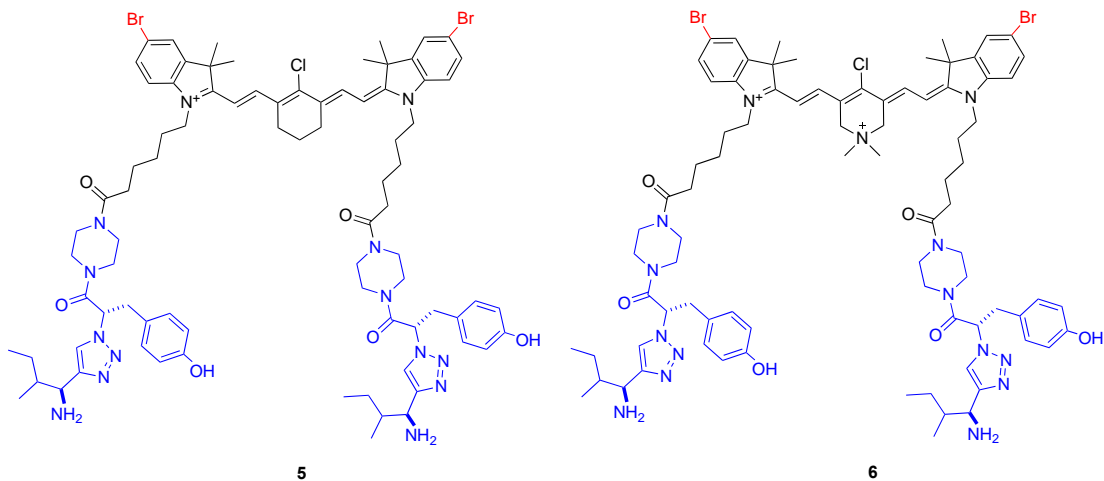
### Investigation Of Cyanine Systems **3** and **4** For Optical Imaging

These studies were outlined in last year's report, and are now published.<sup>1</sup>



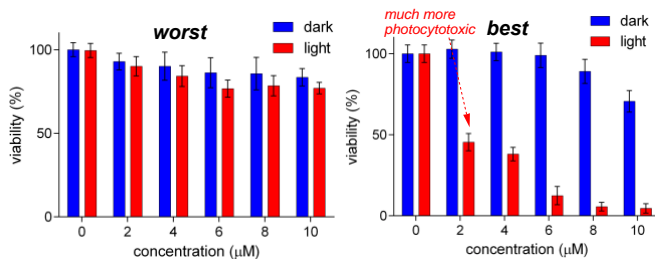
### More Lipophilic Cyanine Systems That Should Be Cleared More Slowly

Compounds **5** and **6** were designed to have cyanine dyes that are less hydrophilic than **3** and **4**. So far we have determined that these systems do indeed bind NIH3T3 TrkC<sup>+</sup> transfectant cells, and metastatic breast cancer in histology experiments (only stained metastatic breast cancer {12 samples} and not normal breast tissue {12 samples}). The water-solubilities of these systems were also determined (**5** is 45  $\mu$ M in 0.5 % DMSO in 1 M PBS, 7.24 pH; **6** is far more soluble). We have not yet been able to determine a  $K_d$  for these compounds binding the TrkC<sup>+</sup> receptor because there is no obvious "blocking group" for use in cells studies; however, we continue to search for a work-around to this problem. In photocytotoxicity experiments compound **5** was not cytotoxic in the dark to NIH3T3 TrkC<sup>+</sup> at 40  $\mu$ M, but was highly toxic when illuminated at 780 nm. Compounds **5** and **6** have the potential to be near-IR imaging agents and PDT therapeutics *in vivo*, but they have not yet been tested.



## Cyanine Dyes In PDT

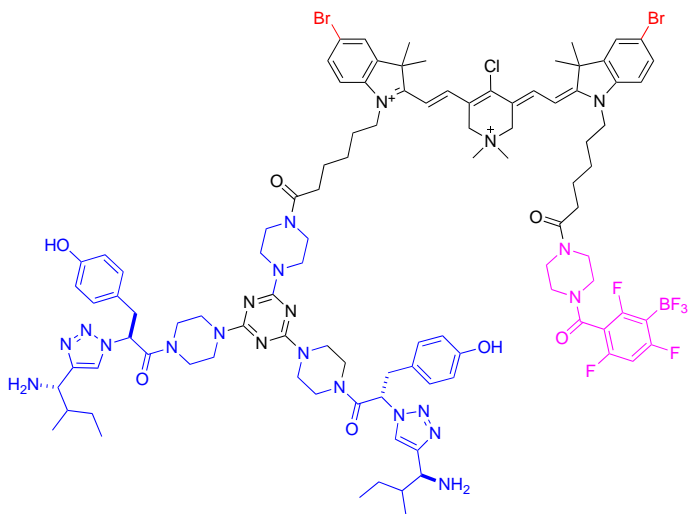
We performed an extensive study on optimizing cyanine dyes for PDT, and this work has now been published.<sup>2</sup> In this paper we made a series of 13 iodinated cyanines and compared their photocytotoxicities. Illustrative data is shown below.



We are confident that these are some of the best photosensitizers for PDT available. They are water soluble, absorb at an ideal wavelength (~780 nm), generate singlet oxygen with reasonable quantum yields, are hardly cytotoxic, but significantly photocytotoxic.

## Potential Fluorescent/PET/PDT Theranostic 7

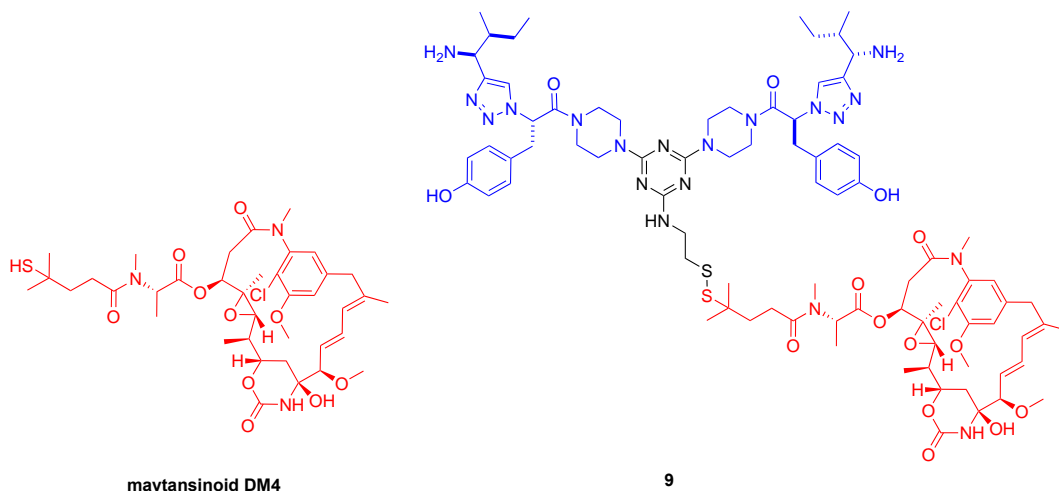
We have also prepared compound **7** which could become our lead theranostic. This structure has the TrkC<sup>+</sup> targeting group (blue), a Perrin <sup>18</sup>F capture unit (purple) and a PDT active cyanine backbone: all the components for a fluorescent/PET/PED theranostic. Currently we are scaling up the synthesis of this molecule, for photophysical measurements, cellular assays particularly light/dark cytotoxicity.



7

## Targeted Maytensinoid Therapeutic 9

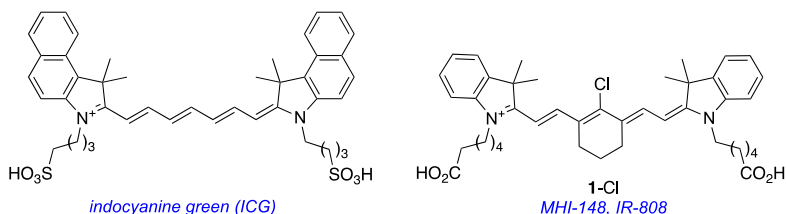
Finally, in collaboration with a biotech company who donated the maytensinoid **DM4**, in our labs we prepared the targeted conjugate **8** equipped with a disulfide linker designed to be cleaved in the cytosol. Cell studies with agent **9** in comparison with **9-control** indicate there is slightly improved cellular therapeutic index. However, we expect the improvements to therapeutic index *in vivo* to be more profound because of pharmacokinetic effects that cannot be replicated in cell culture. *In vivo* studies on this molecule have now been published.<sup>3</sup>



## Tumor-seeking Dyes: Background

Indocyanine green (ICG, **A**), a heptamethine cyanine or “Cy7” dye, is the only near-IR FDA-approved optical marker for clinical use.<sup>4,5</sup> ICG is used in surgical procedures because of its favorable safety profile,<sup>6-8</sup> and absorbance maximum around 750 nm. Below 750 nm, excitation of dyes obscured by more than a few millimeters of tissue become impractical even when using the highest laser powers acceptable in surgical settings. To calibrate, penetration of light of wavelength 800 nm is twice that of light of 630 nm.<sup>9</sup> ICG is used in surgery, but it is not disposed to accumulate in cancer tissue. In fact, ICG collects in the liver and gastrointestinal tract, and tends to wash out of the body within a few hours.<sup>10</sup>

Another Cy7 dye, **1-Cl**, (or MHI-148, and several other similar ones, all having a *meso*-Cl) *accumulates in solid tumors in animal models (eg prostate,<sup>11</sup> gastric,<sup>12</sup> kidney,<sup>13</sup> hepatocytes,<sup>14,15</sup> lung cancer,<sup>16</sup> and glioblastoma<sup>17</sup>) but not in normal cells and tissue.*<sup>18-22</sup> Moreover, these fluors persist in those tumors for at least 1 – 2 d, and in some cases they have been observed there after a much longer period.



The potential importance of near-IR dyes such as **1-Cl** which localizes in solid tumor is that they can be used for *in vivo* experiments,<sup>23</sup> in image guided surgery,<sup>5</sup> and as conjugates to cytotoxic substances.<sup>24-28</sup> Our hypothesis is that these tumor seeking near-IR dyes complement targeted approaches using mAbs or other small

molecule ligands for cell surface receptors, and could surpass them for some applications. Much of this potential is untapped; only five small molecule therapeutics have been conjugated to **1-Cl** (or to close derivatives, throughout). One of these conjugates features a horribly toxic and non-selective mustard-type alkylating agent,<sup>25</sup> another two are monoamine oxidase inhibitors,<sup>27,28</sup> farnesylthiosalicylic acid (an experimental RAS/mTOR inhibitor) has been used,<sup>26</sup> and gemcitabine.<sup>14,15,17†</sup> For this funding cycle, we have some highly encouraging results for conjugating these dyes to *kinase inhibitors*.

## Why Do Tumor-seeking Dyes Localize And Persist In Tumors?

“Tumor-seeking” characteristics of fluor **1-Cl** have been explained by several groups<sup>11,13,14,16-19,22,31</sup> exclusively in terms of uptake via the Organic Anion Transporting Polypeptides (OATPs).<sup>32,33</sup> Tumor compression generates hypoxia and that triggers activation of HIF1 $\alpha$ , which promotes OATPs overexpression in cancer tissue relative to levels found in normal cells.<sup>12,31</sup> The natural role of OATPs is to mediate influx of organic anions and essential metabolites (eg bile salts, steroids, bilirubin, and thyroid hormones). This diversity of substrates means OATPs are not particularly selective and, coincidentally, also import some fluors like **1-Cl**.<sup>34-36</sup> To balance this ion influx, OATPs efflux intracellular bicarbonate, glutathione, and glutathione adducts. Consequently, OATPs promote influx of **1-Cl** into cells, *without pumping it out*.

† There are also a few reports of therapeutics being conjugated by displacement of the *meso*-Cl,<sup>29,30</sup> but our preliminary results featuring albumin conjugations at this position (described in the next section) indicate why these should be considered separately.



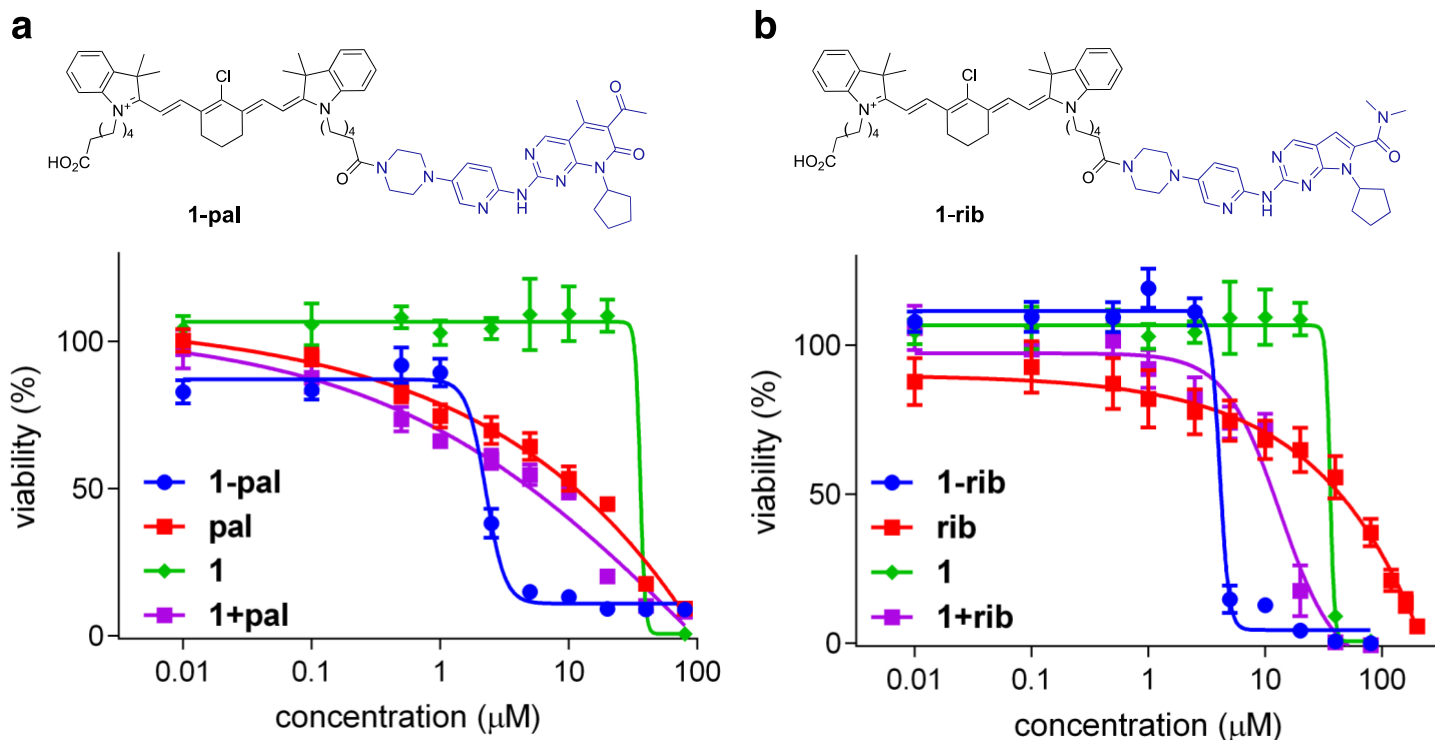
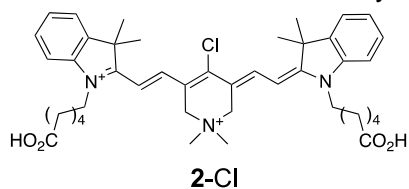


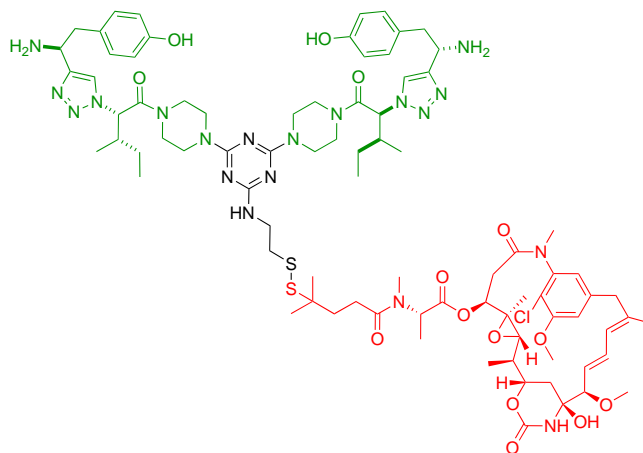
**Figure 1.** Cell viabilities of **1-pal** and **1-rib** determined via an AlamarBlue assay. Error bars represent standard deviation from the mean over three independent experiments.

Excited by the data in Figure 1, we began testing other cell lines that were available in our lab, *and obtained similar data* for HepG2 (liver cancer cells), U87 (glioblastoma cells), A549 (lung cancer), and K562 (leukemia). For non-tumorigenic, HUVEC epithelial cells, however, **pal** and **1-pal** had approximately the same weak effect; thus the Cy-KIs selectively arrest development of cancer cells over normal ones. We have not yet performed other types of cell assays with **1-pal** on the triple negative breast cancer cells, but have studied **1-pal** on HepG2 (liver cancer cells). Those experiments showed: (i) **1-pal** has a more marked effect on cell morphology than equimolar **pal** (**1-Cl** had no effect); (ii) the fluorescence localized in the mitochondria (from confocal microscopy with MitoTracker labels); (iii) in short-term cell culture studies **1-Cl** is imported via OATPs (inhibition by a small molecule inhibitor, but promoted under hypoxic conditions), but after about 30 min **1-Cl** reacts with bovine serum albumin (BSA) in the media to form **1-BSA** which presumably is uptaken into cells via albumin transport mechanisms; and, (iv) in an *in vivo* experiment with rats bearing subcutaneous rat liver tumors from the McA-RH7777 cell line, the fluorescence localized in the tumor tissue and persisted there for >72 h after *iv* injection of **1-pal** (in one animal fluorescence was seen even after 10 d). Additionally, cellular assays similar to (i) – (iii) were performed on some of the other cells lines listed above too, and the observations above seem general. Based on the literature and our data, we would be surprised if triple negative breast cancer cells/tissue behave differently when treated with **1-pal**; those experiments are underway.



One disadvantage of **1-Cl** is that it tends to aggregate in aqueous media. Though not prohibitive, aggregation limits the solubility of this system, and could cause toxicity effects. Consequently, in preliminary studies (recently submitted for publication) we made the quaternary ammonium salt **2-Cl** (QCy); it has complementary solubility properties to **1-Cl** and does not aggregate under the same conditions. Conjugates of QCy to KIs are

currently being made and compared with those of **1-Cl**, primarily as an alternative or back-up option to conjugates of **1-Cl**. Moreover, some other, unexpected, characteristics favor use of **2-Cl** if it does localize in tumors, namely it is much more photostable, and has less inherent toxicity (recall **1-Cl** is weakly cytotoxic).



9-control

### What opportunities for training and professional development has the project provided?

This funding has been used to support postdoctoral fellow Jaya Shrestha, and graduate students Usama Syed, Bosheng Zhou, and Daniel Jiang.

### How were the results disseminated to communities of interest?

These papers acknowledge support from this grant.

- 320 PROTACs Suppression of CDK4/6, Crucial Kinases for Cell Cycle Regulation in Cancer, B. Zhao, K. Burgess, *Angew. Chem.*, 2018, submitted
- 319 A Near-Ir Fluorescent Dasatinib Derivative That Localizes in Cancer Cells, S. M. Usama, B. Zhao, K. Burgess, *Chem Sci*, 2018, submitted.
- 318 QCy: A Simple Heptamethine Cyanine Modification Induces Several Improved Characteristics, S. Thavornpradit, S. M. Usama, J. P. Shrestha, K. Burgess, *Chemical Science*, 2018, submitted.
- 317 Site Specific Labeling of Proteins with Near-IR dyes, C.-M. Lin, S. M. Usama, K. Burgess, *Molecules*, 2018, in the press.
- 316 On the Mechanisms of Uptake of Tumor-seeking Cyanine Dyes, S. M. Usama, C.-M. Lin, K. Burgess, *Bioconjugate Chemistry*, 2018. DOI: 10.1021/acs.bioconjchem.8b00708
- 315 A Zwitterionic Near-infrared Dye Linked TrkC Targeting Agent for Imaging Metastatic Breast Cancer, Z. Yang, S. M. Usama, F. Li, K. Burgess, Z. Li, *Med. Chem. Comm.*, 2018, 9, 1754-1760. DOI: 10.1039/C8MD00190A.
- 314 Targeted Maytansinoid Conjugate Improves Therapeutic Index for Metastatic Breast Cancer Cells, Z. Jiang, Z. Yang, F. Li, Z. Li, N. Fishkin, K. Burgess, *Bioconjugate Chemistry*, 2018, 29, 9, 2920-2926 DOI: 10.1021/acs.bioconjchem.8b00340
- 313 Optimized Heptamethine Cyanines for Photodynamic Therapy, S. Usama, S. Thavornpradit, K. Burgess, *ACS Applied Bio Materials*, 2018, 1, 1195-1205. DOI: 10.1021/acsabm.8b00414.
- 312 Isothiocyanate-Substituted aza-BODIPY as Near-Infrared Fluorescence Chemosensor for Selective Detection of Cyanide Ion in Aqueous Media and Living cells, P. Piyanuch, J. Sirirak, A. Kamakaew, O. Weeranantanapan, K. Burgess, N. Wanichacheva, *Inorganic Chemistry*, 2018, submitted.

- 311 A Click-addressable Cassette for Photoaffinity Labeling, B. Zhao, K. Burgess, *ACS Med. Chem. Letters*, 2018, 9, 155-158. DOI: 10.1021/acsmmedchemlett.7b00516 PMID: 29456805
- 310 Small Molecule Inhibitors of the PCSK9-LDLR Interaction, J. Taechalertrpaisarn, B. Zhao, X. Liang, K. Burgess, *J. Am. Chem. Soc.*, 2018, 140, 3242-3248. DOI: 10.1021/jacs.7b09360 PMID: 29378408

The PI gave a seminar "Active Targeting In Cancer" at the following venues:

EKO: A Simple Idea With Several Applications; University of Amsterdam; Amsterdam, Netherlands, June 11, 2018

Using EKO to Match Small Molecule Conformation to Protein-protein Interactions, German Cancer Research Center (DKFZ), June 21, 2018

Active Targeting of Cancer Cells, City University of Hong Kong, November 2016.

### **What do you plan to do during the next reporting period to accomplish the goals?**

During the next reporting period we will:

- (i) initiate *in vivo* studies (PDT and PET) on some of the compounds already prepared; and,
- (ii) continue the synthetic studies to produce agents with PDT characteristics.

We are absolutely determined to realize the overall goal of this proposal: a theranostic that can be used for diagnosis via histology, imaging via PET, and therapy via PDT.

## **D. Impact**

### **What was the impact on the development of the principle(s) of the project?**

At this early stage, the impact is mostly on improvement of the chemical design of the agents being developed. In this grant period we have begun to make some novel cyanine systems with improved solubility characteristics and suitable for targeted PDT. However, our new discoveries on tumor-seeking dyes conjugated to KIs seems more significant, and we are looking to pursue this further

### **What was the impact on other disciplines?**

In the broader sense we hope to prepare fluorescent and PET imaging agents that can differentiate between TrkA – C *in vivo*. This will be useful as a probe in cell biology, *in vivo*, and potentially (beyond the scope of this proposal) in clinical imaging. Our discoveries on how tumor-seeking dyes are uptaken are likely to have the most impact: they solve a problem that has been outstanding for some time.

### **What was the impact on technology transfer?**

A provisional patent application on Cy-Kis has been submitted.

### **What was the impact on society beyond science and technology?**

Too early to impact society outside science, but eventually the goal of this work is to produce a lead compound that will be iteratively improved to form a “theranostic” for diagnosis, imaging, and therapy.

## **E. Changes/Problems**

### **Changes in approach and reasons for change**

The goal is the same, the particular agents we are preparing to realize the goal are different as detailed above.

### **Actual or anticipated problems or delays and actions or plans to resolve them**

Problems are nearly always encountered in chemical syntheses, but we have anticipated the obvious weak links and constantly consider alternative routes. We have several agents prepared as described above, and more possibilities that we did not detail here.

Last year we reported, “We see more of opportunities to use cyanine dyes that, remarkably, seem to accumulate in all types of cancer cells.” In fact, this has worked out really well and we are hopeful this work can be carried on in an Expansion Award.

### **Changes that had a significant impact on expenditures**

We made a request to re-budget some funds from salaries to equipment to buy an HPLC for preparative isolation of the target molecules. This request was granted, the machine was delivered and it greatly accelerated our progress.

Unfortunately, nearly all the funds for *in vivo* studies are now expended, and very little remains in the chemical budget.

### **Significant changes in use or care of human subjects, vertebrate animals, biohazards, and/or select agents**

None, except that NO ANIMAL STUDIES HAVE BEEN PERFORMED AT TAMU. All the *in vivo* work has therefore been performed at Methodist in Dr Li’s group.

### **Significant changes in use of care of human subjects**

n/a

### **Significant changed in use of care of vertebrate animals**

none

### **Significant changes in use of biohazards and/or select agents**

none

## **F. Products**

### **Publications, conference papers, and presentations**

Please see list of presentations above.

### **Websites or other Internet sites**

none

### **Technologies or techniques**

See above.

## **Inventions, patent application, and/or licenses**

See patent issued cited above

## **Other Products**

none

## **G. Participants & Other Collaborating Organizations**

### **What individuals have worked on the project?**

Zhengyang (Daniel) Jiang, graduate student at TAMU, 50% time, 1 year.

Syed Usama, graduate student at TAMU 50% time for 7 months, 25% time for 1 month, 8 months total work.

Bosheng Zhao, graduate student at TAMU 50% time for 6 months, 25% time for 1 month, 7 months total work.

Dr Chen-Ming Lin, postdoctoral associate, 5 months effort at 100 %.

Dr Jay Shrestha, postdoctoral associate, 100% time for 8 months.

### **Has there been a change in the active other support of the PD/PI(s) or senior/key personnel?**

no

### **What other organizations were in involved as partners?**

Dr Li, co-PI at Methodist is about to begin.

## **Special Reporting Requirements**

none

## **H. Appendices (attached journal articles, reprints, CV, patent applications)**

Reprints of our most important papers are attached.

- 317 Site Specific Labeling of Proteins with Near-IR dyes, C.-M. Lin, S. M. Usama, K. Burgess, *Molecules*, 2018, 23, 2900. DOI: 10.3390/molecules23112900
- 316 On the Mechanisms of Uptake of Tumor-seeking Cyanine Dyes, S. M. Usama, C.-M. Lin, K. Burgess, *Bioconjugate Chemistry*, 2018. DOI: 10.1021/acs.bioconjchem.8b00708
- 315 A Zwitterionic Near-infrared Dye Linked TrkC Targeting Agent for Imaging Metastatic Breast Cancer, Z. Yang, S. M. Usama, F. Li, K. Burgess, Z. Li, *Med. Chem. Comm.*, 2018, 9, 1754-1760. DOI: 10.1039/C8MD00190A.
- 314 Targeted Maytansinoid Conjugate Improves Therapeutic Index for Metastatic Breast Cancer Cells, Z. Jiang, Z. Yang, F. Li, Z. Li, N. Fishkin, K. Burgess, *Bioconjugate Chemistry*, 2018, 29, 9, 2920-2926 DOI: 10.1021/acs.bioconjchem.8b00340
- 313 Optimized Heptamethine Cyanines for Photodynamic Therapy, S. Usama, S. Thavornpradit, K. Burgess, *ACS Applied Bio Materials*, 2018, 1, 1195-1205. DOI: 10.1021/acsabm.8b00414.

1. A Zwitterionic Near-infrared Dye Linked TrkC Targeting Agent for Imaging Metastatic Breast Cancer, Z. Yang, S. M. Usama, F. Li, K. Burgess, and Z. Li, *Med. Chem. Comm.*, 2018, **9**, 1754-60.
2. Optimized Heptamethine Cyanines for Photodynamic Therapy, S. M. Usama, S. Thavornpradit, and K. Burgess, *ACS Appl. Bio Mater.*, 2018, **1**, 1195-205.
3. Targeted Maytansinoid Conjugate Improves Therapeutic Index for Metastatic Breast Cancer Cells, Z. Jiang, Z. Yang, F. Li, Z. Li, N. Fishkin, and K. Burgess, *Bioconjugate Chem.*, 2018, **29**, 2920-6.
4. Near infrared fluorescence for image-guided surgery, S. L. Gibbs, *Quant Imaging Med Surg*, 2012, **2**, 177-87.
5. Fluorescence-Guided Surgery, T. Nagaya, A. Nakamura Yu, L. Choyke Peter, and H. Kobayashi, *Front Oncol*, 2017, **7**, 314.
6. In vivo near-infrared fluorescence imaging, J. V. Frangioni, *Curr. Opin. Chem. Biol.*, 2003, **7**, 626-34.
7. Image-guided surgery using invisible near-infrared light: fundamentals of clinical translation, S. Gioux, H. S. Choi, and J. V. Frangioni, *Mol. Imaging*, 2010, **9**, 237-55.
8. Image-guided cancer surgery using near-infrared fluorescence, A. L. Vahrmeijer, M. Hutteman, J. R. van der Vorst, C. J. H. van de Velde, and J. V. Frangioni, *Nat. Rev. Clin. Oncol.*, 2013, **10**, 507-18.
9. The Role of Porphyrin Chemistry in Tumor Imaging and Photodynamic Therapy, M. Ethirajan, Y. Chen, P. Joshi, and R. K. Pandey, *Chem. Soc. Rev.*, 2011, **40**, 340-62.
10. Synthesis and In Vivo Fate of Zwitterionic Near-Infrared Fluorophores, H.-S. Choi, K. Nasr, S. Alyabyev, D. Feith, J.-H. Lee, S.-H. Kim, Y. Ashitate, H. Hyun, G. Patonay, L. Strekowski, M. Henary, and J. V. Frangioni, *Angew. Chem., Int. Ed.*, 2011, **50**, 6258-63.
11. Near-Infrared Fluorescence Imaging of Prostate Cancer Using Heptamethine Carbocyanine Dyes, J. Yuan, X. Yi, F. Yan, F. Wang, W. Qin, G. Wu, X. Yang, C. Shao, and L. W. K. Chung, *Mol. Med. Rep.*, 2015, **11**, 821-8.
12. Optical Imaging of Gastric Cancer With Near-Infrared Heptamethine Carbocyanine Fluorescence Dyes, N. Zhao, C. Zhang, Y. Zhao, B. Bai, J. An, H. Zhang, C. Shi, and B. Wu Jason, *Oncotarget*, 2016, **7**, 57277-89.
13. Optical Imaging of Kidney Cancer with Novel Near Infrared Heptamethine Carbocyanine Fluorescent Dyes, X. Yang, C. Shao, R. Wang, C.-Y. Chu, P. Hu, V. Master, A. O. Osunkoya, H. L. Kim, H. E. Zhau, and L. W. K. Chung, *J. Urol.*, 2013, **189**, 702-10.
14. Heptamethine Carbocyanine DZ-1 Dye for Near-Infrared Fluorescence Imaging of Hepatocellular Carcinoma, J. An, N. Zhao, C. Zhang, Y. Zhao, D. Tan, Y. Zhao, B. Bai, H. Zhang, C. Shi, J. An, and J. Wu Boyang, *Oncotarget*, 2017, **8**, 56880-92.
15. The Application of Heptamethine Cyanine Dye DZ-1 and Indocyanine Green for Imaging and Targeting in Xenograft Models of Hepatocellular Carcinoma, C. Zhang, Y. Zhao, H. Zhang, X. Chen, N. Zhao, D. Tan, H. Zhang, and C. Shi, *Int. J. Mol. Sci.*, 2017, **18**,
16. A Multifunctional Heptamethine Near-Infrared Dye for Cancer Theranosis, S. Luo, X. Tan, Q. Qi, Q. Guo, X. Ran, L. Zhang, E. Zhang, Y. Liang, L. Weng, H. Zheng, T. Cheng, Y. Su, and C. Shi, *Biomaterials*, 2013, **34**, 2244-51.



17. Near-Infrared Fluorescence Heptamethine Carbocyanine Dyes Mediate Imaging and Targeted Drug Delivery for Human Brain Tumor, J. B. Wu, C. Shi, G. C.-Y. Chu, Q. Xu, Y. Zhang, Q. Li, J. S. Yu, H. E. Zhau, and L. W. K. Chung, *Biomaterials*, 2015, **67**, 1-10.
18. Near IR Heptamethine Cyanine Dye-Mediated Cancer Imaging, X. Yang, C. Shi, R. Tong, W. Qian, H. E. Zhau, R. Wang, G. Zhu, J. Cheng, V. W. Yang, T. Cheng, M. Henary, L. Strekowski, and L. W. K. Chung, *Clin. Cancer Res.*, 2010, **16**, 2833-44.
19. A near-infrared fluorescent heptamethine indocyanine dye with preferential tumor accumulation for in vivo imaging, C. Zhang, T. Liu, Y. Su, S. Luo, Y. Zhu, X. Tan, S. Fan, L. Zhang, Y. Zhou, T. Cheng, and C. Shi, *Biomaterials*, 2010, **31**, 6612-7.
20. Newly Emerging Theranostic Agents for Simultaneous Cancer targeted Imaging and Therapy, S. Luo, X. Yang, and C. Shi, *Curr. Med. Chem.*, 2016, **23**, 483-97.
21. Fluorescent chemical probes for accurate tumor diagnosis and targeting therapy, M. Gao, F. Yu, C. Lv, J. Choo, and L. Chen, *Chem. Soc. Rev.*, 2017, **46**, 2237-71.
22. A NIR Heptamethine Dye With Intrinsic Cancer Targeting, Imaging and Photosensitizing Properties, X. Tan, S. Luo, D. Wang, Y. Su, T. Cheng, and C. Shi, *Biomaterials*, 2012, **33**, 2230-9.
23. Review on near-infrared heptamethine cyanine dyes as theranostic agents for tumor imaging, targeting, and photodynamic therapy, C. Shi, B. Wu Jason, and D. Pan, *J. Biomed. Opt.*, 2016, **21**, 50901:1 - :11.
24. Mitochondria-targeted prostate cancer therapy using a near-infrared fluorescence dye-monoamine oxidase A inhibitor conjugate, Q. Lv, X. Yang, M. Wang, J. Yang, Z. Qin, Q. Kan, H. Zhang, Y. Wang, D. Wang, and Z. He, *J. Controlled Release*, 2018, **279**, 234-42.
25. Mechanistic study of IR-780 dye as a potential tumor targeting and drug delivery agent, E. Zhang, S. Luo, X. Tan, and C. Shi, *Biomaterials*, 2014, **35**, 771-8.
26. Improving Therapeutic Potential of Farnesylthiosalicylic Acid: Tumor Specific Delivery via Conjugation with Heptamethine Cyanine Dye, Y. Guan, Y. Zhang, L. Xiao, J. Li, J.-p. Wang, M. D. Chordia, Z.-Q. Liu, L. W. K. Chung, W. Yue, and D. Pan, *Mol. Pharmaceutics*, 2017, **14**, 1-13.
27. Monoamine Oxidase A Inhibitor-Near-Infrared Dye Conjugate Reduces Prostate Tumor Growth, J. B. Wu, T.-P. Lin, J. D. Gallagher, S. Kushal, L. W. K. Chung, H. E. Zhau, B. Z. Olenyuk, and J. C. Shih, *J. Am. Chem. Soc.*, 2015, **137**, 2366-74.
28. Monoamine oxidase A (MAO A) inhibitors decrease glioma progression, S. Kushal, W. Wang, V. P. Vaikari, R. Kota, K. Chen, T.-S. Yeh, N. Jhaveri, S. L. Groshen, B. Z. Olenyuk, T. C. Chen, H. F. M., and J. C. Shih, *Oncotarget*, 2016, **7**, 13842-53.
29. Folate-based Near-infrared Fluorescent Theranostic Gemcitabine Delivery, Z. Yang, H. Lee Jae, M. Jeon Hyun, H. Han Ji, N. Park, Y. He, H. Lee, S. Hong Kwan, C. Kang, and S. Kim Jong, *J. Am. Chem. Soc.*, 2013, in press.
30. Targeted Methotrexate Prodrug Conjugated With Heptamethine Cyanine Dye Improving Chemotherapy and Monitoring Itself Activating by Dual-Modal Imaging, S. Li, Z. Sun, X. Meng, G. Deng, J. Zhang, K. Zhou, W. Li, L. Zhou, P. gong, and L. Cai, *Frontiers in Materials*, 2018, **5**, 1-12.

31. Near-infrared fluorescence imaging of cancer mediated by tumor hypoxia and HIF1 $\alpha$ /OATPs signaling axis, J. B. Wu, C. Shao, X. Li, C. Shi, Q. Li, P. Hu, Y.-T. Chen, X. Dou, D. Sahu, W. Li, H. Harada, Y. Zhang, R. Wang, H. E. Zhau, and L. W. K. Chung, *Biomaterials*, 2014, **35**, 8175-85.
32. Role of Organic Anion-Transporting Polypeptides (OATPs) in Cancer Therapy, N. Thakkar, A. C. Lockhart, and W. Lee, *AAPS Journal*, 2015, **17**, 535-45.
33. E. Kotsampasakou, and G. F. Ecker, "Organic Anion Transporting Polypeptides as Drug Targets, in Transporters as Drug Targets", Transporters as Drug Targets. H. H. Sitte, G. F. Ecker, R. Mannhold, H. Buschmann and R. P. Clausen ed. 2017 Wiley - VCH Verlag GmbH & Co. KGaA.
34. Classification of Inhibitors of Hepatic Organic Anion Transporting Polypeptides (OATPs): Influence of Protein Expression on Drug-Drug Interactions, M. Karlgren, A. Vildhede, U. Norinder, J. R. Wisniewski, E. Kimoto, Y. Lai, U. Haglund, and P. Artursson, *J. Med. Chem.*, 2012, **55**, 4740-63.
35. The expression and function of organic anion transporting polypeptides in normal tissues and in cancer, A. Obaidat, M. Roth, and B. Hagenbuch, *Annu. Rev. Pharmacol. Toxicol.*, 2012, **52**, 135-51.
36. OATPs, OATs and OCTs: the organic anion and cation transporters of the SLCO and SLC22A gene superfamilies, M. Roth, A. Obaidat, and B. Hagenbuch, *Br. J. Pharmacol.*, 2012, **165**, 1260-87.
37. On the Mechanisms of Update of Tumor-Seeking Cyanine Dyes, S. M. Usama, C.-M. Lin, and K. Burgess, *Bioconjugate Chem.*, 2018, accepted.
38. Site-Specific Labeling of Proteins With Near-IR Dyes, C.-M. Lin, S. M. Usama, and K. Burgess, *Molecules*, 2018, submitted.
39. Albumin binding ligands and albumin conjugate uptake by cancer cells, E. Frei, *Diabetol. Metab. Syndr.*, 2011, **3**, 11.
40. Albumin-based drug delivery: harnessing nature to cure disease, T. Larsen Maja, M. Kuhlmann, L. Hvam Michael, and A. Howard Kenneth, *Mol Cell Ther*, 2016, **4**, 3.
41. Serum proteins as drug carriers of anticancer agents: a review, F. Kratz, and U. Beyer, *Drug Delivery*, 1998, **5**, 281-99.
42. Impact of albumin on drug delivery - New applications on the horizon, B. Elsadek, and F. Kratz, *J. Controlled Release*, 2012, **157**, 4-28.
43. Unraveling the mysteries of serum albumin-more than just a serum protein, A. M. Merlot, D. S. Kalinowski, and D. R. Richardson, *Front Physiol*, 2014, **5**, 299.
44. Simple bioconjugate chemistry serves great clinical advances: albumin as a versatile platform for diagnosis and precision therapy, Z. Liu, and X. Chen, *Chem. Soc. Rev.*, 2016, **45**, 1432-56.
45. Interactive association of drugs binding to human serum albumin, F. Yang, Y. Zhang, and H. Liang, *Int. J. Mol. Sci.*, 2014, **15**, 3580-95.
46. Human serum albumin homeostasis: a new look at the roles of synthesis, catabolism, renal and gastrointestinal excretion, and the clinical value of serum albumin measurements, D. G. Levitt, and M. D. Levitt, *Int. J. Gen. Med.*, 2016, **9**, 229-55.

47. Validation of the SCID-hu Thy/Liv mouse model with four classes of licensed antiretrovirals, C. A. Stoddart, C. A. Bales, J. C. Bare, G. Chkhenkeli, S. A. Galkina, A. N. Kinkade, M. E. Moreno, J. M. Rivera, R. E. Ronquillo, B. Sloan, and P. L. Black, *PLoS One*, 2007, **2**, e655.
48. Albumin-conjugated C34 Peptide HIV-1 Fusion Inhibitor: equipotent to C34 and T-20 in vitro with sustained activity in SCID-hu Thy/Liv mice, C. A. Stoddart, G. Nault, S. A. Galkina, K. Thibaudeau, P. Bakis, N. Bousquet-Gagnon, M. Robitaille, M. Bellomo, V. Paradis, P. Liscourt, A. Lobach, M.-E. Rivard, R. G. Ptak, M. K. Mankowski, D. Bridon, and O. Quraishi, *J. Biol. Chem.*, 2008, **283**, 34045-52.
49. A Novel Macromolecular Prodrug Concept Exploiting Endogenous Serum Albumin as a Drug Carrier for Cancer Chemotherapy, F. Kratz, R. Mueller-Driver, I. Hofmann, J. Dreves, and C. Unger, *J. Med. Chem.*, 2000, **43**, 1253-6.
50. INNO-206, the (6-maleimidocaproyl hydrazone derivative of doxorubicin), shows superior antitumor efficacy compared to doxorubicin in different tumor xenograft models and in an orthotopic pancreas carcinoma model, R. Graeser, N. Esser, H. Unger, I. Fichtner, A. Zhu, C. Unger, and F. Kratz, *Invest. New Drugs*, 2010, **28**, 14-9.
51. Probing the Cysteine-34 Position of Endogenous Serum Albumin with Thiol-Binding Doxorubicin Derivatives. Improved Efficacy of an Acid-Sensitive Doxorubicin Derivative with Specific Albumin-Binding Properties Compared to That of the Parent Compound, F. Kratz, A. Warnecke, K. Scheuermann, C. Stockmar, J. Schwab, P. Lazar, P. Drucekes, N. Esser, J. Dreves, D. Rognan, C. Bissantz, C. Hinderling, G. Folkers, I. Fichtner, and C. Unger, *J. Med. Chem.*, 2002, **45**, 5523-33.
52. An albumin-exendin-4 conjugate engages central and peripheral circuits regulating murine energy and glucose homeostasis, L. L. Baggio, Q. Huang, X. Cao, and D. J. Drucker, *Gastroenterology*, 2008, **134**, 1137-47.
53. Development and characterization of a glucagon-like peptide 1-albumin conjugate: The ability to activate the glucagon-like peptide 1 receptor in vivo, J.-G. Kim, L. L. Baggio, D. P. Bridon, J.-P. Castaigne, M. F. Robitaille, L. Jette, C. Benquet, and D. J. Drucker, *Diabetes*, 2003, **52**, 751-9.
54. CDK4/6 inhibition in breast cancer: current practice and future directions, S. Pernas, M. Tolaney Sara, P. Winer Eric, and S. Goel, *Ther Adv Med Oncol*, 2018, **10**, 1758835918786451.
55. CDK4/6 Inhibition in Cancer: Beyond Cell Cycle Arrest, S. Goel, M. J. DeCristo, S. S. McAllister, and J. J. Zhao, *Trends Cell Biol.*, 2018, Ahead of Print.
56. Treating cancer with selective CDK4/6 inhibitors, B. O'Leary, R. S. Finn, and N. C. Turner, *Nat. Rev. Clin. Oncol.*, 2016, **13**, 417-30.
57. Specific inhibition of cyclin-dependent kinase 4/6 by PD 0332991 and associated antitumor activity in human tumor xenografts, D. W. Fry, P. J. Harvey, P. R. Keller, W. L. Elliott, M. Meade, E. Trachet, M. Albassam, X. Zheng, W. R. Leopold, N. K. Pryer, and P. L. Toogood, *Mol. Cancer Ther.*, 2004, **3**, 1427-38.
58. CDK4/6 Inhibitors: The Mechanism of Action May Not Be as Simple as Once Thought, M. E. Klein, M. Kovatcheva, L. E. Davis, W. D. Tap, and A. Koff, *Cancer Cell*, 2018, **34**, 9-20.

## Article

# Site-Specific Labeling of Proteins with Near-IR Heptamethine Cyanine Dyes

Chen-Ming Lin , Syed Muhammad Usama  and Kevin Burgess \*

Department of Chemistry, Texas A & M University, Box 30012, College Station, TX 77842, USA; chen-ming\_lin@tamu.edu (C.-M.L.); syed.usama@chem.tamu.edu (S.M.U.)

\* Correspondence: burgess@tamu.edu; Tel.: +1-979-845-4345

Academic Editor: Maged Henary

Received: 19 October 2018; Accepted: 6 November 2018; Published: 7 November 2018



**Abstract:** Convenient labeling of proteins is important for observing its function under physiological conditions. In tissues particularly, heptamethine cyanine dyes (Cy-7) are valuable because they absorb in the near-infrared (NIR) region (750–900 nm) where light penetration is maximal. In this work, we found Cy-7 dyes with a *meso*-Cl functionality covalently binding to proteins with free Cys residues under physiological conditions (aqueous environments, at near neutral pH, and 37 °C). It transpired that the *meso*-Cl of the dye was displaced by free thiols in protein, while nucleophilic side-chains from amino acids like Tyr, Lys, and Ser did not react. This finding shows a new possibility for convenient and selective labeling of proteins with NIR fluorescent probes.

**Keywords:** heptamethine cyanine; protein labeling; thiol labeling; cancer targeting; vimentin

## 1. Introduction

Hydrophilic near-infrared (NIR) fluorescent dyes are valued for in-depth imaging in tissues, and heptamethine cyanines, or Cy-7 dyes, which absorb in the NIR region (700–900 nm), are amongst the most widely used [1]. Indocyanine green (ICG, Figure 1), the only FDA-approved Cy-7 dye, has been widely used in medical and clinical diagnostics [2–4].

Many applications of Cy-7 dyes require that they be covalently conjugated to, for example, antibodies, cell surface targeting peptides/biomarkers, and small molecule substrates. This is often achieved by modifying Cy-7 derivatives with coupling functionalities such as maleimide, succinimide esters, isocyanates, or sulfonyl halides. The challenge with strategies like this is balancing the demands of experimental convenience with selectivity towards targeted amino acid types. Extensive modifications to Cy-7 dyes can also alter their solubility and photophysical properties [5].

Figure 1 shows dyes featured in this study. Probes of this type, i.e., with a 1-chloro-2,6-disubstituted cyclohexane (i.e., MHI-148, IR-780, IR-783, and DZ-1) [6–8], are known for their tumor localizing properties [9–12]. Therefore, these Cy-7 dyes are potential carriers of cytotoxic payload for combined cancer targeted therapy and imaging [13–16]. In our research in this area, we happened to make a surprising finding regarding such a conjugation process. Specifically, when investigating in vitro reactions and cell lysates featuring MHI-148, it was found to covalently bind to several proteins with high selectivity as evidenced by gel electrophoresis and NIR imaging at around 800 nm.

We hypothesized that the *meso*-Cl of MHI-148 was substituted by nucleophilic functional groups of amino acids (Cys, Ser, Tyr and Lys) of proteins. This paper provides data to support this hypothesis and understand the selectivity.

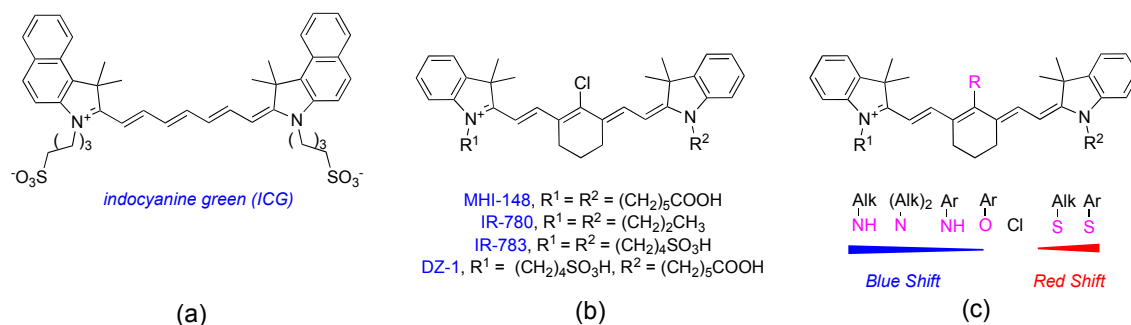
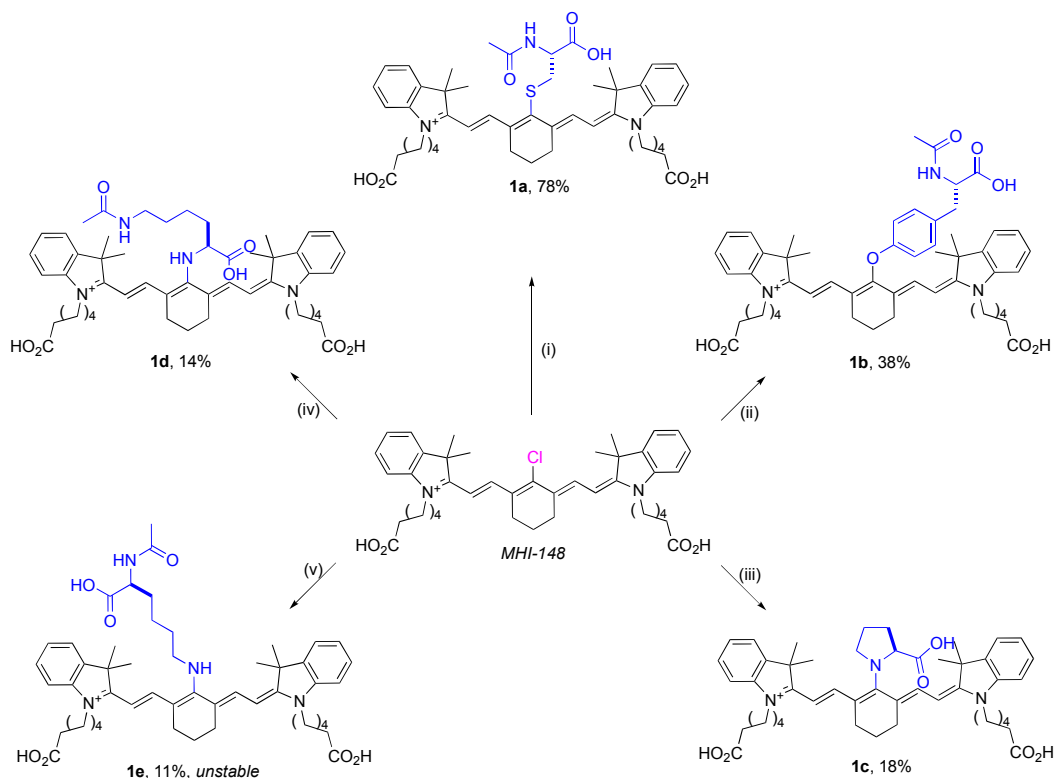


**Figure 1.** Structures of: (a) ICG; (b) cancer-tissue-targeting Cy-7 dyes and their *meso*-substituted derivatives; and (c) graphical representation of the effects of *meso*-substitution on electronic spectra.

## 2. Results and Discussion

### 2.1. Syntheses of Amino-Acid-Substituted Cy-7 Dyes

Reactions under controlled conditions were used to test if nucleophilic substitution of the chloride of MHI-148 possibly occurred in DMF solvent. Thus, several amino acids with different nucleophilic side-chains (*N*-acetyl-L-cysteine, *N*-acetyl-L-tyrosine, *N* $\alpha$ -acetyl-L-lysine, *N* $\epsilon$ -acetyl-L-lysine, and L-proline) were reacted with MHI-148 under conditions that were varied to force the reactions to proceed. The corresponding amino-acid-substituted Cy-7 dyes were indeed formed (Scheme 1); these were isolated, characterized (see supplementary materials for NMR and mass spectrometry), and later used as standards for comparison of high-performance liquid chromatography (HPLC) retention times. Serine was excluded from these experiments because alcohol hydroxyl groups are known to not substitute the *meso*-Cl without complications [17–20].



**Scheme 1.** Preparation of amino-acid-substituted Cy-7 dyes. (i) *N*-acetyl-L-cysteine (1 eq.), <sup>i</sup>Pr<sub>2</sub>NEt (1.5 eq.), DMF, 25 °C, 1 h (ii) *N*-acetyl-L-tyrosine (1 eq.), NaH, DMF, 25 °C, 18 h (iii) proline (1 eq.), <sup>i</sup>Pr<sub>2</sub>NEt (1 eq.), DMF, 60 °C, 2 h (iv) *N* $\epsilon$ -acetyl-L-lysine (1 eq.), <sup>i</sup>Pr<sub>2</sub>NEt (1 eq.), DMF/H<sub>2</sub>O, 60 °C, 20 h (v) *N* $\alpha$ -acetyl-L-lysine (1 eq.), <sup>i</sup>Pr<sub>2</sub>NEt (1 eq.), DMF, 60 °C, 20 h.

*N*-Acetyl-L-cysteine was the most reactive nucleophile of the five amino acids studied. In the presence of Hünig's base, MHI-148 was completely converted to the thiol-substituted product within 1 h at 25 °C in DMF (0.1 M 1:1 dye:Cys-derivative, LC-MS analyses). Four other amino acid nucleophiles studied required a stronger base (Tyr) and/or elevated temperatures (Pro and Lys), and even then, a significant amount of unreacted MHI-148 was observed after several hours. *N*α-Acetyl-L-lysine reacted faster than those three, giving the substituted product **1e**, which can be isolated by reversed-phase flash chromatography; however, significant decomposition was observed (color change from blue to pink) in organic solvents after only 20 min. The instability caused by delocalization of a lone pair of electrons by primary amine at *meso* position is also reported by other groups [21,22]. Overall, this data indicated the *meso*-Cl substitution reactivity was thiol > phenol > 2° amine > 1° amine, which corresponds to the observations in the literature [23]. At this stage, we did not know if these reactivities would also be observed in aqueous media, but preferential conjugation of MHI-148 to Cys residues seemed more likely.

## 2.2. Optical Properties of Amino-Acid-Substituted Cy-7 Dyes

Figure 2 shows absorbance and fluorescence of compounds **1a–d** in 10 mM PBS buffer. The *S*- or *O*-substituted compounds (**1a** and **1b**) had absorbance and fluorescence spectra similar to those of MHI-148. Significant red-shifts of absorbance and fluorescence were observed for both *N*-substituted Cy-7 dyes (**1c** and **1d**), which have been attributed [24,25] to conjugation of the nitrogen lone pair with the Cy-7 core. Interestingly, the peaks for the *N*-substituted products are significantly broader, implying more vibrational fine structures than the *S*- or *O*-substituted products [26].

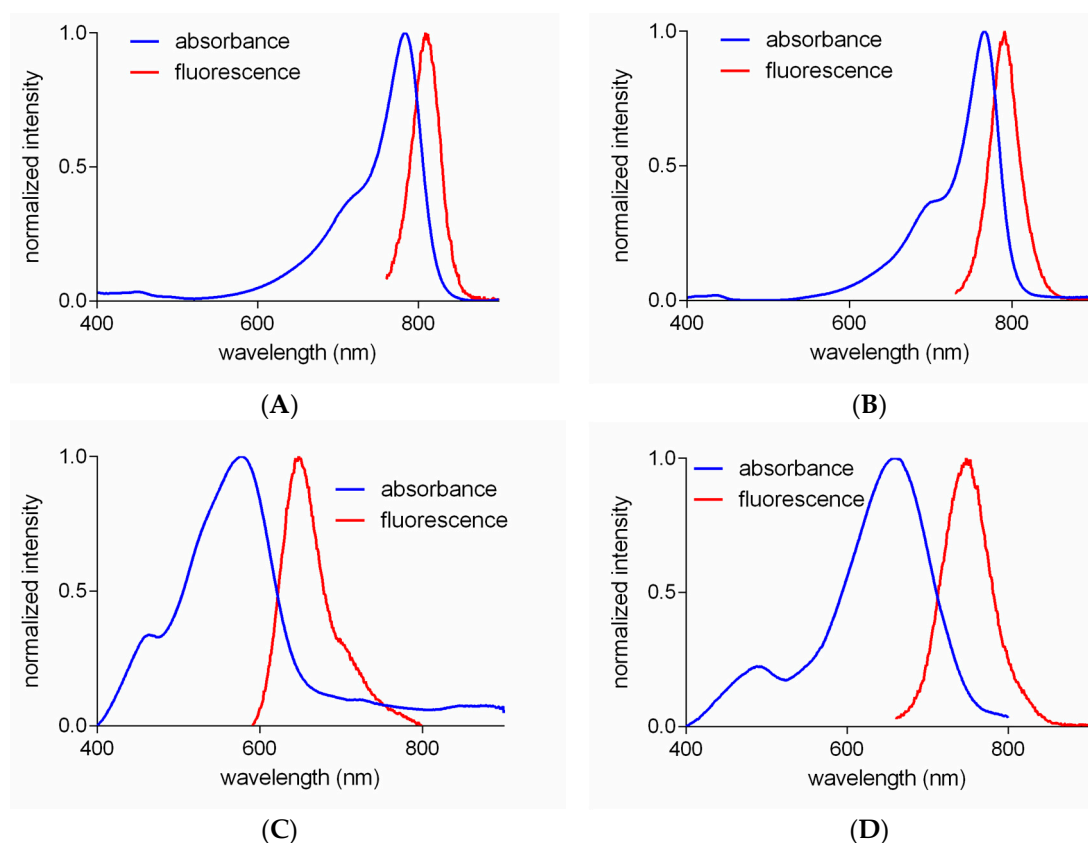


**Figure 2.** Normalized absorbance and fluorescence of compounds **1a–d** (6  $\mu$ M, 37 °C) in pH 7.24 10 mM PBS buffer. (A) compound **1a**:  $\lambda_{\text{max abs}}$  783 nm (blue),  $\lambda_{\text{max emiss}}$  809 nm (red). (B) compound **1b**:  $\lambda_{\text{max abs}}$  766 nm (blue),  $\lambda_{\text{max emiss}}$  791 nm (red). (C) compound **1c**:  $\lambda_{\text{max abs}}$  578 nm (blue),  $\lambda_{\text{max emiss}}$  648 nm (red). (D) compound **1d**:  $\lambda_{\text{max abs}}$  658 nm (blue),  $\lambda_{\text{max emiss}}$  748 nm (red).

### 2.3. Meso-Cl Functionality of Cy-7 Dyes Is Essential for Cys-Selective Protein Labeling

Vimentin, a structural protein, was chosen for study because it has only one Cys residue (C328). Vimentin (1  $\mu$ g, 1  $\mu$ M) was incubated with Cy-7 dyes containing *meso*-Cl (MHI-148, IR-780, IR-783, and DZ-1; 10  $\mu$ M) and with Cy-7 dyes without *meso*-Cl (ICG and **1a**) for comparison (throughout, 10  $\mu$ M in 50 mM pH 7.24 HEPES buffer at 37  $^{\circ}$ C for up to 24 h). An equal amount of the samples (100 ng) was electrophoresed under reducing conditions, and the gel was analyzed using an NIR imager. Only the Cy-7 dyes containing *meso*-Cl reacted to give a band observable at 800 nm (Figure 3).

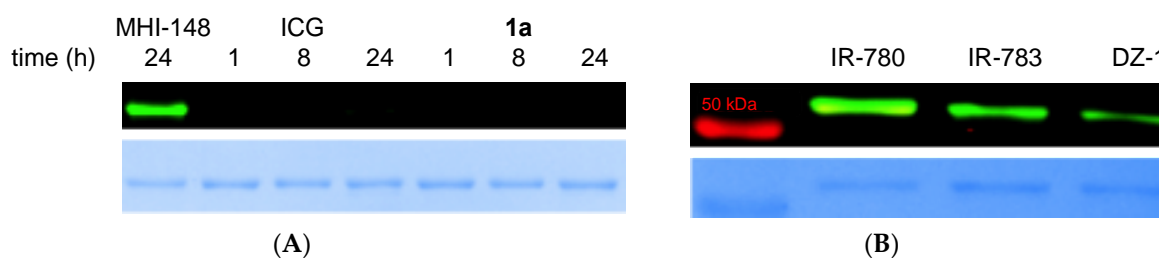
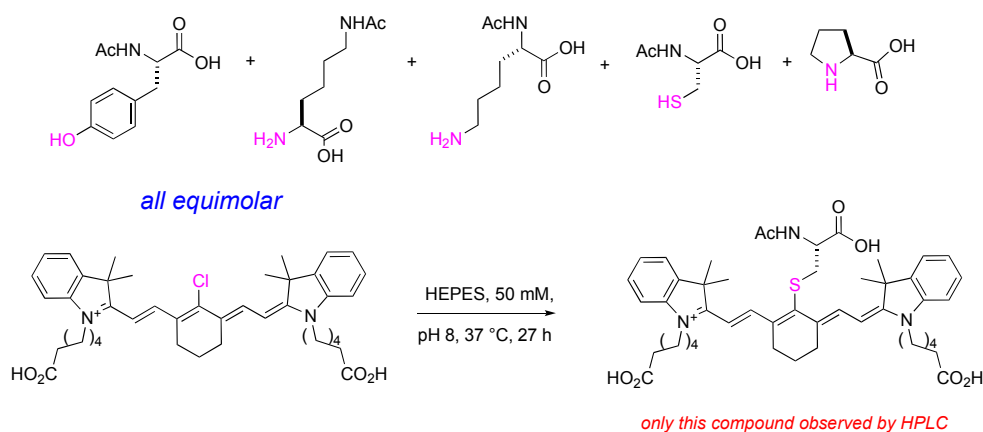


**Figure 3.** Near-infrared (NIR) fluorescent gel image of (A) vimentin (1  $\mu$ M) incubated with different cyanines (10  $\mu$ M) in 50 mM pH 7.24 HEPES buffer at different incubation times; (B) vimentin (1  $\mu$ M) incubated with IR-780, IR-783, and DZ-1 in the same buffer as (A) for 24 h. CBB-G250 staining indicated an equal amount of protein (100 ng) was loaded into gel.

Further evidence for the superior reactivities of Cys side-chains over other nucleophilic amino acid residues was obtained via competition experiments. Thus, MHI-148 (200  $\mu$ M) in 50 mM pH 8.0 HEPES buffer was incubated with equimolar amounts of five amino acids (Scheme 2) at 37  $^{\circ}$ C, and the reaction was monitored by HPLC up to 27 h. Prototypes of this experiment were intended to measure relative rates, however, only formation of the Cys-product **1a** occurred (HPLC spike with the standard from Scheme 1 (Figure 4) and LC-MS analyses). Under these conditions, approximately 32% of MHI-148 was substituted and 68% remained after 15 h. The reaction did not go to completion due to equilibrium of the reaction or due to oxidation of cysteines in aqueous conditions. This observation implied amine, alcohol, and phenol side-chains in the protein did not react with the dye.



**Scheme 2.** Competition study of MHI-148 with amino acids in aqueous buffer.

Blocking experiments were performed to be absolutely sure that the vimentin Cys was the reactive group for coupling to MHI-148 in aqueous buffer at 37  $^{\circ}$ C. Thus, maleimide-blocked protein [27,28] was formed by incubating vimentin with 6-maleimidohexanoic acid (6-MA; 18 h in 50 mM pH 7.24 HEPES buffer at 37  $^{\circ}$ C). Vimentin and the thiol-blocked vimentin were incubated with MHI-148 for different incubation times, then analyzed using SDS-PAGE gel electrophoresis. Figure 4C shows that the concentration of MHI-148 covalently bound to vimentin progressively increased (NIR fluorescence at  $\sim$ 800 nm), whereas no fluorescent band was observed for the thiol-blocked vimentin.

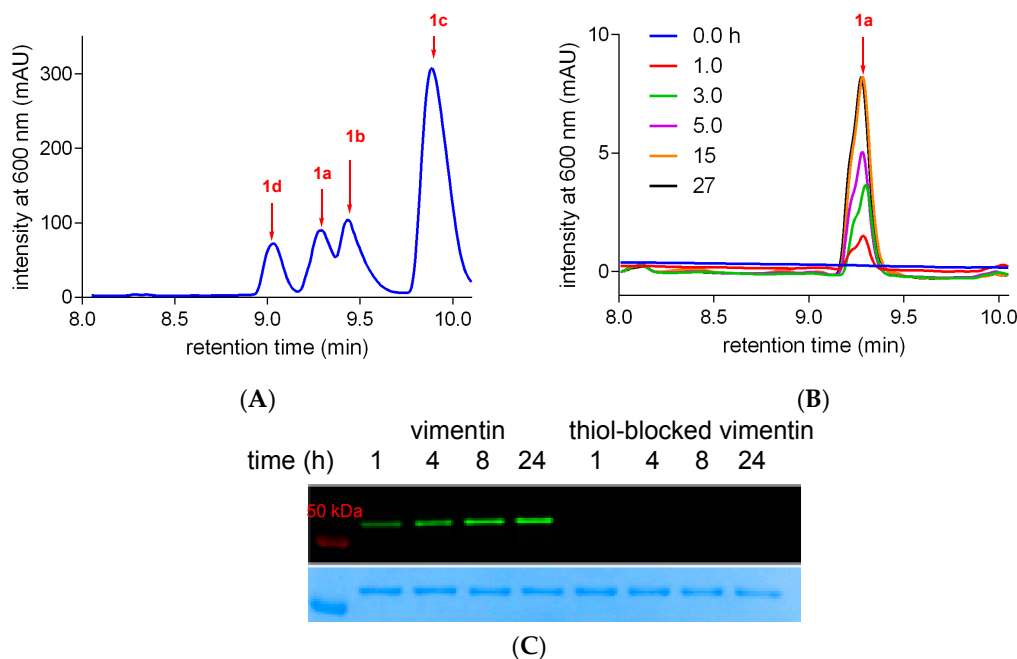


**Figure 4.** High-performance liquid chromatography (HPLC) analysis of (A) 200  $\mu$ M of each amino-acid-conjugate standard 1a–d in 50 mM pH 8.0 HEPES buffer; (B) kinetic study for 200  $\mu$ M of MHI-148 with 200  $\mu$ M of each amino acid (*N*-acetyl-L-Cys, *N*-acetyl-L-Tyr, *N* $\alpha$ -acetyl-L-Lys, *N* $\epsilon$ -acetyl-L-Lys, and L-proline) in 50 mM pH 8.0 HEPES buffer incubating at 37  $^{\circ}$ C; (C) NIR fluorescent gel image of vimentin or 6-MA-blocked vimentin (1  $\mu$ M) incubated with MHI-148 (1  $\mu$ M) in 50 mM pH 7.24 HEPES buffer at different incubation times.

Overall, based on all the experiments above, we concluded that MHI-148 selectively binds the only free Cys in vimentin, C328, in aqueous buffer at 37  $^{\circ}$ C, and went on to calibrate the efficiency of binding. Thus, NIR fluorescence ( $>800$  nm) in gel electrophoresis was quantitative for vimentin (1  $\mu$ M in 50 mM pH 7.24 HEPES buffer) when incubated with MHI-148 (0–30  $\mu$ M, 3 h at 37  $^{\circ}$ C). Fluorescence intensities of the salient band saturated at 10  $\mu$ M (Figure 5a), which means the tested fluorescent compound can quantitatively label the protein at a 10:1 ratio within 3 h when incubated under these conditions in HEPES aqueous buffer. Experiments to test sensitivity revealed labeled vimentin was detectable at concentrations as low as 1 ng on our gel imaging apparatus (Figure 5b).

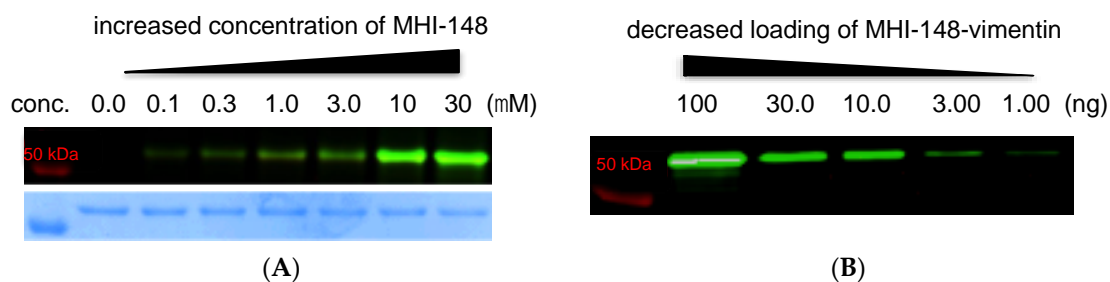


**Figure 5.** NIR fluorescent gel image of (A) vimentin (1  $\mu$ M) incubated with different concentrations of MHI-148 in 50 mM pH 7.24 HEPES buffer for 3 h at 37  $^{\circ}$ C (B) 10:1 concentration ratio of MHI-148:vimentin sample was loaded into 10% SDS-PAGE gel with different amounts of vimentin sample.

#### 2.4. Labeling of Other Proteins Using MHI-148

Several proteins with and without free Cys residues were labeled to test the robustness of the method developed for vimentin. NEDD8-activating enzyme (NAE) [29], Ubc12 [30], and PCSK9 [31] contain free thiols (reduced Cys residues), whereas NEDD8 [29] (no Cys in sequences), truncated suPAR

(residues 1–281, 12 disulfides) [32], and EGFR (25 disulfides) [33] have none. Figure 6 shows that only the proteins containing sulfhydryl groups reacted under the standard conditions. NAE consists of two subunits (APPBP1 and UBA3) which each contain free Cys; hence, two NIR fluorescence bands were observed for that sample.

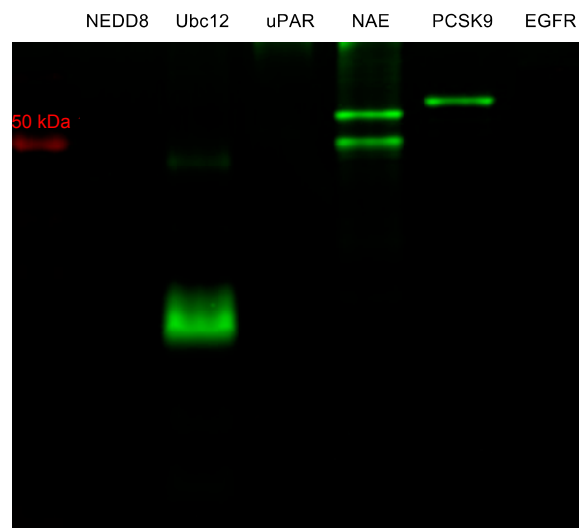


**Figure 6.** NIR fluorescent gel image of diverse proteins (4  $\mu$ M) incubated with MHI-148 (4  $\mu$ M) for 3 h using 50 mM pH 7.24 HEPES buffer at 37  $^{\circ}$ C.

### 3. Materials and Methods

#### 3.1. General Information

All reactions were carried out with dry solvents under anhydrous conditions under an inert atmosphere (argon). Glassware was dried in an oven at 140  $^{\circ}$ C for a minimum of 6 h prior to use for all reactions. IR-783 and IR-780 were purchased from Sigma Aldrich (Atlanta, GA, USA) and abcr GmbH (Karlsruhe, Germany), respectively, and DZ-1 and MHI-148 were synthesized according to literature protocol [7,12,14,34]. All other reagents were purchased at a high commercial quality (typically 97% or higher) and used without further purification, unless otherwise stated. Products were purified using a reverse-phase column on a preparative high-performance liquid chromatography (prep HPLC) (Agilent, Santa Clara, CA, USA) obtained from solid-phase synthesis in 10%–95% MeCN/water with 0.05% trifluoroacetic acid over 20 min. High-field NMR spectra were recorded with Bruker Avance III (Billerica, MA, USA) at 400 MHz for  $^1$ H, and 100 MHz for  $^{13}$ C for all compounds. All spectra were calibrated using residual nondeuterated solvent as an internal reference (MeOD- $d_4$ :  $^1$ H-NMR = 3.30,  $^{13}$ C-NMR = 49.0, DMSO- $d_6$ :  $^1$ H-NMR = 2.50,  $^{13}$ C-NMR = 39.5). The following abbreviations were used to explain the multiplicities: s = singlet, d = doublet, t = triplet, q = quartet, quint = quintet, dd = double doublet, dt = double triplet, dq = double quartet, and m = multiplet. Electrospray ionization mass spectrometry (ESI-MS) data were collected on a triple-stage quadrupole instrument (Thermo Scientific, Waltham, MA, USA) in a positive mode. All statistical analyses were carried out by GraphPad Prism version 6.0 (GraphPad Software, La Jolla, CA, USA).

#### 3.2. Synthesis and Characterization

2-((E)-2-((E)-2-(((R)-2-acetamido-2-carboxyethyl)thio)-3-(2-((E)-1-(5-carboxypentyl)-3,3-dimethylindolin-2-ylidene)ethylidene)cyclohex-1-en-1-yl)vinyl)-1-(5-carboxypentyl)-3,3-dimethyl-3H-indol-1-ium (**1a**)

To a solution of MHI-148 (25.0 mg, 0.04 mmol) in DMF (1.00 mL), *N*-acetyl-L-cysteine (5.98 mg, 0.04 mmol) and  $^i$ Pr $_2$ NEt (9.41  $\mu$ L, 0.06 mmol) were added and the reaction was stirred at 25  $^{\circ}$ C for

1 h. Solvent was removed under a stream of nitrogen gas and purified by preparative reversed-phase HPLC (10%–95% CH<sub>3</sub>CN/water containing 0.05% TFA). Compound was lyophilized to obtain green solid (23.4 mg, 78%). <sup>1</sup>H-NMR (400 MHz, MeOD) δ 8.77 (d, *J* = 13.9 Hz, 2H), 7.49 (d, *J* = 7.3 Hz, 2H), 7.45–7.36 (m, 2H), 7.27 (dd, *J* = 14.9, 7.6 Hz, 4H), 6.28 (d, *J* = 13.8 Hz, 2H), 4.55 (dd, *J* = 7.5, 5.3 Hz, 1H), 4.15 (t, *J* = 6.9 Hz, 4H), 3.40 (dd, *J* = 13.4, 5.3 Hz, 1H), 3.12 (dd, *J* = 13.4, 7.5 Hz, 1H), 2.75–2.54 (m, 4H), 2.31 (t, *J* = 7.3 Hz, 4H), 1.98–1.92 (m, 2H), 1.95 (s, 3H), 1.90–1.80 (m, 4H), 1.74 (s, 12H), 1.72–1.64 (m, 4H), 1.55–1.45 (m, 4H). <sup>13</sup>C-NMR (100 MHz, MeOD) δ 177.23, 173.86, 173.21, 172.93, 157.83, 146.46, 143.72, 142.48, 134.54, 129.83, 126.27, 123.46, 112.00, 102.20, 54.36, 50.51, 50.49, 49.85, 44.97, 39.51, 34.61, 28.44, 28.02, 27.38, 25.65, 22.75, 22.03. HRMS calculated for C<sub>47</sub>H<sub>60</sub>N<sub>3</sub>O<sub>7</sub>S<sup>+</sup> (M)<sup>+</sup>: 810.4146; found 810.4166.

6-((E)-2-((E)-2-(2-(4-(2-acetamido-2-carboxyethyl)phenoxy)-3-((E)-2-(1-(5-carboxypentyl)-3,3-dimethyl-3H-indol-1-ium-2-yl)vinyl)cyclohex-2-en-1-ylidene)ethylidene)-3,3-dimethylindolin-1-yl)hexanoate (**1b**)

NaH (0.89 mg, 0.04 mmol) was added to a solution of *N*-acetyl-L-tyrosine (8.25 mg, 0.04 mmol) in DMF (1.00 mL) and the reaction was stirred at 25 °C for 30 min. MHI-148 (25.0 mg, 0.04 mmol) was then added to the above reaction and the reaction was stirred for an additional 18 h at 25 °C. Solvent was removed under a stream of nitrogen gas and purified by preparative reversed-phase HPLC (10%–95% CH<sub>3</sub>CN/water containing 0.05% TFA). Compound was lyophilized to obtain green solid (12.2 mg, 38%). <sup>1</sup>H-NMR (400 MHz, MeOD) δ 8.01–7.92 (m, 2H), 7.36 (t, *J* = 7.8 Hz, 4H), 7.31–7.15 (m, 6H), 7.05 (d, *J* = 8.7 Hz, 2H), 6.13 (d, *J* = 14.2 Hz, 2H), 4.54 (dd, *J* = 9.1, 5.2 Hz, 1H), 4.09 (t, *J* = 7.3 Hz, 4H), 3.14 (dd, *J* = 14.0, 5.2 Hz, 1H), 2.84 (dd, *J* = 14.2, 9.2 Hz, 1H), 2.73 (t, *J* = 5.8 Hz, 4H), 2.30 (t, *J* = 7.3 Hz, 4H), 2.04 (t, *J* = 7.3 Hz, 2H), 1.84 (s, 3H), 1.83–1.73 (m, 4H), 1.67 (dd, *J* = 15.1, 7.5 Hz, 4H), 1.46 (t, *J* = 7.7 Hz, 4H), 1.33 (s, 12H). <sup>13</sup>C-NMR (100 MHz, MeOD) δ 177.20, 174.59, 173.75, 173.05, 165.43, 160.25, 143.57, 143.34, 142.51, 132.96, 132.16, 129.76, 126.19, 123.40, 123.20, 115.75, 111.94, 100.93, 55.48, 50.27, 44.85, 37.62, 34.59, 28.25, 27.96, 27.33, 25.63, 25.21, 22.48, 22.39. HRMS calculated for C<sub>53</sub>H<sub>64</sub>N<sub>3</sub>O<sub>8</sub><sup>+</sup> (M)<sup>+</sup>: 870.4688; found 870.4675.

1-(5-Carboxypentyl)-2-((E)-2-((E)-3-(2-((E)-1-(5-carboxypentyl)-3,3-dimethylindolin-2-ylidene)ethylidene)-2-((S)-2-carboxypyrrolidin-1-yl)cyclohex-1-en-1-yl)vinyl)-3,3-dimethyl-3H-indol-1-ium (**1c**)

To a solution of MHI-148 (25.0 mg, 0.04 mmol) in DMF (1.00 mL), L-proline (4.26 mg, 0.04 mmol) and <sup>i</sup>Pr<sub>2</sub>NEt (6.27 μL, 0.04 mmol) were added and the reaction was stirred at 60 °C monitored by Agilent LC-MS. The reaction reached equilibrium after 2 h and the solvent was removed under a stream of nitrogen gas and purified by preparative reversed-phase HPLC (10%–95% CH<sub>3</sub>CN/water containing 0.05% TFA). Compound was lyophilized to obtain blue solid (5.18 mg, 18%). <sup>1</sup>H-NMR (400 MHz, DMSO) δ 7.42 (d, *J* = 7.3 Hz, 2H), 7.28 (t, *J* = 7.7 Hz, 2H), 7.11 (d, *J* = 7.7 Hz, 2H), 7.04 (t, *J* = 7.2 Hz, 2H), 5.68 (d, *J* = 12.4 Hz, 2H), 4.96 (d, *J* = 7.3 Hz, 2H), 4.02–3.97 (m, 1H), 3.90–3.87 (m, 4H), 2.76–2.57 (m, 3H), 2.46–2.29 (m, 3H), 2.28–2.18 (m, 1H), 2.20 (t, *J* = 7.3 Hz, 4H), 2.09–1.98 (m, 3H), 1.79–1.70 (m, 2H), 1.70–1.62 (m, 4H), 1.57 (s, 6H), 1.61–1.48 (m, 4H), 1.54 (s, 6H), 1.45–1.30 (m, 4H). <sup>13</sup>C-NMR (100 MHz, DMSO) δ 174.29, 172.71, 166.02, 158.00, 142.99, 139.74, 136.52, 128.11, 123.13, 122.28, 122.00, 109.00, 94.22, 64.69, 56.49, 46.93, 42.26, 33.52, 30.04, 29.59, 28.65, 28.11, 26.70, 25.81, 24.22, 20.65. HRMS calculated for C<sub>47</sub>H<sub>60</sub>N<sub>3</sub>O<sub>6</sub><sup>+</sup> (M)<sup>+</sup>: 762.4477; found 762.4457.

2-((E)-2-((E)-2-(((S)-5-acetamido-1-carboxypentyl)amino)-3-(2-((E)-1-(5-carboxypentyl)-3,3-dimethylindolin-2-ylidene)ethylidene)cyclohex-1-en-1-yl)vinyl)-1-(5-carboxypentyl)-3,3-dimethyl-3H-indol-1-ium (**1d**)

To a solution of MHI-148 (25.0 mg, 0.04 mmol) in DMF/H<sub>2</sub>O (1:1; 1.00 mL), *N*ε-acetyl-L-lysine (6.96 mg, 0.04 mmol) and <sup>i</sup>Pr<sub>2</sub>NEt (6.27 μL, 0.04 mmol) were added and the reaction was stirred at 60 °C monitored by Agilent LC-MS. The reaction reached equilibrium after 20 h and the solvent was removed under a stream of nitrogen gas and purified by preparative reversed-phase HPLC (10%–95% CH<sub>3</sub>CN/water containing 0.05% TFA). Compound was lyophilized to obtain blue solid (4.33 mg, 18%).

$^1\text{H}$ -NMR (400 MHz, DMSO)  $\delta$  8.02 (d,  $J$  = 9.4 Hz, 1H), 7.78 (d,  $J$  = 12.9 Hz, 2H), 7.45 (d,  $J$  = 7.2 Hz, 2H), 7.35–7.28 (m, 2H), 7.24 (dd,  $J$  = 11.6, 3.9 Hz, 1H), 7.17 (d,  $J$  = 8.0 Hz, 2H), 7.09 (t,  $J$  = 7.4 Hz, 2H), 7.05–7.00 (m, 1H), 5.85 (d,  $J$  = 13.2 Hz, 2H), 4.43 (dd,  $J$  = 13.9, 8.8 Hz, 1H), 4.00–3.95 (m, 4H), 3.68–3.61 (m, 4H), 3.01 (t,  $J$  = 5.4 Hz, 2H), 2.56 (dd,  $J$  = 13.9, 7.2 Hz, 2H), 2.42–2.33 (m, 2H), 2.20 (dd,  $J$  = 13.4, 6.3 Hz, 4H), 1.75 (s, 3H), 1.72–1.63 (m, 6H), 1.60 (s, 12H), 1.52 (dd,  $J$  = 14.8, 7.4 Hz, 6H), 1.43–1.34 (m, 8H).  $^{13}\text{C}$ -NMR (100 MHz, DMSO)  $\delta$  174.22, 173.25, 168.88, 167.91, 142.71, 140.05, 128.12, 127.58, 122.74, 122.42, 121.96, 120.58, 109.39, 108.49, 95.36, 47.32, 43.24, 42.35, 38.21, 33.47, 28.99, 28.01, 27.60, 25.94, 25.77, 25.62, 24.45, 24.18, 24.11, 24.05, 22.53. HRMS calculated for  $\text{C}_{50}\text{H}_{67}\text{N}_4\text{O}_7^+$  (M) $^+$ : 835.5004; found 835.4972.

### 3.3. UV-Vis and Fluorescence Analysis

Here, 6  $\mu\text{M}$  of compounds **1a–d** samples in 10 mM PBS buffer was prepared by diluting their corresponding stock solution (20 mM) in DMSO using pH 7.24 10 mM PBS buffer. The absorbance and fluorescence of these samples were analyzed using a Varian Cary 100 UV-Vis spectrometer and Varian Cary Eclipse fluorescence spectrophotometer, respectively. The excitation wavelength for compounds **1a–d** was set as 740, 720, 580, and 650 nm, respectively. The normalized absorbance and fluorescence data were plotted using GraphPad Prism version 6.0 (GraphPad Software).

### 3.4. NIR Gel Image Protocol

Different cyanines (10  $\mu\text{M}$ ; 20 mM stock in DMSO) were incubated with vimentin (1  $\mu\text{M}$ ; 1  $\mu\text{g}$ ) in pH 7.24 HEPES buffer (50 mM) at 37  $^\circ\text{C}$  monitored up to 24 h. For this, 100 ng of each cyanine-vimentin conjugate samples was treated under reducing condition with heating at 95  $^\circ\text{C}$  for 10 min and loaded into 15% SDS-PAGE for electrophoresis. The gel was washed with deionized water (10 min  $\times$  3 times), and the gel was analyzed by an Odyssey imager to detect the NIR fluorescence.

### 3.5. Preparation of Thiol-Blocked Vimentin

Using pH 7.24 HEPES buffer (50 mM), thiol-blocked vimentin was prepared by incubating 6-maleimide-hexanoic acid (6-MA, 10  $\mu\text{M}$ ) with vimentin (1  $\mu\text{g}$ , 1  $\mu\text{M}$ ) for 18 h at 37  $^\circ\text{C}$ . The thiol-blocked vimentin solution was directly used to incubate with MHI-148 (1  $\mu\text{M}$ ) without further purifications.

### 3.6. Kinetic Study of MHI-148 with Amino Acids in Aqueous Buffer

To a solution of MHI-148 (400  $\mu\text{M}$ ) in pH 8.00 HEPES buffer (500  $\mu\text{L}$ ), 100  $\mu\text{L}$  of each amino acid solution (2.00 mM) in pH 8.00 HEPES buffer was added to make a final concentration of 200  $\mu\text{M}$  of each reagent. The reaction was incubated and shaken at 37  $^\circ\text{C}$  and was monitored using HPLC at 600 nm from 0 to 27 h to reach reaction equilibrium. The data was plotted using GraphPad Prism version 6.0 (GraphPad Software).

### 3.7. NIR Gel Image of MHI-148 with Different Proteins

Different proteins, including NEDD8, Ubc12, truncated suPAR (residues 1–281), NAE, PCSK9, and EGFR (4  $\mu\text{M}$ ; 1  $\mu\text{g}$ ), were incubated with MHI-148 (4  $\mu\text{M}$ ) in pH 7.24 HEPES buffer (50 mM) at 37  $^\circ\text{C}$  for 3 h. For this, 500 ng of each protein samples were treated under nonreducing condition with heating at 95  $^\circ\text{C}$  for 10 min and loaded into 10% SDS-PAGE for electrophoresis. The gel was washed with deionized water (10 min  $\times$  3 times), and the gel was analyzed by an Odyssey imager to detect the NIR fluorescence.

## 4. Conclusions

MHI-148 can label proteins that have free Cys residues such as serum albumin [35] and vimentin. Other Cy-7 dyes containing *meso*-Cl were only used to label vimentin in this work, but it would

be unsurprising if they can be used. It seems clear that this methodology could be applied with a high probability of success to conveniently conjugate *meso*-CI NIR dyes to antibodies, monobodies, and nanobodies to form selective agents for optical imaging in vivo. Traditional conjugation techniques tend to require modification of the dye to include maleimide or succinimide functionality [28,36,37], but the method developed here circumvents that process.

**Supplementary Materials:** The NMR and mass spectrometry of compounds **1a–d** and picture of Coomassie blue staining for SDS-PAGE are available online.

**Author Contributions:** C.-M.L. designed the research. C.-M.L. and S.M.U. carried out the experiments and analyzed the data. All authors contributed to write the manuscript.

**Funding:** Financial support was provided by a DoD BCRP Breakthrough Award [BC141561], CPRIT [RP150559 and RP170144], The Robert A. Welch Foundation [A-1121], Texas A&M University [RP180875], and The National Science Foundation [M1603497]. The NMR instrumentation of Texas A&M University was supported by a grant from the National Science Foundation [DBI-9970232] and the Texas A&M University system.

**Acknowledgments:** We would like to thank Raquel Sitcheran's laboratory at Texas A&M University for the use of the Odyssey CLx NIR imager. The use of chemistry Mass Spectrometry Facility at Texas A&M University is acknowledged.

**Conflicts of Interest:** The authors declare no conflict of interest.

## References

1. Shi, C.; Wu Jason, B.; Pan, D. Review on near-infrared heptamethine cyanine dyes as theranostic agents for tumor imaging, targeting, and photodynamic therapy. *J. Biomed. Opt.* **2016**, *21*, 50901. [[CrossRef](#)] [[PubMed](#)]
2. Schaafsma, B.E.; Mieog, J.S.D.; Hutteman, M.; van der Vorst, J.R.; Kuppen, P.J.K.; Loewik, C.W.G.M.; Frangioni, J.V.; van de Velde, C.J.H.; Vahrmeijer, A.L. The clinical use of indocyanine green as a near-infrared fluorescent contrast agent for image-guided oncologic surgery. *J. Surg. Oncol.* **2011**, *104*, 323–332. [[CrossRef](#)] [[PubMed](#)]
3. Alander, J.T.; Kaartinen, I.; Laakso, A.; Patila, T.; Spillmann, T.; Tuchin, V.V.; Venermo, M.; Valisuo, P. A review of indocyanine green fluorescent imaging in surgery. *Int. J. Biomed. Imaging* **2012**, *2012*. [[CrossRef](#)] [[PubMed](#)]
4. Nagahara, R.; Onda, N.; Yamashita, S.; Kojima, M.; Inohana, M.; Eguchi, A.; Nakamura, M.; Matsumoto, S.; Yoshida, T.; Shibutani, M. Fluorescence tumor imaging by i.v. administered indocyanine green in a mouse model of colitis-associated colon cancer. *Cancer Sci.* **2018**, *109*, 1638–1647. [[CrossRef](#)] [[PubMed](#)]
5. Luo, S.; Zhang, E.; Su, Y.; Cheng, T.; Shi, C. A review of NIR dyes in cancer targeting and imaging. *Biomaterials* **2011**, *32*, 7127–7138. [[CrossRef](#)] [[PubMed](#)]
6. James, N.S.; Chen, Y.; Joshi, P.; Ohulchanskyy, T.Y.; Ethirajan, M.; Henary, M.; Streckowski, L.; Pandey, R.K. Evaluation of polymethine dyes as potential probes for near infrared fluorescence imaging of tumors: Part-1. *Theranostics* **2013**, *3*, 692–702. [[CrossRef](#)] [[PubMed](#)]
7. Yang, X.; Shi, C.; Tong, R.; Qian, W.; Zhau, H.E.; Wang, R.; Zhu, G.; Cheng, J.; Yang, V.W.; Cheng, T.; et al. Near IR heptamethine cyanine dye-mediated cancer imaging. *Clin. Cancer Res.* **2010**, *16*, 2833–2844. [[CrossRef](#)] [[PubMed](#)]
8. Henary, M.; Pannu, V.; Owens, E.A.; Aneja, R. Near infrared active heptacyanine dyes with unique cancer-imaging and cytotoxic properties. *Bioorg. Med. Chem. Lett.* **2012**, *22*, 1242–1246. [[CrossRef](#)] [[PubMed](#)]
9. Yuan, J.; Yi, X.; Yan, F.; Wang, F.; Qin, W.; Wu, G.; Yang, X.; Shao, C.; Chung, L.W.K. Near-infrared fluorescence imaging of prostate cancer using heptamethine carbocyanine dyes. *Mol. Med. Rep.* **2015**, *11*, 821–828. [[CrossRef](#)] [[PubMed](#)]
10. Zhao, N.; Zhang, C.; Zhao, Y.; Bai, B.; An, J.; Zhang, H.; Shi, C.; Wu Jason, B. Optical imaging of gastric cancer with near-infrared heptamethine carbocyanine fluorescence dyes. *Oncotarget* **2016**, *7*, 57277–57289. [[CrossRef](#)] [[PubMed](#)]
11. Yang, X.; Shao, C.; Wang, R.; Chu, C.-Y.; Hu, P.; Master, V.; Osunkoya, A.O.; Kim, H.L.; Zhau, H.E.; Chung, L.W.K. Optical imaging of kidney cancer with novel near infrared heptamethine carbocyanine fluorescent dyes. *J. Urol.* **2013**, *189*, 702–710. [[CrossRef](#)] [[PubMed](#)]

12. Zhang, C.; Zhao, Y.; Zhang, H.; Chen, X.; Zhao, N.; Tan, D.; Zhang, H.; Shi, C. The application of heptamethine cyanine Dye DZ-1 and indocyanine green for imaging and targeting in xenograft models of hepatocellular carcinoma. *Int. J. Mol. Sci.* **2017**, *18*, 1332. [[CrossRef](#)] [[PubMed](#)]
13. Wu, J.B.; Lin, T.-P.; Gallagher, J.D.; Kushal, S.; Chung, L.W.K.; Zhau, H.E.; Olenyuk, B.Z.; Shih, J.C. Monoamine oxidase a inhibitor-near-infrared dye conjugate reduces prostate tumor growth. *J. Am. Chem. Soc.* **2015**, *137*, 2366–2374. [[CrossRef](#)] [[PubMed](#)]
14. Wu, J.B.; Shi, C.; Chu, G.C.-Y.; Xu, Q.; Zhang, Y.; Li, Q.; Yu, J.S.; Zhau, H.E.; Chung, L.W.K. Near-infrared fluorescence heptamethine carbocyanine dyes mediate imaging and targeted drug delivery for human brain tumor. *Biomaterials* **2015**, *67*, 1–10. [[CrossRef](#)] [[PubMed](#)]
15. Guan, Y.; Zhang, Y.; Xiao, L.; Li, J.; Wang, J.-P.; Chordia, M.D.; Liu, Z.-Q.; Chung, L.W.K.; Yue, W.; Pan, D. Improving therapeutic potential of farnesylthiosalicylic acid: Tumor specific delivery via conjugation with heptamethine cyanine dye. *Mol. Pharm.* **2017**, *14*, 1–13. [[CrossRef](#)] [[PubMed](#)]
16. Lv, Q.; Yang, X.; Wang, M.; Yang, J.; Qin, Z.; Kan, Q.; Zhang, H.; Wang, Y.; Wang, D.; He, Z. Mitochondria-targeted prostate cancer therapy using a near-infrared fluorescence dye-monoamine oxidase A inhibitor conjugate. *J. Control. Release* **2018**, *279*, 234–242. [[CrossRef](#)] [[PubMed](#)]
17. Streckowski, L.; Lipowska, M.; Patonay, G. Facile derivatizations of heptamethine cyanine dyes. *Synth. Commun.* **1992**, *22*, 2593–2598. [[CrossRef](#)]
18. Streckowski, L.; Lipowska, M.; Patonay, G. Substitution reactions of a nucleofugal group in heptamethine cyanine dyes. Synthesis of an isothiocyanato derivative for labeling of proteins with a near-infrared chromophore. *J. Org. Chem.* **1992**, *57*, 4578–4580. [[CrossRef](#)]
19. Cha, J.; Nani, R.R.; Luciano, M.P.; Broch, A.; Kim, K.; Namgoong, J.-M.; Kulkarni, R.A.; Meier, J.L.; Kim, P.; Schnermann, M.J. A chemically stable fluorescent marker of the ureter. *Bioorg. Med. Chem. Lett.* **2018**, *28*, 2741–2745. [[CrossRef](#)] [[PubMed](#)]
20. Nani, R.R.; Shaum, J.B.; Gorka, A.P.; Schnermann, M.J. Electrophile-integrating smiles rearrangement provides previously inaccessible C4'-O-alkyl heptamethine cyanine fluorophores. *Org. Lett.* **2015**, *17*, 302–305. [[CrossRef](#)] [[PubMed](#)]
21. Samanta, A.; Vendrell, M.; Das, R.; Chang, Y.T. Development of photostable near-infrared cyanine dyes. *Chem. Commun. (Camb)* **2010**, *46*, 7406–7408. [[CrossRef](#)] [[PubMed](#)]
22. Das, R.K.; Samanta, A.; Ha, H.H.; Chang, Y.T. Solid phase synthesis of ultra-photostable cyanine NIR dye library. *RSC Adv.* **2011**, *1*, 573–575. [[CrossRef](#)]
23. Pascal, S.; Haelele, A.; Monnerneau, C.; Charaf-Eddin, A.; Jacquemin, D.; Le Guennic, B.; Andraud, C.; Maury, O. Expanding the polymethine paradigm: Evidence for the contribution of a bis-dipolar electronic structure. *J. Phys. Chem. A* **2014**, *118*, 4038–4047. [[CrossRef](#)] [[PubMed](#)]
24. Guo, Z.; Zhu, W.; Zhu, M.; Wu, X.; Tian, H. Near-infrared cell-permeable Hg<sup>2+</sup>-selective ratiometric fluorescent chemodosimeters and fast indicator paper for MeHg<sup>+</sup> based on tricarbocyanines. *Chem. Eur. J.* **2010**, *16*, 14424–14432. [[CrossRef](#)] [[PubMed](#)]
25. Njiojob, C.N.; Owens, E.A.; Narayana, L.; Hyun, H.; Choi, H.S.; Henary, M. Tailored near-infrared contrast agents for image guided surgery. *J. Med. Chem.* **2015**, *58*, 2845–2854. [[CrossRef](#)] [[PubMed](#)]
26. Peng, X.; Song, F.; Lu, E.; Wang, Y.; Zhou, W.; Fan, J.; Gao, Y. Heptamethine cyanine dyes with a large Stokes shift and strong fluorescence: A paradigm for excited-state intramolecular charge transfer. *J. Am. Chem. Soc.* **2005**, *127*, 4170–4171. [[CrossRef](#)] [[PubMed](#)]
27. Warnecke, A.; Fichtner, I.; Garmann, D.; Jaehde, U.; Kratz, F. Synthesis and biological activity of water-soluble maleimide derivatives of the anticancer drug carboplatin designed as albumin-binding prodrugs. *Bioconjugate Chem.* **2004**, *15*, 1349–1359. [[CrossRef](#)] [[PubMed](#)]
28. Nanda, J.S.; Lorsch, J.R. Labeling of a protein with fluorophores using maleimide derivitization. In *Methods Enzymol.*; Lorsch, J.R., Ed.; Elsevier: San Diego, CA, USA, 2014; Volume 536, pp. 79–86.
29. Walden, H.; Podgorski, M.S.; Huang, D.T.; Miller, D.W.; Howard, R.J.; Minor, D.L., Jr.; Holton, J.M.; Schulman, B.A. The structure of the APPBP1-UBA3-NEDD8-ATP complex reveals the basis for selective ubiquitin-like protein activation by an E1. *Mol. Cell* **2003**, *12*, 1427–1437. [[CrossRef](#)]
30. Huang, D.T.; Miller, D.W.; Mathew, R.; Cassell, R.; Holton, J.M.; Roussel, M.F.; Schulman, B.A. A unique E1-E2 interaction required for optimal conjugation of the ubiquitin-like protein NEDD8. *Nat. Struct. Mol. Biol.* **2004**, *11*, 927–935. [[CrossRef](#)] [[PubMed](#)]

31. Cunningham, D.; Danley, D.E.; Geoghegan, K.F.; Griffor, M.C.; Hawkins, J.L.; Subashi, T.A.; Varghese, A.H.; Ammirati, M.J.; Culp, J.S.; Hoth, L.R.; et al. Structural and biophysical studies of PCSK9 and its mutants linked to familial hypercholesterolemia. *Nat. Struct. Mol. Biol.* **2007**, *14*, 413–419. [[CrossRef](#)] [[PubMed](#)]
32. Llinas, P.; Le Du, M.H.; Gardsvoll, H.; Dano, K.; Ploug, M.; Gilquin, B.; Stura, E.A.; Menez, A. Crystal structure of the human urokinase plasminogen activator receptor bound to an antagonist peptide. *Embo J.* **2005**, *24*, 1655–1663. [[CrossRef](#)] [[PubMed](#)]
33. Ogiso, H.; Ishitani, R.; Nureki, O.; Fukai, S.; Yamanaka, M.; Kim, J.-H.; Saito, K.; Sakamoto, A.; Inoue, M.; Shirouzu, M.; et al. Crystal structure of the complex of human epidermal growth factor and receptor extracellular domains. *Cell* **2002**, *110*, 775–787. [[CrossRef](#)]
34. Usama, S.M.; Thavornpradit, S.; Burgess, K. Optimized Heptamethine Cyanines for Photodynamic Therapy. *ACS Appl. Bio Mater.* **2018**, *1*, 1195–1205. [[CrossRef](#)]
35. Usama, S.M.; Lin, C.-M.; Burgess, K. On the mechanisms of uptake of tumor-seeking cyanine dyes. *Bioconjugate Chem.* **2018**. [[CrossRef](#)] [[PubMed](#)]
36. Sato, K.; Gorka, A.P.; Nagaya, T.; Michie, M.S.; Nakamura, Y.; Nani, R.R.; Coble, V.L.; Vasalatiy, O.V.; Swenson, R.E.; Choyke, P.L.; et al. Effect of charge localization on the in vivo optical imaging properties of near-infrared cyanine dye/monoclonal antibody conjugates. *Mol. Biosyst.* **2016**, *12*, 3046–3056. [[CrossRef](#)] [[PubMed](#)]
37. Nani, R.R.; Gorka, A.P.; Nagaya, T.; Kobayashi, H.; Schnermann, M.J. Near-IR light-mediated cleavage of antibody-drug conjugates using cyanine photocages. *Angew. Chem. Int. Ed.* **2015**, *54*, 13635–13638. [[CrossRef](#)] [[PubMed](#)]

**Sample Availability:** Samples of the compounds **1a–d** are available from the authors.



© 2018 by the authors. Licensee MDPI, Basel, Switzerland. This article is an open access article distributed under the terms and conditions of the Creative Commons Attribution (CC BY) license (<http://creativecommons.org/licenses/by/4.0/>).

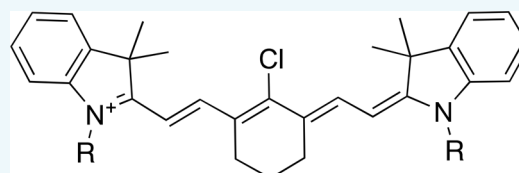
# On the Mechanisms of Uptake of Tumor-Seeking Cyanine Dyes

Syed Muhammad Usama,<sup>1</sup> Chen-Ming Lin, and Kevin Burgess<sup>1\*</sup>

Department of Chemistry, Texas A&M University, Box 30012, College Station, Texas 77842, United States

## S Supporting Information

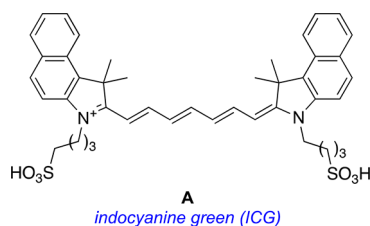
**ABSTRACT:** Molecular entities that localize in tumor tissue are clinically important for targeted delivery of diagnostic, imaging, and therapeutic reagents. Often these targeting entities are designed for specific receptors (e.g., EGFR or integrin receptors). However, there is a subset of cyanine-7 dyes that apparently localize in every type of solid tumor tissue (at least, no exceptions have been reported so far), and they persist there for several days. Consequently, these dyes can be used for near-IR optical imaging of tumors in animal studies, they can be conjugated with cytotoxic species to give experimental theranostics, and there is potential for expanding their use into the development of clinically useful derivatives. Data presented in the literature and in this work indicate that the half-lives of these compounds in serum at 37 °C is on the order of minutes to a few hours, so what accounts for the persistent fluorescence of these dyes in tumor tissue over periods of several days? Literature, solely based on tissue culture experiments featuring a particular receptor blocker, indicates that uptake of these dyes is mediated by the organic anion transporter proteins (OATPs). Data presented in this paper agrees with that conclusion for short-term uptake, but significantly expands understanding of the likely reasons for long-term uptake and persistent tumor localization *in vivo*.



“tumor-seeking” near-IR dyes  
half life in serum: minutes to hours  
*in vivo* tumor fluorescence: several days  
what accounts for the difference?

## INTRODUCTION

Indocyanine green (ICG, **A**), a heptamethine cyanine or “Cy-7” dye, is the only near-IR FDA-approved optical marker for clinical use.<sup>1,2</sup> ICG is used in surgical procedures because of its favorable safety profile,<sup>3–5</sup> and because it is fluorescent with an absorbance maximum around 750 nm. Below 750 nm, excitation of dyes obscured by more than a few millimeters of tissue becomes impractical with even the highest laser powers acceptable in surgical settings. To calibrate, penetration of light of wavelength 800 nm is twice that of light of 630 nm.<sup>6</sup>



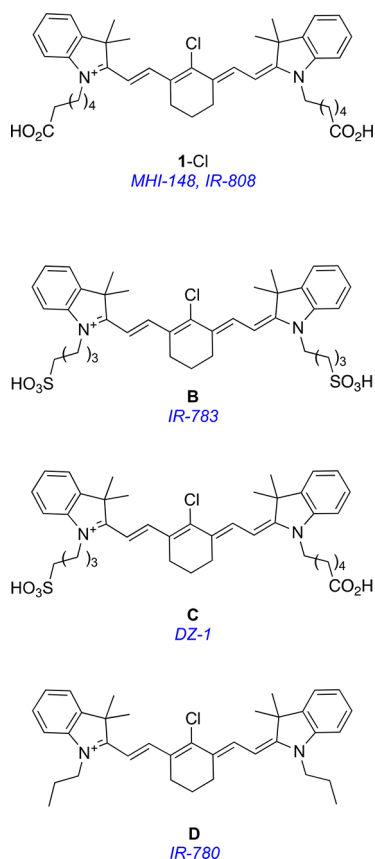
Fluor **A** can be used in surgery, but it is not disposed of especially accumulate in cancer tissue. In fact, ICG collects in the liver and gastrointestinal tract, and tends to mostly wash out of the body within a few hours.<sup>7</sup> However, at least in animal models, other heptamethine cyanine dyes like **1-Cl** and **B–D** do accumulate in solid tumors (e.g., prostate,<sup>8</sup> gastric,<sup>9</sup> kidney,<sup>10</sup> hepatocytes,<sup>11,12</sup> lung cancer,<sup>13</sup> and glioblastoma<sup>14</sup>) but not in normal cells and tissue.<sup>15–19</sup> Moreover, fluor **B–D** tend to persist in those tumors; they can still be observed there after 1–2 days. There is an enormous amount of literature on antibody–drug conjugates (illustrative reviews<sup>20,21</sup>), and a growing volume

on small molecules that target tumor tissue conjugated to cytotoxic species (illustrative reviews<sup>22,23</sup>). Consequently, the potential importance of near-IR dyes that localize in, apparently, any solid tumor is immense; they can be used for *in vivo* experiments,<sup>24</sup> have the potential in image guided surgery,<sup>2</sup> and can be conjugated to cytotoxic substances for theranostic approaches (near-IR imaging and chemotherapy,<sup>25–29</sup> in this case). These tumor seeking near-IR dyes at the very least complement targeted approaches, and in some cases could surpass them.

Many reports (for example<sup>8,10,11,13–16,19,30</sup>) explain the “tumor-seeking” characteristics of fluor **1-Cl** and **B–D** in terms of uptake via the Organic Anion Transporter Proteins (OATPs).<sup>31,32</sup> Hypoxia (common in compressed solid tumors) triggers activation of HIF1 $\alpha$ , and promotes OATPs overexpression in cancer tissue relative to levels found in normal cells.<sup>9,30</sup> The natural role of OATPs is to mediate influx of organic anions and some neutral materials that are important to cells (e.g., bile salts, steroids, bilirubin, and thyroid hormones). This diversity of substrates means OATPs are not particularly selective and, coincidentally, these receptors also import some drug structures and fluor **1-Cl**, **B–D**.<sup>33–35</sup> To balance this ion influx, OATPs efflux intracellular bicarbonate, glutathione, and glutathione adducts. Consequently, OATPs can promote influx of fluor **1-Cl**, **B–D** into cells, without pumping the same ones out.

A chance discovery in our laboratories led us to question the assumption that import via the OATPs predominantly accounts for the tumor-seeking characteristics of fluor **1-Cl**, **B–D**. In this

Received: October 5, 2018



event, data presented in this paper indicates that OATPs are a mechanism of import in *ex vivo* cellular experiments, but an alternative mechanism accounts for the persistent fluorescence of tumors in animal experiments featuring fluors of this category.

## RESULTS AND DISCUSSION

**Observation of a Fluorescent Protein in Cell Lysates after Treatment with Fluor 1-Cl.** The following is a typical literature procedure for treatment of cancer cells with fluor 1-Cl. The cells (in our case a leukemia line, K562) are suspended in RPMI-1640 medium with 10% FBS added, then seeded to 24-well plates. Various concentrations of 1-Cl in the same medium are added to the cells to give final fluor concentrations of 0–30  $\mu\text{M}$ . After 20 h incubation at 37  $^{\circ}\text{C}$ , the cells are collected, and washed twice with ice-cold PBS buffer.

In a particular experiment in our laboratory, RIPA lysis buffer containing of 1% of a pan protease inhibitor was added to the cells after the procedure outlined above. The cell samples were gently shaken on ice for 30 min, and the lysates were centrifuged to remove cell debris. Supernatants were collected and the protein concentrations were determined using a colorimetric protein assay kit. Equal total protein amounts were electrophoresed under reducing conditions on 15% SDS-PAGE. The gel was washed with deionized water, then analyzed with an imager designed to detect the near IR fluorescence ( $>800\text{ nm}$ ); this gave a conspicuous fluorescent band at over 50 kDa. We were surprised by the selectivity with which this band formed, excited by the prospect of identifying this fluorescent conjugate (Figure 1a), then, later, amused by the result (Figure 1b).

After a few false starts, we hypothesized the pronounced fluorescent band in the gel shown in Figure 1a was derived from bovine serum albumin (BSA) in the FBS medium. Consistent with this assertion, Figure 1b shows the band from the lysate was

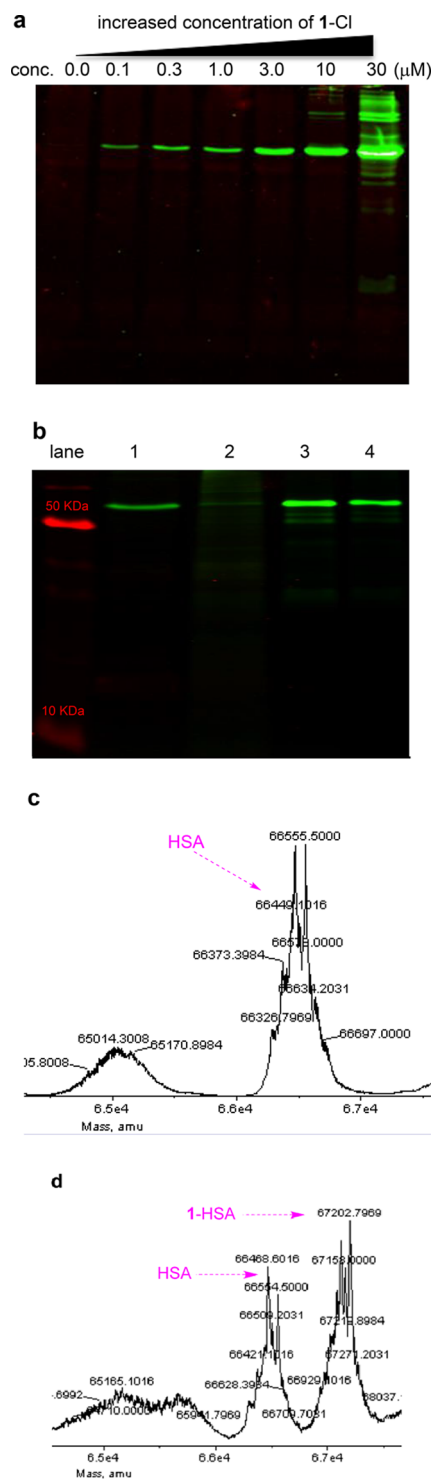


**Figure 1.** (a) NIR-fluorescent gel image ( $>800\text{ nm}$ ) of K562 cell lysate prior treated with different concentrations of 1-Cl for 20 h in RPMI-1640 medium containing 10% FBS. (b) Lane 1, K562 cell lysates treated with 10  $\mu\text{M}$  of 1-Cl as in (a). Lane 2, K562 cell lysates treated with 10  $\mu\text{M}$  of 1-Cl as in (a) except serum-free RPMI-1640 medium was used. Lane 3, 10  $\mu\text{M}$  of 1-Cl incubated with RPMI-1640 medium containing 10% FBS for 20 h as in (a) but without cells. Lane 4, 10  $\mu\text{M}$  of 1-Cl as in (a), except no cells were used and 10  $\mu\text{M}$  BSA was added in their place. Staining the gel with Coomassie Blue G250 showed an equal amount of protein was loaded into each well (Figure S10). Electrospray ionization (ESI) mass spectra of: (c) free HSA; and (d) ESI MS of 1-Cl covalently bound to HSA formed by reacting the two components in a 2.5:1 ratio (1 M HEPES buffer).

not formed when FBS was excluded from the culture medium (lane 2), but it was formed when FBS was present without cells, or when only BSA was added (i.e., no cells and no FBS; lanes 3 and 4, respectively). Albumin concentrations in FBS vary between 20 and 36 mg/mL;<sup>36–38</sup> assuming a conservative mid-range figure of 25 mg/mL BSA in FBS, this corresponds to 38  $\mu$ M. Thus, cellular experiments involving 10  $\mu$ M 1-Cl would have almost a 4-fold excess of BSA (38  $\mu$ M) to react with.

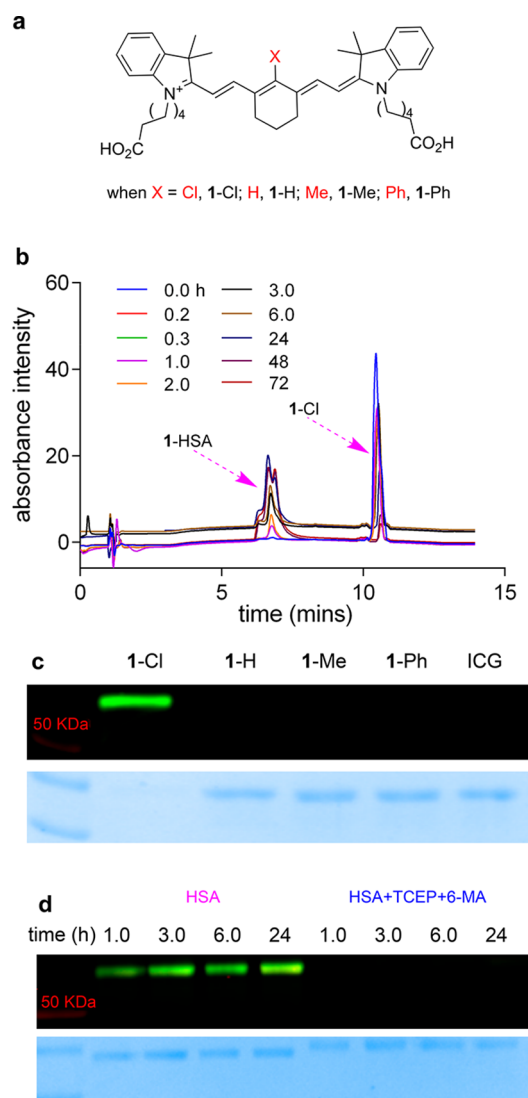


**Figure 2.** (a) Structures of 1-Cl and *meso*-blocked derivatives. (b) Analytical HPLC analyses for reactions of 0.5 mM HSA with 0.2 mM 1-Cl (in 1 M HEPES buffer pH 7.4) at 37 °C. NIR-fluorescent gel image (>800 nm) of (c) HSA (1  $\mu$ M, 1  $\mu$ g) incubated with cyanines 1 (10  $\mu$ M) for 3 h in 50 mM pH 7.4 HEPES buffer, 30 ng of HSA with 1-Cl, and 100 ng of HSA with other derivatives of 1 were loaded into gel; and (d) HSA (15  $\mu$ M, 1  $\mu$ g) and “thiol-blocked HSA” treated with 1-Cl (15  $\mu$ M) for the incubation times indicated.

In a control experiment, human serum albumin (HSA) was reacted with 2.5 equiv of 1-Cl at 37 °C in 1 M HEPES buffer. This 1-Cl:albumin molar ratio was selected because it is approximately that used in cell culture experiments to probe uptake of this dye. Figure 1c shows the ESI mass spectra of HSA, and Figure 1d shows that a product formed when HSA combined with 1-Cl; the molecular mass formed correspond to a 1:1 covalent adduct between 1-Cl (after loss of Cl) and HSA. This is

consistent with the fact that HSA has one free Cys residue (and 34, oxidized, i.e., disulfide-linked, Cys residues).

At this stage we hypothesized that the 1:1 covalent adduct is formed by displacement of the *meso*-Cl from 1-Cl by a nucleophile on HSA, and that nucleophile was probably the free Cys thiol. Three derivatives of 1 (Figure 2a) that had *meso*-functionalities that cannot readily be leaving groups were made and reacted with HSA to test a *meso*-leaving group was required for covalent binding. It emerged that ICG (A), 1-H, 1-Me, and 1-Ph do not react with HSA at 37 °C in aqueous buffer (Figures S4 and S7), under the conditions that 1-Cl does combine with HSA (Figure 2b); in fact, nearly all the 1-Cl is consumed after 72 h.

At this stage it seemed probable that 1-Cl reacts with a free thiol on albumin. To exclude the possibility that other nucleophilic amino acid side-chains might be involved (e.g., Lys, Tyr, Ser) experiments were performed using HSA that was first treated with 6-maleimide-hexanoic acid to selectively block free thiols.<sup>39,40</sup> Unexpectedly, this experiment still gave a fluorescent band, but we concluded that there was some 1-Cl noncovalently bound to albumin, and this became covalently bound after the protein had been reduced for loading onto the gel. To test this assertion the experimental design was modified in the following way. HSA was first completely reduced with tris(2-carboxyethyl)-phosphine (TCEP) to break all its disulfide bonds, and then the product was thiol-blocked using 6-maleimido-hexanoic acid, and finally this sample was treated with 1-Cl. This approach is imperfect because it tests the interaction of 1-Cl with reduced albumin, but it is sufficient to prove that O- and N-based nucleophilic side-chains (specifically those not derived from cysteine) of the reduced protein did not combine with 1-Cl. Thus, binding of free Cys to 1-Cl is implicated in the covalent binding step (Figure 2d).

Noncovalent interactions of the dyes 1 with HSA were also explored. Thus, 10  $\mu$ M solutions of ICG, 1-Cl, 1-H, 1-Me, and 1-Ph were mixed with varied concentrations of HSA and the interaction was followed by UV spectroscopy. Absorbance saturation was observed for 1-Cl at a 1:1 ratio with HSA, but for the other compounds, none of which have a leaving group at the *meso*-position, saturation was achieved at around 1.5 equiv of HSA (Figures S5 and S6).

**Uptake of Fluor 1-Cl and 1-HSA into Cells.** Figure 2b indicates that albumin and 1-Cl at approximately the ratio typically used in cell culture experiments (2.5:1.0, see above) react over time periods that are similar to the span of a typical cell culture experiment. Consequently, we set out to test first where the fluorescent signal localizes in cells if albumin is excluded from the medium, then to determine if 1-HSA is imported and, if so, where it localizes.

Figure 3 shows confocal images for uptake of 1-Cl into a human glioblastoma cell line (U87-MG) cultured in a medium without albumin. Under these conditions, the dye was imported into the cells after 30 min incubation, and localized in the mitochondria.

Figure 4 are data from a set of experiments nearly identical to those in Figure 3, except featuring preformed 1-HSA (i.e. not 1-Cl), also in medium not containing albumin. At 30 min of incubation, it was clear that 1-HSA was also imported into the cells, but this adduct preferentially localizes in the lysosome and Golgi, i.e., different organelles to 1-Cl.

Data in Figure 3 should be compared with literature reports describing import of 1-Cl, but in medium containing albumin, into various cells. For instance, the following cell lines have been tested, and localization was observed in the mitochondria: human cervical cancer cell line (HeLa) and Lewis lung carcinoma (LLC), rat transformed mesenchymal stem cells (rTDMCs).<sup>19</sup> In our

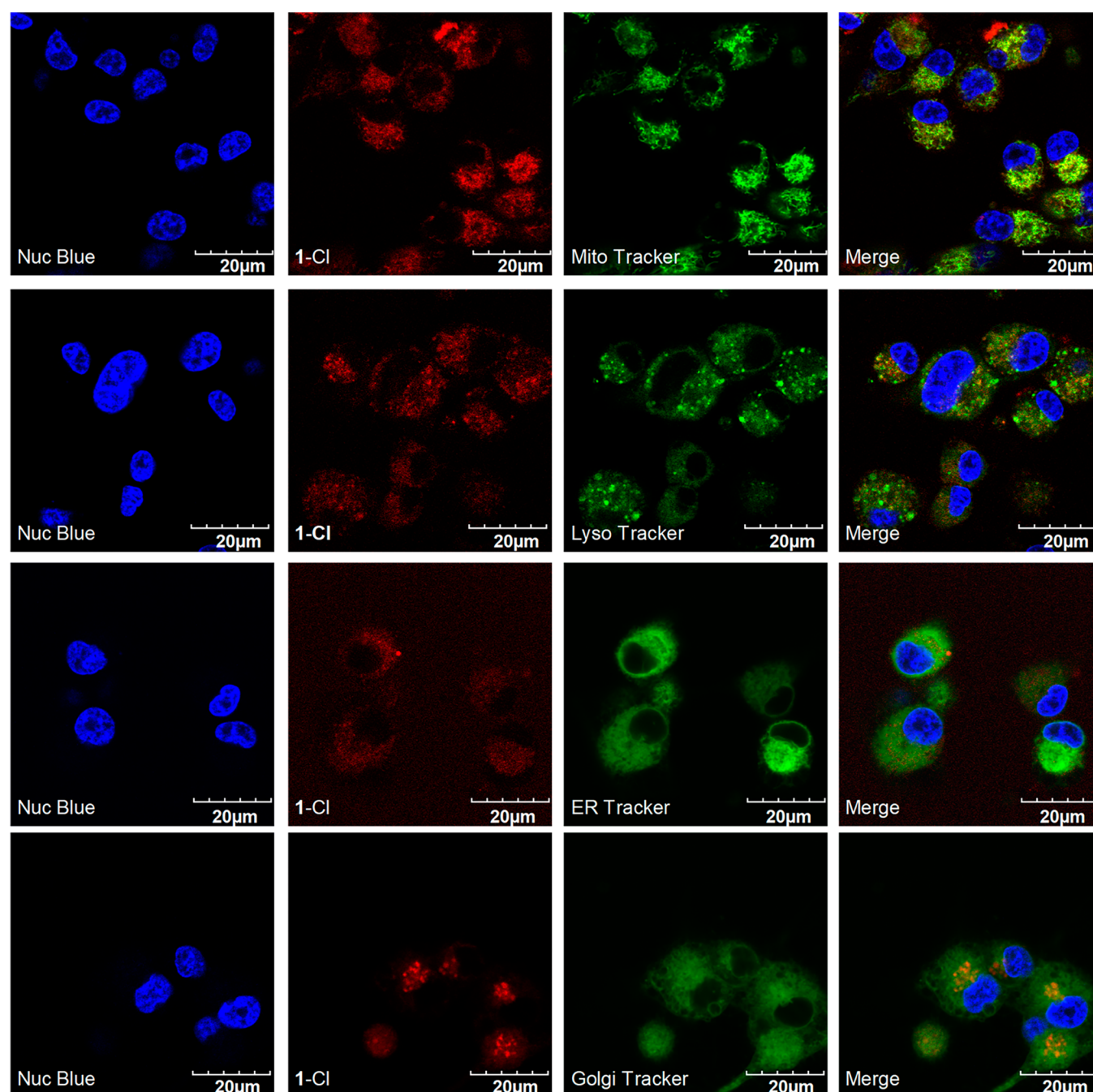


**Figure 3.** Uptake of **1-Cl** ( $20\ \mu\text{M}$ ) into U87-MG cells incubated in serum free medium for 30 min. Colocalization with trackers for mitochondria, lysosome, ER, and Golgi are featured. Images were taken using Olympus confocal microscope at  $60\times/1.2$  water immerse objective after 30 min of incubation. Most colocalization was seen with the mitochondria.

laboratory we also investigated uptake of **1-Cl** but, unlike in our experiments described above, in media containing albumin, into U87 glioblastoma cells and found fluorescence was observed mostly in the mitochondria; consequently, the absence of albumin in the experiments described above did not somehow change the localization.

As far as we are aware, without exception, the evidence for OATPs mediated uptake of **1-Cl** in tissue culture is based on the same experimental format. Briefly, cells are allowed to attach to imaging chamber overnight in a medium containing BSA at  $37\ ^\circ\text{C}$ , **1-Cl** is added in the same medium, and after 30 min at  $37\ ^\circ\text{C}$  the cells are collected, and washed twice with ice-cold PBS buffer. Microscopy is then used to qualitatively monitor the uptake.

This protocol is performed side-by-side with two similar experiments but where the medium contains the pan-OATP inhibitor BSP (bromosulphophthalein),<sup>41</sup> or in which the cells were treated with an agent to induce hypoxia (DMOG, dimethyloxallylglycine<sup>42,43</sup>). Under these conditions, BSP suppresses the fluorescence observed in the cells (presumably by inhibiting OATP-mediated uptake), whereas under hypoxic conditions for which OATPs are overexpressed, the fluorescence uptake was increased. We were intrigued to explore how **1-HSA** would behave under these conditions because the data above indicates that at least partial conversion of **1-Cl** to **1-HSA** occurs in these types of cellular experiments featuring albumin in the medium. These experiments would reveal if **1-HSA** was

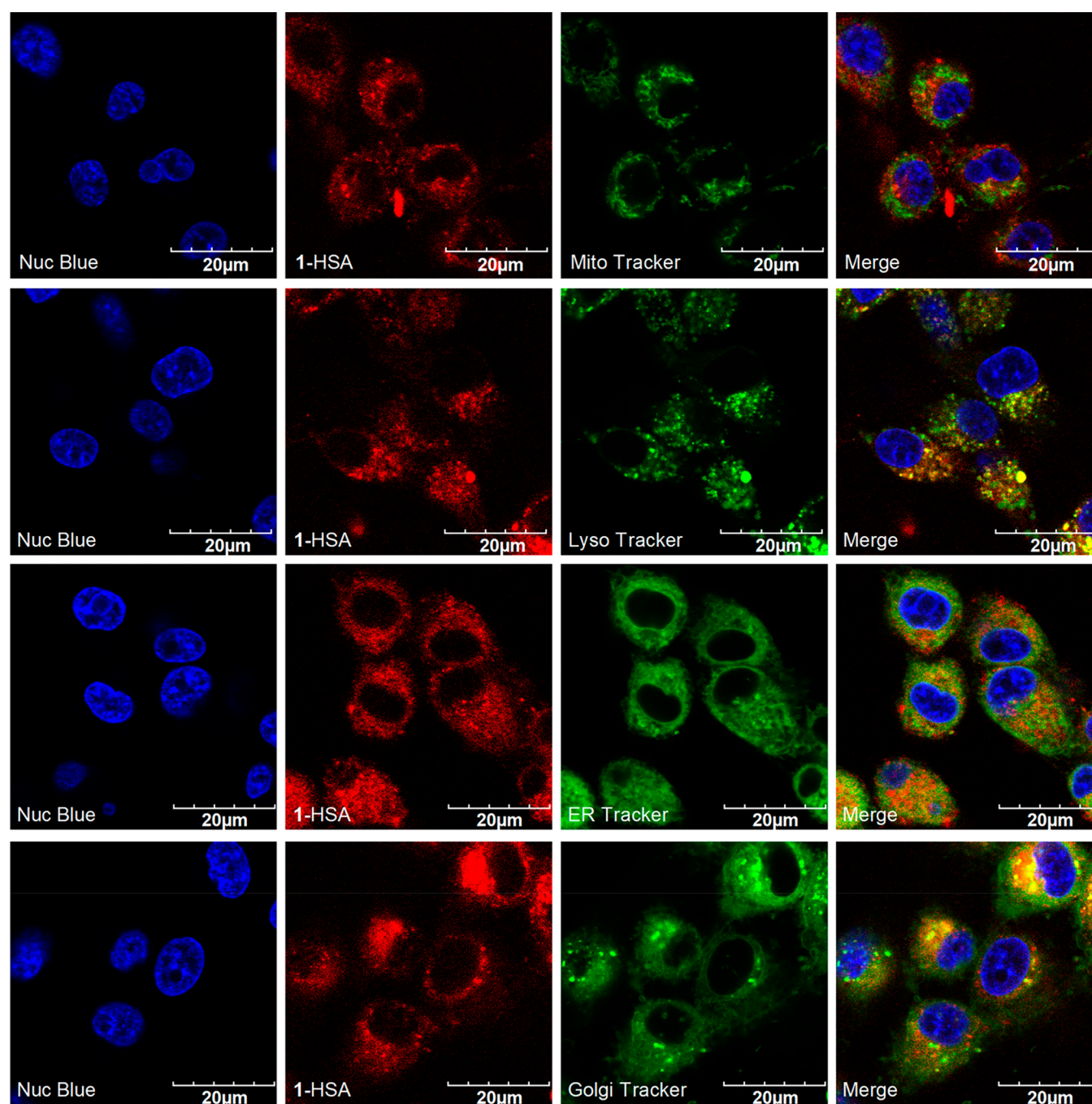


**Figure 4.** Uptake of 1-HSA (20  $\mu$ M) into U87-MG cells incubated in serum free medium. Colocalization with trackers for mitochondria, lysosome, ER, and Golgi was featured. Images were taken using Olympus confocal microscope at 60 $\times$ /1.2 water immersion objective after 30 min of incubation. Most colocalization was seen with lysosome and Golgi.

imported into the cells and, if so, how its uptake responds to the pan-OATP inhibitor, BSP.

Data in Figure 5 shows that 1-HSA is imported into the glioblastoma cells (first row). Import of 1-HSA is conspicuously *increased* when the cells are pretreated with pan-OATP inhibitor, BSP. Hypoxic and normoxic cells import about the same amount of fluorescence from 1-HSA (rows 3 and 1), but cooling the cells to retard active transport mechanisms also diminishes uptake of fluorescence from 1-HSA. Whereas 1-Cl uptake in the cell was enhanced in hypoxia condition but reduced in the presence of BSP or at low temperatures, implying the uptake was dependent on active transport via OATPs (Figure S8). Collectively these

data show uptake of 1-HSA is enhanced by active transport mechanisms, but not via the OATPs. Figure S9 shows data from similar experiments that show 1-HSA uptake was (i) not inhibited by an inhibitor of clathrin mediated endocytosis (PitStop2),<sup>44</sup> but was by (ii) a micropinocytosis inhibitor (amiloride)<sup>45</sup> and (iii) an inhibitor of lipid raft endocytosis ( $M\beta$ CD).<sup>46</sup>

Albumin (Figure 6; from PDB 1AO6) has 14 disulfide bonds and one unique, free cysteine residue, Cys34. It is present in high concentrations in the blood where it acts as a carrier for small molecules, many of which noncovalently bind one of the two binding sites indicated. Consequently, electrophilic small molecules might react with Cys34 directly, or possibly associate with

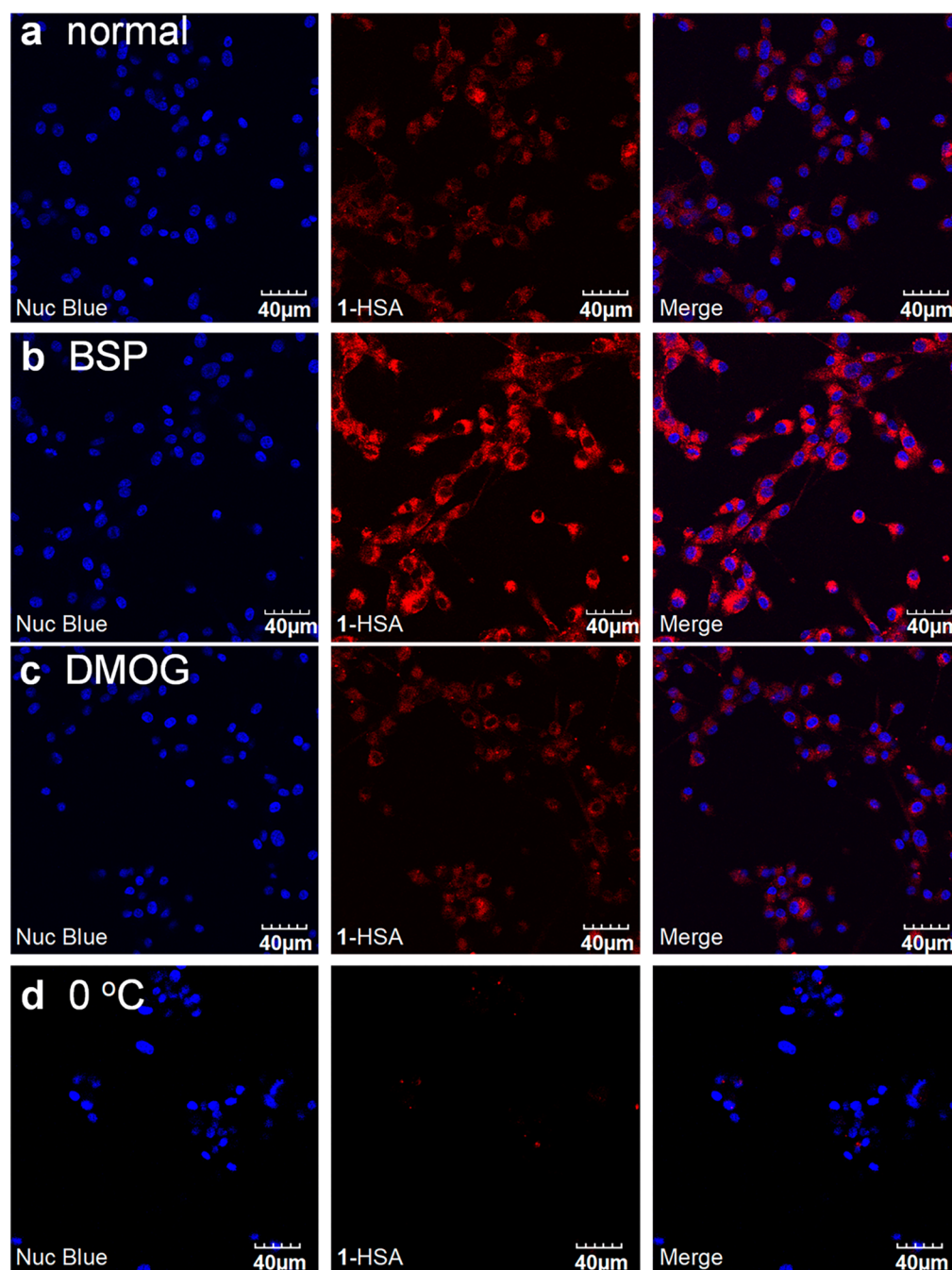


**Figure 5.** Experiments to test uptake of 1-HSA (20  $\mu$ M) into U87-MG cells (grown in DMEM medium supplemented with 10% FBS, i.e., containing approximately 0.038 mM BSA). (a) Without any blocking agents or abnormal conditions; (b) pretreated with 250  $\mu$ M BSP to block OATPs for 10 min; (c) after the cells were pretreated with 1 mM DMOG for 24 h to induce hypoxia; and (d) when the cells were maintained at 0  $^{\circ}$ C for 30 min to retard active transport. All images were collected using a Olympus confocal microscope at 20 $\times$  magnification.

one of the binding sites, then be relayed to that free thiol. Albumin is known to be imported into cells via several mechanisms<sup>47</sup> and particularly into cancer cells<sup>48,49</sup> though, to the best of our knowledge, those mechanisms do not include OATP-mediated pathways.

Both noncovalent and covalent binding to albumin have dramatic effects on the pharmacokinetics of small molecules.<sup>50,51</sup> Some small molecule drugs associate with albumin;<sup>52</sup> this can be problematic if they are not released, but in other situations it is an advantage due to the prolonged half-life of the compound in the blood. Small molecules also have been covalently bound to albumin via Cys34 to improve their pharmacokinetics.<sup>47</sup> This is

frequently achieved by attaching a maleimide functionality to the small molecule and either reacting it with HSA<sup>53,54</sup> or simply allowing the drug to combine with HSA *in situ* in a novel prodrug approach.<sup>55–59</sup> Albumin itself has been estimated to have a turnover rate of over 20 days in humans,<sup>60</sup> so it seems likely that most covalent small molecule-to-albumin adducts would be long-lived *in vivo*.

Albumin is the most abundant protein in the blood, being present at around 35–50 g/L or 0.53–0.73 mM (human and mouse). We estimate (see [Supporting Information](#)) that by injecting 1-Cl into a 25 g mouse at 10 mg/kg (a typical dose in an *in vivo* experiment featuring this dye), the initial concentration in the blood

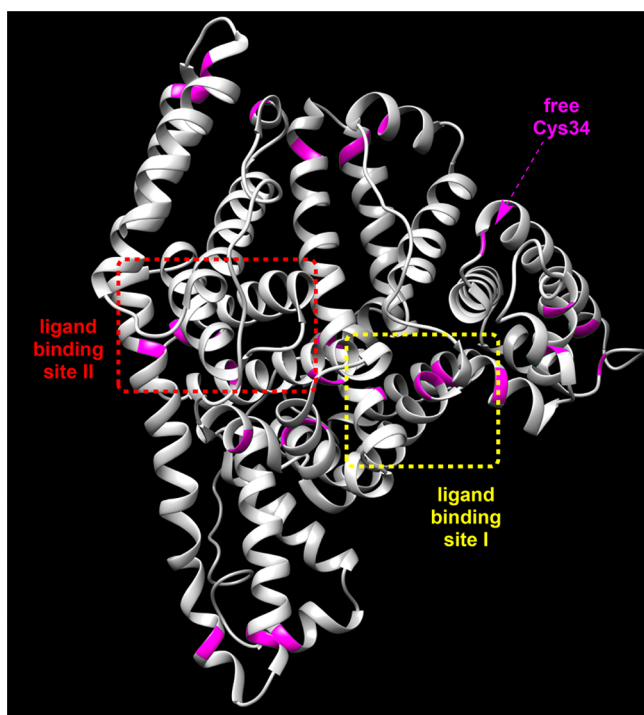


**Figure 6.** HSA structure from PDB 1AO6. Figure S1 depicts the HSA with different helical structures and binding domains whereas Figures S2–S4 show diagrams emphasizing cysteine 34 pointing outside in the solvent.

would also be in the same range,  $\sim 0.53$  mM. After the injection, clearance mechanisms would rapidly decrease the amount of free 1-Cl in the blood; consequently, excess albumin is always present. Our data indicates that 1-Cl would be converted to 1-HSA (and presumably to lesser amounts of adducts with other serum proteins like LDL) reasonably quickly.

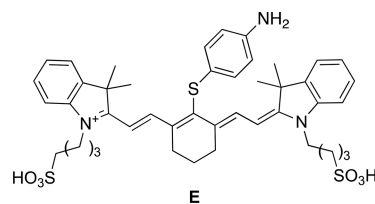
There does not appear to be published *in vivo* work on the lifetime of 1-Cl in the blood, but a very careful study of derivative E has reported the half-life of this compound in mice to be 36 min. Formation of covalent adducts to albumin and other serum proteins with free thiols<sup>61</sup> must account, at least in part, for the rapidly decreasing 1-Cl concentration in the blood in that study. Assuming the same half-life for 1-Cl, and considering that the blood circulates in about 1 min, it is reasonable to conclude that some 1-Cl does enter cancer cells *in vivo* shortly after administration i.v. However, once inside the cells then 1-Cl encounters high concentrations of other nucleophilic thiols, notably, glutathione. In unpublished work, performed in parallel to this, we have also proved that 1-Cl has a similar reactivity toward Cys as to albumin, so it seems likely that this chloride would be short-lived inside cells. However, the fluorescence observed inside tumors *in vivo* persists for days.<sup>10,15,27</sup>

## CONCLUSIONS

The observations outlined above explains why heptamethine cyanine dyes with a *meso*-chloride tend to be much longer-lived in tumors than Cy-7 derivatives without a *meso*-chloride, e.g., ICG.<sup>24</sup> Thus, the weight of the evidence points to short-term ( $\sim 30$  min) accumulation of 1-Cl in cancer tissue *in vivo*, but, after this, transformation into covalent adducts with biomolecules possessing free thiols, particularly including serum proteins in the blood. Albumin adducts would be especially favored, because of the abundance of the high blood concentrations of this protein. This

accounts for persistent fluorescence from cancer tissue *in vivo* after injection of 1-Cl. Various factors might contribute to persistent localization of covalent adducts formed *in situ*, e.g., 1-albumin, including slow efflux, and the EPR effect.

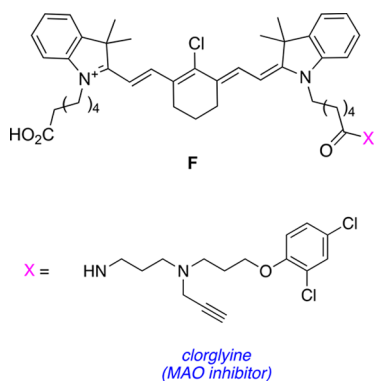
The data interpretation outlined above is consistent with many observations in the literature. Our assertion that 1-Cl and similar Cy7 dyes with *meso*-chlorines (e.g., B–D) probably have parallel pharmacokinetics is consistent with observations that describe these types of fluors being retained in tumor tissues (e.g., kidney, brain, breast, and liver) for many days (e.g., 5–20 d),<sup>10–12,16,26</sup> in fact, for periods that are comparable with the half-life albumin *in vivo* (20 d). Conversely, ICG (no *meso*-chlorine) is cleared *in vivo* in  $<24$  h,<sup>11,12,16</sup> and a direct analog of 1, but substituted at the *meso* position, i.e., E, was observed not be retained in an embedded prostate tumor.<sup>15</sup> We thank a referee for pointing out that another group has observed an immediate UV  $\lambda_{\max}$  red-shift for 1-Cl when added to albumin *in vitro*, followed by a gradual blue-shift to another  $\lambda_{\max}$  after 1.5 h.<sup>62</sup> Those researchers did not attempt to explain that observation, but it is easily interpreted in light of our work. We suggest under those conditions 1-Cl rapidly forms a non-covalent adduct with albumin, that is slowly transformed into a covalent one.



Increased uptake of 1-HSA by the pan-OATP inhibitor BSP (Figure 5) surprised us, but, in retrospect, perhaps it should not have. BSP is a venerable, old small molecule that rose to fame as a probe for testing liver function; it binds albumin<sup>63</sup> as well as inhibiting OATPs.<sup>64</sup> In fact, molecules like this tend to bind lots of proteins nonselectively, so much that they are described by some as a PAIN (Pan Assay Interference compound).<sup>65</sup> BSP is an inexpensive and convenient probe for testing inhibition of OATPs, and in many cases it may be the only logistically feasible option to do so. However, BSP has limitations associated with its interactions with other receptors on cells, and proteins in tissue culture medium, and data from cell uptake experiments using this probe should not be over-interpreted.

Small molecules attached to albumin in covalent adducts can be fluorescein derivatives as in the conjugate manufactured by Orpegen Pharma (Heidelberg, Germany) for intraoperative fluorescence staining of brain tumors during surgery.<sup>66,67</sup> Related to this, the prospect of conjugating near-IR dyes to albumin for optical imaging has been described in a patent application,<sup>68</sup> but without the realization that 1-Cl could be combined simply via direct displacement of the *meso*-Cl via Cys34 in that protein. Moreover, there is growing interest in drugs conjugated to 1-Cl<sup>25–27</sup> (like F).<sup>28,29</sup> It is reasonable to assume that these too would combine with albumin *in situ* when injected into the blood; this might be advantageous insofar as it would generate theranostics for optical imaging and therapy with largely predictable, and extended, blood plasma lifetimes *in vivo*.

Data presented here also explains some observations in the literature, and some misconceptions to be avoided. For instance, a recent paper noted exceptionally different photophysical



properties of a dye related to 1-Cl in the presence and absence of albumin;<sup>69</sup> it may be that a covalent adduct is implicated. With regard to pitfalls, there are two quite different ways to go about making drug-adducts with the core of cyanine 1. When peripheral carboxylic acids are used to make amides or esters, e.g., E, then these will accumulate in tumors and persist there for a long time as albumin and similar adducts. However, conjugation of drugs to 1-Cl via displacement of the *meso*-chloride<sup>70</sup> is likely to give products that persist for much shorter times in tumor tissue.

## MATERIALS AND METHODS

**Photophysical Properties.** ICG was bought from Ark Pharm where as human serum albumin (HSA) was bought from Sigma-Aldrich. HSA was stored in  $-20^{\circ}\text{C}$  and fresh 0.5 mM (33 mg in 1 mL) solution was prepared for experiments.

**UV Absorbance with HSA.** 10  $\mu\text{M}$  of 1-Cl, 1-H, 1-Me, 1-Ph, and ICG was dissolved in PBS pH 7.4 and different concentrations of HSA were added and stirred for 90 min in dark. Afterwards, absorbance was determined using a Cary-Varian 100 UV-vis NIR spectrophotometer.

**Kinetics Experiment.** 200  $\mu\text{M}$  of 1-Cl, 1-H, 1-Me, 1-Ph, and ICG was dissolved in 500  $\mu\text{M}$  of PBS pH 7.4 containing HSA. The reaction mixture was kept in incubator at  $37^{\circ}\text{C}$  for up to 72 h and it was observed at different time points using C18 column on Agilent 1200 LC/MS. The detection wavelength was set up at 600 nm to observe ICG, 1-Cl, 1-H, 1-Me, and 1-Ph and their respective conjugate with HSA.

**Mass Spec Analysis.** 200  $\mu\text{M}$  of 1-Cl, 1-H, 1-Me, 1-Ph, and ICG was dissolved in 500  $\mu\text{M}$  of HSA in PBS pH 7.4 for 3 h at  $37^{\circ}\text{C}$  in an incubator set to shake at 90 rpm. Afterward, the mixture was concentrated using 10 kDa (GE Health) cutoff filter and washed thrice with 50 mM ammonium carbonate to replace the solvent.

**In Vitro Assays.** U87-MG cells were grown in Dulbecco's Modified Eagle's medium (DMEM) containing 10% fetal bovine serum (FBS). Cells were grown in an incubator at  $37^{\circ}\text{C}$ , humidified atmosphere containing 5%  $\text{CO}_2$ . Cells were grown in T-75 culture flask until 70% confluency before splitting into next passage.

**Live Cell Staining.** Intracellular localization of dyes with the U87-MG cells was measured using Olympus Fluoview FV1000. The images were taken at  $60\times/1.20$  water immersed objective. Lysosome, Mitochondria, and Nucleus were stained using LysoTracker Green DND 26, Mitotracker Green FM, and NucBlue, respectively, bought from Life Technologies. 488 nm laser was used for green channel, 405 nm laser was used for nucleus, and 633 nm laser was used for compound 1-Cl and 1-HSA.

**Blocking Experiment.** Briefly, 50,000 cells were seeded on 4 well chambers (Nunc Lab-Tek) and allowed to adhere overnight. The cells were incubated with 20  $\mu\text{M}$  of compound 2 for

30 min, washed twice with PBS, and incubated with organelle stains according to manufacturer's instructions. The cells were washed twice again and stained with Nuc Blue for 10 min.

Mode of uptake of 1-Cl and 1-HSA was determined on using Olympus FV1000 confocal microscope at  $20\times/0.75$ . Briefly, cells were either preblocked with 250  $\mu\text{M}$  BSP for 10 min or treated with 1 mM DMOG for 24 h before treating with the dye. After 30 min incubation with 1-Cl and 1-HSA, cells were washed twice with PBS and stained with NucBlue for 10 min and taken for imaging.

For endocytosis inhibitors, cells were starved for 20 h and different routes of endocytosis were blocked using Pitstop (20  $\mu\text{M}$ ), Amiloride (1 mM), and M $\beta$ CD (15  $\mu\text{M}$ ) for 15 min. After 30 min incubation with 1-Cl and 1-HSA, cells were washed twice with PBS and stained with NucBlue for 10 min and were imaged under confocal microscope as mentioned above.

**NIR Gel Image Protocol.** Incubation of 1-Cl with K562 Cells. RPMI-1640 with 10% FBS medium was used for K562 cell suspensions which were seeded to 24-well plates with  $3 \times 10^5$  cells/well (500  $\mu\text{L}$ ). Various concentrations of 1-Cl (20 mM stock in DMSO) were prepared in the same medium and added to 24-well plate containing cells (500  $\mu\text{L}$ /well) to make final concentrations from 0 to 30  $\mu\text{M}$ . After 20 h incubation, the cells were collected, washed twice with ice-cold PBS buffer, and RIPA lysis buffer (60  $\mu\text{L}$ ) containing 1% protease inhibitor was added to each cell sample. Each cell sample was gently shaken on ice for 30 min, and the lysate samples were centrifuged at 19,000 rcf for 25 min at  $4^{\circ}\text{C}$  to remove cell debris. The supernatant was collected and the protein concentration was determined using Pierce BSA protein assay kit (cat. #23225). Equal total protein amounts (30  $\mu\text{g}$ ) were electrophoresed in a 15% SDS-PAGE. The gel was washed with deionized water (10 min  $\times$  3 times), and the gel was analyzed by an Odyssey imager to detect the Near IR fluorescence. The preparation of K562 lysate sample (10  $\mu\text{M}$  of 1-Cl used) from serum free medium is the same except serum free RPMI-1640 medium was used.

**Incubation of 1-Cl, 1-H, 1-Me, and 1-Ph with HSA.** Different cyanines (10  $\mu\text{M}$ ; 20 mM stock in DMSO) were incubated with HSA (1  $\mu\text{M}$ ; 1  $\mu\text{g}$ ) in pH 7.4 HEPES buffer (50 mM) for 3 h at  $37^{\circ}\text{C}$ . 30 ng of 1-HSA and 100 ng of other cyanine-HSA conjugates were treated with reducing condition and loaded into 10% SDS-PAGE for electrophoresis. The gel was washed with deionized water (10 min  $\times$  3 times), and the gel was analyzed by an Odyssey imager to detect the Near IR fluorescence.

**Preparation of Thiol-Blocked HSA.** Using pH 7.4 HEPES buffer (50 mM), thiol-blocked HSA was prepared by reducing disulfide bonds of HSA (15  $\mu\text{M}$ ) with incubation of tris(2-carboxyethyl)phosphine) (TCEP, 1.5 mM, 100-fold) for 2 h at  $25^{\circ}\text{C}$ , and followed by addition and incubation of 6-maleimide-hexanoic acid (6-MA, 6 mM) for another 18 h at  $37^{\circ}\text{C}$ .

## ASSOCIATED CONTENT

### Supporting Information

The Supporting Information is available free of charge on the ACS Publications website at DOI: 10.1021/acs.bioconjchem.8b00708.

Synthesis and characterization of compounds 1-Cl, 1-H, 1-Me, and 1-Ph and supporting figures (PDF)

## AUTHOR INFORMATION

### Corresponding Author

\*E-mail: burgess@tamu.edu.

ORCID 

Syed Muhammad Usama: 0000-0002-7487-1568

Kevin Burgess: 0000-0001-6597-1842

## Notes

The authors declare no competing financial interest.

## ■ ACKNOWLEDGMENTS

We would like to thank Dr. Larry Dangott, Maritess Arancillo, and Zhengyang Jiang at Texas A&M University for their advice and help, particularly Larry who suggested that the mystery fluorescent band in Figure 1a might be associated with albumin. Financial support was provided by a DoD BCRP Breakthrough Award (BC141561), CPRIT (RP170144), The Robert A. Welch Foundation (A-1121), and The National Science Foundation (CHE1608009). The Microscopy and Imaging Center facility used is supported by Texas A&M University. The Olympus FV1000 confocal microscope acquisition was supported by the Office of the Vice President for Research at Texas A&M University.

## ■ REFERENCES

- (1) Gibbs, S. L. (2012) Near infrared fluorescence for image-guided surgery. *Quant Imaging Med. Surg.* 2, 177–187.
- (2) Nagaya, T., Nakamura, A., Choyke, L., and Kobayashi, H. (2017) Fluorescence-Guided Surgery. *Front. Oncol.* 7, 314.
- (3) Frangioni, J. V. (2003) In vivo near-infrared fluorescence imaging. *Curr. Opin. Chem. Biol.* 7, 626–634.
- (4) Gioux, S., Choi, H. S., and Frangioni, J. V. (2010) Image-guided surgery using invisible near-infrared light: fundamentals of clinical translation. *Mol. Imaging* 9, 237–255.
- (5) Vahrmeijer, A. L., Hutteman, M., van der Vorst, J. R., van de Velde, C. J. H., and Frangioni, J. V. (2013) Image-guided cancer surgery using near-infrared fluorescence. *Nat. Rev. Clin. Oncol.* 10, 507–518.
- (6) Ethirajan, M., Chen, Y., Joshi, P., and Pandey, R. K. (2011) The Role of Porphyrin Chemistry in Tumor Imaging and Photodynamic Therapy. *Chem. Soc. Rev.* 40, 340–362.
- (7) Choi, H.-S., Nasr, K., Alyabyev, S., Feith, D., Lee, J.-H., Kim, S.-H., Ashitate, Y., Hyun, H., Patonay, G., Strekowski, L., et al. (2011) Synthesis and In Vivo Fate of Zwitterionic Near-Infrared Fluorophores. *Angew. Chem., Int. Ed.* 50, 6258–6263.
- (8) Yuan, J., Yi, X., Yan, F., Wang, F., Qin, W., Wu, G., Yang, X., Shao, C., and Chung, L. W. K. (2015) Near-Infrared Fluorescence Imaging of Prostate Cancer Using Heptamethine Carbocyanine Dyes. *Mol. Med. Rep.* 11, 821–828.
- (9) Zhao, N., Zhang, C., Zhao, Y., Bai, B., An, J., Zhang, H., Shi, C., and Wu, Jason, B. (2016) Optical Imaging of Gastric Cancer With Near-Infrared Heptamethine Carbocyanine Fluorescence Dyes. *Oncotarget* 7, 57277–57289.
- (10) Yang, X., Shao, C., Wang, R., Chu, C.-Y., Hu, P., Master, V., Osunkoya, A. O., Kim, H. L., Zhau, H. E., and Chung, L. W. K. (2013) Optical Imaging of Kidney Cancer with Novel Near Infrared Heptamethine Carbocyanine Fluorescent Dyes. *J. Urol.* 189, 702–710.
- (11) An, J., Zhao, N., Zhang, C., Zhao, Y., Tan, D., Zhao, Y., Bai, B., Zhang, H., Shi, C., An, J., et al. (2017) Heptamethine Carbocyanine DZ-1 Dye for Near-Infrared Fluorescence Imaging of Hepatocellular Carcinoma. *Oncotarget* 8, 56880–56892.
- (12) Zhang, C., Zhao, Y., Zhang, H., Chen, X., Zhao, N., Tan, D., Zhang, H., and Shi, C. (2017) The Application of Heptamethine Cyanine Dye DZ-1 and Indocyanine Green for Imaging and Targeting in Xenograft Models of Hepatocellular Carcinoma. *Int. J. Mol. Sci.* 18, 1332.
- (13) Luo, S., Tan, X., Qi, Q., Guo, Q., Ran, X., Zhang, L., Zhang, E., Liang, Y., Weng, L., Zheng, H., et al. (2013) A Multifunctional Heptamethine Near-Infrared Dye for Cancer Theranosis. *Biomaterials* 34, 2244–2251.
- (14) Wu, J. B., Shi, C., Chu, G. C.-Y., Xu, Q., Zhang, Y., Li, Q., Yu, J. S., Zhau, H. E., and Chung, L. W. K. (2015) Near-Infrared Fluorescence Heptamethine Carbocyanine Dyes Mediate Imaging and Targeted Drug Delivery for Human Brain Tumor. *Biomaterials* 67, 1–10.
- (15) Yang, X., Shi, C., Tong, R., Qian, W., Zhau, H. E., Wang, R., Zhu, G., Cheng, J., Yang, V. W., Cheng, T., et al. (2010) Near IR Heptamethine Cyanine Dye-Mediated Cancer Imaging. *Clin. Cancer Res.* 16, 2833–2844.
- (16) Zhang, C., Liu, T., Su, Y., Luo, S., Zhu, Y., Tan, X., Fan, S., Zhang, L., Zhou, Y., Cheng, T., et al. (2010) A near-infrared fluorescent heptamethine indocyanine dye with preferential tumor accumulation for in vivo imaging. *Biomaterials* 31, 6612–6617.
- (17) Luo, S., Yang, X., and Shi, C. (2016) Newly Emerging Theranostic Agents for Simultaneous Cancer targeted Imaging and Therapy. *Curr. Med. Chem.* 23, 483–497.
- (18) Gao, M., Yu, F., Lv, C., Choo, J., and Chen, L. (2017) Fluorescent chemical probes for accurate tumor diagnosis and targeting therapy. *Chem. Soc. Rev.* 46, 2237–2271.
- (19) Tan, X., Luo, S., Wang, D., Su, Y., Cheng, T., and Shi, C. (2012) A NIR Heptamethine Dye With Intrinsic Cancer Targeting, Imaging and Photosensitizing Properties. *Biomaterials* 33, 2230–2239.
- (20) Chari, R. V. J., Miller, M. L., and Widdison, W. C. (2014) Antibody-Drug Conjugates: An Emerging Concept in Cancer Therapy. *Angew. Chem., Int. Ed.* 53, 3796–3827.
- (21) Casi, G., and Neri, D. (2015) Antibody-Drug Conjugates and Small Molecule-Drug Conjugates: Opportunities and Challenges for the Development of Selective Anticancer Cytotoxic Agents. *J. Med. Chem.* 58, 8751–8761.
- (22) Srinivasarao, M., and Low, P. S. (2017) Ligand-Targeted Drug Delivery. *Chem. Rev.* 117, 12133–12164.
- (23) Kue, C. S., Kamkaew, A., Burgess, K., Kiew, L. V., Chung, L. Y., and Lee, H. B. (2016) Small Molecules for Active Targeting in Cancer. *Med. Res. Rev.* 36, 494–575.
- (24) Shi, C., Wu, B., and Pan, D. (2016) Review on near-infrared heptamethine cyanine dyes as theranostic agents for tumor imaging, targeting, and photodynamic therapy. *J. Biomed. Opt.* 21, 50901.
- (25) Lv, Q., Yang, X., Wang, M., Yang, J., Qin, Z., Kan, Q., Zhang, H., Wang, Y., Wang, D., and He, Z. (2018) Mitochondria-targeted prostate cancer therapy using a near-infrared fluorescence dye-monoamine oxidase A inhibitor conjugate. *J. Controlled Release* 279, 234–242.
- (26) Zhang, E., Luo, S., Tan, X., and Shi, C. (2014) Mechanistic study of IR-780 dye as a potential tumor targeting and drug delivery agent. *Biomaterials* 35, 771–778.
- (27) Guan, Y., Zhang, Y., Xiao, L., Li, J., Wang, J.-p., Chordia, M. D., Liu, Z.-Q., Chung, L. W. K., Yue, W., and Pan, D. (2017) Improving Therapeutic Potential of Farnesylthiosalicylic Acid: Tumor Specific Delivery via Conjugation with Heptamethine Cyanine Dye. *Mol. Pharmaceutics* 14, 1–13.
- (28) Wu, J. B., Lin, T.-P., Gallagher, J. D., Kushal, S., Chung, L. W. K., Zhau, H. E., Olenyuk, B. Z., and Shih, J. C. (2015) Monoamine Oxidase A Inhibitor-Near-Infrared Dye Conjugate Reduces Prostate Tumor Growth. *J. Am. Chem. Soc.* 137, 2366–2374.
- (29) Kushal, S., Wang, W., Vaikari, V. P., Kota, R., Chen, K., Yeh, T.-S., Jhaveri, N., Groshen, S. L., Olenyuk, B. Z., Chen, T. C., et al. (2016) Monoamine oxidase A (MAO A) inhibitors decrease glioma progression. *Oncotarget* 7, 13842–13853.
- (30) Wu, J. B., Shao, C., Li, X., Shi, C., Li, Q., Hu, P., Chen, Y.-T., Dou, X., Sahu, D., Li, W., et al. (2014) Near-infrared fluorescence imaging of cancer mediated by tumor hypoxia and HIF1 $\alpha$ /OATPs signaling axis. *Biomaterials* 35, 8175–8185.
- (31) Thakkar, N., Lockhart, A. C., and Lee, W. (2015) Role of Organic Anion-Transporting Polypeptides (OATPs) in Cancer Therapy. *AAPS J.* 17, 535–545.
- (32) Kotsampasakou, E., and Ecker, G. F. (2017) Organic Anion Transporting Polypeptides as Drug Targets, in *Transporters as Drug Targets* (Sitte, H. H., Ecker, G. F., Mannhold, R., Buschmann, H., and Clausen, R. P., Eds.) 271–324.
- (33) Karlgren, M., Vildhede, A., Norinder, U., Wisniewski, J. R., Kimoto, E., Lai, Y., Haglund, U., and Artursson, P. (2012) Classification

of Inhibitors of Hepatic Organic Anion Transporting Polypeptides (OATPs): Influence of Protein Expression on Drug-Drug Interactions. *J. Med. Chem.* 55, 4740–4763.

(34) Obaidat, A., Roth, M., and Hagenbuch, B. (2012) The expression and function of organic anion transporting polypeptides in normal tissues and in cancer. *Annu. Rev. Pharmacol. Toxicol.* 52, 135–151.

(35) Roth, M., Obaidat, A., and Hagenbuch, B. (2012) OATPs, OATs and OCTs: the organic anion and cation transporters of the SLCO and SLC22A gene superfamilies. *Br. J. Pharmacol.* 165, 1260–1287.

(36) Okamura, K., Dummer, P., Kopp, J., Qiu, L., Levi, M., Faubel, S., and Blaine, J. (2013) Endocytosis of albumin by podocytes elicits an inflammatory response and induces apoptotic cell death. *PLoS One* 8, e54817.

(37) Peters, J. T. (1995) *All About Albumin: Biochemistry, Genetics, and Medical Applications*.

(38) Gonyar, L. A., Gray, M. C., Christianson, G. J., Mehrad, B., and Hewlett, E. L. (2017) Albumin, in the presence of calcium, elicits a massive increase in extracellular Bordetella adenylate cyclase toxin. *Infect. Immun.* 85, e00198/1–e00198/19.

(39) Spicer, C. D., and Davis, B. G. (2014) Selective chemical protein modification. *Nat. Commun.* 5, 4740.

(40) Kim, Y., Ho, S. O., Gassman, N. R., Korlann, Y., Landorf, E. V., Collart, F. R., and Weiss, S. (2008) Efficient Site-Specific Labeling of Proteins via Cysteines. *Bioconjugate Chem.* 19, 786–791.

(41) Kullak-Ublick, G.-A., Hagenbuch, B., Stieger, B., Wolkoff, A. W., and Meier, P. J. (1994) Functional characterization of the basolateral rat liver organic anion transporting polypeptide. *Hepatology* 20, 411–416.

(42) Milkiewicz, M., Pugh, C. W., and Egginton, S. (2004) Inhibition of endogenous HIF inactivation induces angiogenesis in ischemic skeletal muscles of mice. *J. Physiol.* 560, 21–26.

(43) Jaakkola, P., Mole, D. R., Tian, Y.-M., Wilson, M. I., Gielbert, J., Gaskell, S. J., von Kriegsheim, A., Hebestreit, H. F., Mukherji, M., Schofield, C. J., et al. (2001) Targeting of HIF- $\alpha$  to the von Hippel-Lindau ubiquitylation complex by O<sub>2</sub>-regulated prolyl hydroxylation. *Science* 292, 468–472.

(44) Dutta, D., Williamson, D., Cole, B., and Donaldson, G. (2012) Pitstop 2 is a potent inhibitor of clathrin-independent endocytosis. *PLoS One* 7, e45799.

(45) Koivusalo, M., Welch, C., Hayashi, H., Scott, C. C., Kim, M., Alexander, T., Touret, N., Hahn, K. M., and Grinstein, S. (2010) Amiloride inhibits macropinocytosis by lowering submembranous pH and preventing Rac1 and Cdc42 signaling. *J. Cell Biol.* 188, 547–563.

(46) Dutta, D., and Donaldson, G. (2012) Search for inhibitors of endocytosis: Intended specificity and unintended consequences. *Cell Logist* 2, 203–208.

(47) Liu, Z., and Chen, X. (2016) Simple bioconjugate chemistry serves great clinical advances: albumin as a versatile platform for diagnosis and precision therapy. *Chem. Soc. Rev.* 45, 1432–1456.

(48) Frei, E. (2011) Albumin binding ligands and albumin conjugate uptake by cancer cells. *Diabetol. Metab. Syndr.* 3, 11.

(49) Stehle, G., Sinn, H., Wunder, A., Schrenk, H. H., Schutt, S., Maier-Borst, W., and Heene, D. L. (1997) The loading rate determines tumor targeting properties of methotrexate-albumin conjugates in rats. *Anti-Cancer Drugs* 8, 677–685.

(50) Elsadek, B., and Kratz, F. (2012) Impact of albumin on drug delivery - New applications on the horizon. *J. Controlled Release* 157, 4–28.

(51) Larsen, T., Kuhlmann, M., Hvam, L., and Howard, A. (2016) Albumin-based drug delivery: harnessing nature to cure disease. *Mol. Cell Ther* 4, 3.

(52) Yang, F., Zhang, Y., and Liang, H. (2014) Interactive association of drugs binding to human serum albumin. *Int. J. Mol. Sci.* 15, 3580–3595.

(53) Stoddart, C. A., Bales, C. A., Bare, J. C., Chkhenkeli, G., Galkina, S. A., Kinkade, A. N., Moreno, M. E., Rivera, J. M., Ronquillo, R. E., Sloan, B., et al. (2007) Validation of the SCID-hu Thy/Liv mouse model with four classes of licensed antiretrovirals. *PLoS One* 2, e655.

(54) Stoddart, C. A., Nault, G., Galkina, S. A., Thibaudeau, K., Bakis, P., Bousquet-Gagnon, N., Robitaille, M., Bellomo, M., Paradis, V.,

Liscourt, P., et al. (2008) Albumin-conjugated C34 Peptide HIV-1 Fusion Inhibitor: equipotent to C34 and T-20 in vitro with sustained activity in SCID-hu Thy/Liv mice. *J. Biol. Chem.* 283, 34045–34052.

(55) Kratz, F., Mueller-Driver, R., Hofmann, I., Dreves, J., and Unger, C. (2000) A Novel Macromolecular Prodrug Concept Exploiting Endogenous Serum Albumin as a Drug Carrier for Cancer Chemotherapy. *J. Med. Chem.* 43, 1253–1256.

(56) Graeser, R., Esser, N., Unger, H., Fichtner, I., Zhu, A., Unger, C., and Kratz, F. (2010) INNO-206, the (6-maleimidocaproyl hydrazine derivative of doxorubicin), shows superior antitumor efficacy compared to doxorubicin in different tumor xenograft models and in an orthotopic pancreas carcinoma model. *Invest. New Drugs* 28, 14–19.

(57) Kratz, F., Warnecke, A., Scheuermann, K., Stockmar, C., Schwab, J., Lazar, P., Drucekes, P., Esser, N., Dreves, J., Rognan, D., et al. (2002) Probing the Cysteine-34 Position of Endogenous Serum Albumin with Thiol-Binding Doxorubicin Derivatives. Improved Efficacy of an Acid-Sensitive Doxorubicin Derivative with Specific Albumin-Binding Properties Compared to That of the Parent Compound. *J. Med. Chem.* 45, 5523–5533.

(58) Baggio, L. L., Huang, Q., Cao, X., and Drucker, D. J. (2008) An albumin-xendin-4 conjugate engages central and peripheral circuits regulating murine energy and glucose homeostasis. *Gastroenterology* 134, 1137–1147.

(59) Kim, J.-G., Baggio, L. L., Bridon, D. P., Castaigne, J.-P., Robitaille, M. F., Jette, L., Benquet, C., and Drucker, D. J. (2003) Development and characterization of a glucagon-like peptide 1-albumin conjugate: The ability to activate the glucagon-like peptide 1 receptor in vivo. *Diabetes* 52, 751–759.

(60) Levitt, D. G., and Levitt, M. D. (2016) Human serum albumin homeostasis: a new look at the roles of synthesis, catabolism, renal and gastrointestinal excretion, and the clinical value of serum albumin measurements. *Int. J. Gen. Med.* 9, 229–255.

(61) Kratz, F., and Beyer, U. (1998) Serum proteins as drug carriers of anticancer agents: a review. *Drug Delivery* 5, 281–299.

(62) Awasthi, K., and Nishimura, G. (2011) Modification of near-infrared cyanine dyes by serum albumin protein. *Photochem. Photobiol. Sci.* 10, 461–463.

(63) Rosenthal, S. M., and White, E. C. (1925) Clinical Application of the Bromsulphalein Test for Hepatic Function. *J. Am. Med. Assoc.* 84, 1112–1114.

(64) Jacquemin, E., Hagenbuch, B., Stieger, B., Wolkoff, A. W., and Meier, P. J. (1994) Expression cloning of a rat liver Na<sup>+</sup>-independent organic anion transporter. *Proc. Natl. Acad. Sci. U. S. A.* 91, 133–137.

(65) Baell, J. B., and Holloway, G. A. (2010) New Substructure Filters for Removal of Pan Assay Interference Compounds (PAIS) from Screening Libraries and for Their Exclusion in Bioassays. *J. Med. Chem.* 53, 2719–2740.

(66) Ding, R., Frei, E., Fardanesh, M., Schrenk, H.-H., Kremer, P., and Haefeli, W. E. (2011) Pharmacokinetics of 5-aminofluorescein-albumin, a novel fluorescence marker of brain tumors during surgery. *J. Clin. Pharmacol.* 51, 672–678.

(67) Kremer, P., Fardanesh, M., Ding, R., Pritsch, M., Zoubaa, S., and Frei, E. (2009) Intraoperative fluorescence staining of malignant brain tumors using 5-aminofluorescein-labeled albumin. *Neurosurgery* 64, 53–61.

(68) Frangioni, J. V., and Onishi, S. (2005) Serum albumin conjugated to fluorescent substances for imaging. US20080308744A1.

(69) Li, B., Lu, L., Zhao, M., Lei, Z., and Zhang, F. (2018) An Efficient 1064 nm NIR-II Excitation Fluorescent Molecular Dye for Deep-Tissue High-Resolution Dynamic Bioimaging. *Angew. Chem., Int. Ed.* 57, 7483–7487.

(70) De los Reyes-Berbel, E., Salto-Gonzalez, R., Ortega-Munoz, M., Reche-Perez, F. J., Jodar-Reyes, A. B., Hernandez-Mateo, F., Giron-Gonzalez, M. D., and Santoyo-Gonzalez, F. (2018) PEI-NIR Heptamethine Cyanine Nanotheranostics for Tumor Targeted Gene Delivery. *Bioconjugate Chem.* 29, 2561–2575.

## RESEARCH ARTICLE

 View Article Online  
View Journal | View Issue

 Cite this: *Med. Chem. Commun.*,  
2018, 9, 1754

# A zwitterionic near-infrared dye linked TrkC targeting agent for imaging metastatic breast cancer†

 Zhen Yang,<sup>‡a</sup> Syed Muhammad Usama,<sup>id</sup>†<sup>b</sup> Feng Li,<sup>a</sup>  
Kevin Burgess<sup>id</sup>\*<sup>b</sup> and Zheng Li<sup>id</sup>\*<sup>a</sup>

Much effort has been devoted to targeting agents for imaging and chemotherapy of tumors in cancer research, but there remain significant unmet needs in that area. We have reported a series of preclinical TrkC targeting agents for diagnoses and treatment of metastatic breast cancer; however, with respect to optical imaging, there are limitations to the agents already disclosed. In this work, a TrkC targeting fragment was equipped with a zwitterionic cyanine dye to give a near-infrared probe for *in vivo* imaging of metastatic breast tumors, with excitation and emission wavelengths of 760 and 780 nm, respectively, and facilitate the aqueous dissolution of the final design. To our delight, the newly developed probe maintained the specific targeting to TrkC<sup>+</sup> 4T1 metastatic breast tumor cells as well as the TrkC<sup>+</sup> metastatic breast tumor tissue. Upon injection into 4T1-tumor-bearing mice, the tumor was visualized *in vivo* and *ex vivo* through the fluorescence signal of the probe. These data seem to encourage further investigations toward developing a TrkC targeting agent for the diagnosis of metastatic breast tumors.

 Received 6th April 2018,  
Accepted 25th July 2018

DOI: 10.1039/c8md00190a

rsc.li/medchemcomm

## Introduction

Development of imaging probes that selectively associate with metastatic tumor cells enhances useful diagnostic tools for the therapeutic assessment of cancer treatment.<sup>1,2</sup> For breast cancer, there is an emerging demand for imaging probes that are capable for the recognition of *metastatic*, not just normal, breast tumor cells.<sup>3,4</sup> Tropomyosin kinase receptor C (TrkC) has been identified as a characteristic regulator of breast cancer cell growth and metastasis and tends to be overexpressed in metastatic breast tumor cells.<sup>5,6</sup> Consequently, it is a potential target for the active targeting of metastatic breast cancer.

Most often, monoclonal antibodies (mAbs) are used as targeting agents.<sup>7,8</sup> Small-molecule alternatives, however, have advantages with respect to cost, reagent stabilities, immunogenic effects, circulation times in the course of patient imaging, and, most importantly, superior perme-

ation into solid tumors.<sup>1,9</sup> Consequently, the focus of our research is on small molecules for active targeting of TrkC.

Targeting TrkC with small molecules has featured a bivalent targeting fragment (IY-IY, blue color throughout diagrams in this paper).<sup>10–12</sup> In this work, that fragment, “IY-IY”, was covalently linked to a zwitterionic cyanine dye (purple color throughout) to give a near-infrared probe for TrkC targeted imaging. The polar, zwitterionic characteristics of the dye were anticipated to foster aqueous dissolution for *in vivo* administration and simultaneously diminish net-charges that might otherwise induce non-specific binding.<sup>13</sup> Since the intrinsic structure of the IY-IY fragment was preserved, we hypothesized that the final assembly of the probe would maintain its characteristics of TrkC targeting.

## Results and discussion

### Probe design

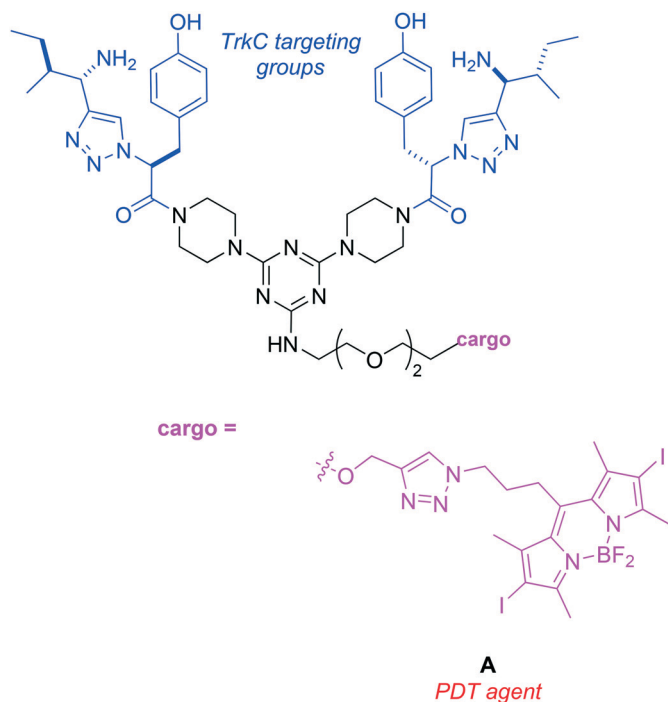
Motivation for these studies came from positive results obtained from a study of the photodynamic therapy (PDT) agent A in mice impregnated with 4T1 mouse breast tumors.<sup>14</sup> In that work, one single 10 mg kg<sup>−1</sup> dose followed by illumination for 10 min caused near complete regression of the primary tumor over 28 days and inhibited metastatic spread relative to untreated control animals.

<sup>a</sup> Center for Bioenergetics, Houston Methodist Research Institute, Houston, TX 77030, USA. E-mail: zli@houstonmethodist.org

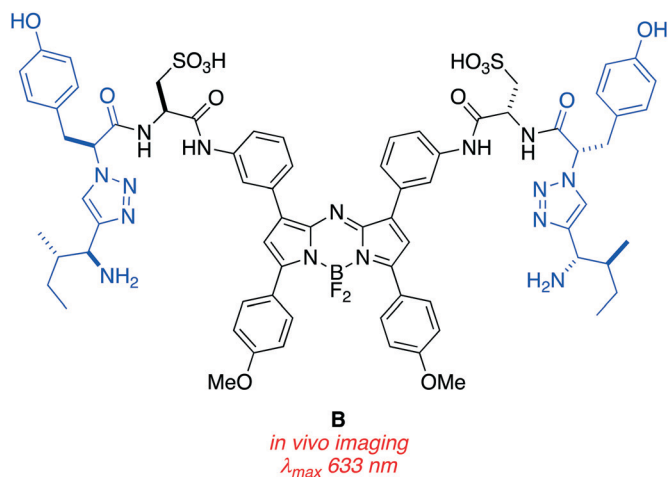
<sup>b</sup> Department of Chemistry, Texas A & M University, Box 30012, College Station, TX 77842, USA. E-mail: burgess@tamu.edu

† Electronic supplementary information (ESI) available: The scheme and full details of compound syntheses and characterization and the *in vitro* cell uptake study. See DOI: 10.1039/c8md00190a

‡ Both authors contributed equally to this work.



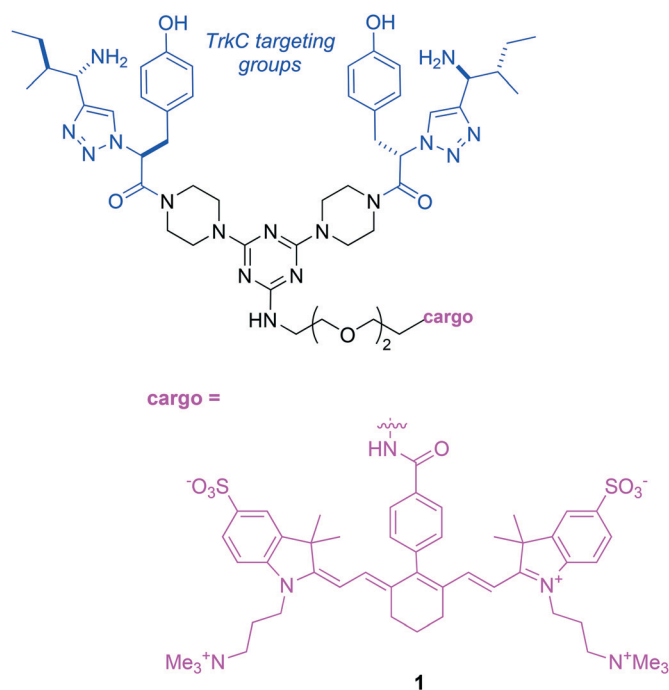
The next step in our research was to develop a TrkC-targeted compound for optical imaging *in vivo*. Agent A, and especially its non-iodinated analog, stained 4T1 cells (that are TrkC<sup>+</sup>) well in culture,<sup>15</sup> but it is unsuitable for *in vivo* imaging because it absorbs light maximally at only 530 nm. Dyes that absorb above 750 nm are preferred for *in vivo* imaging because tissue is most permeable to light above that wavelength, hence the fluorophores can be excited in more deeply situated tumors. Consequently, we designed and studied agent B which contains aza-BODIPY.<sup>16,17</sup>



The outcome of our studies on B was a mixed success.<sup>10</sup> Agent B selectively accumulated in the TrkC<sup>+</sup> 4T1 tumors (relative to an isomeric, non-TrkC targeting control similar to that shown below). That observation means that the different linker and spacing of the TrkC-targeting groups in B relative

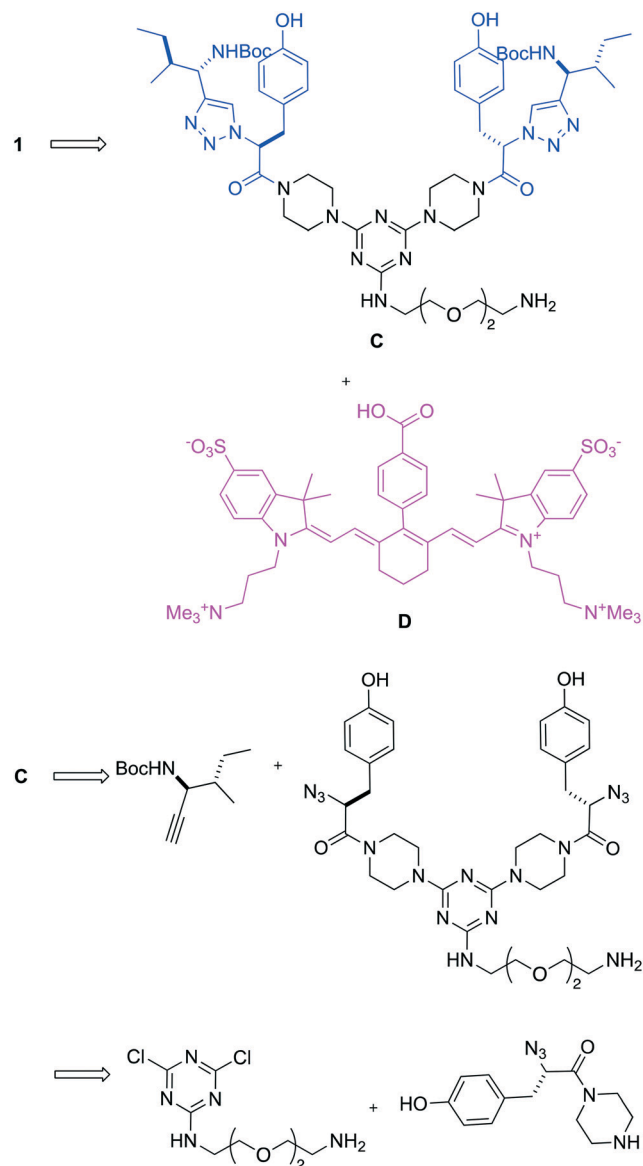
to A did not perturb its honing ability; other work has shown that that is not always the case.<sup>18</sup> On the other hand, a shortcoming was that B absorbs at 633 nm which, though more appropriate than 540 nm in A, is still not a long enough wavelength. Another shortcoming was that B accumulated about three times more in the liver than in the tumor, and it had a long residence time there (still observed after 48 h).

Based on the studies outlined above, the current study was initiated to change the fluorophore completely to a hydrophilic cyanine dye as in 1. Structure 1 has the same IY-IY targeting arrangement as our original lead A, and a more water-soluble fluorophore than B that absorbs light maximally at around 760 nm. Consequently, the visibility of this probe *in vivo* should be superior to A and B, and we anticipated that it would be less retained in the liver than the lipophilic azaBODIPY system B. The parameter that could not be anticipated was the effect of the targeting groups in 1 offset by the pharmacokinetic influence of the cyanine fragment. Important work, particularly by Henary and co-workers, on the distribution of cyanine dyes *in vivo* enables some predictions to be made with more confidence,<sup>19–24</sup> but, nevertheless, experimentation is necessary.



### Probe synthesis and optical properties

The IY-IY targeting group has been made many times previously in these labs, but for the current study an improved procedure was developed to facilitate synthesis on a larger scale. Details of the modified route are given in the ESI,<sup>†</sup> and the concept is outlined in Scheme 1. The last step involved a coupling of the targeting fragment C with the activated cyanine part D.<sup>25</sup> The innovation in the modification was in the construction of C. Previously, IY-piperazine fragments had

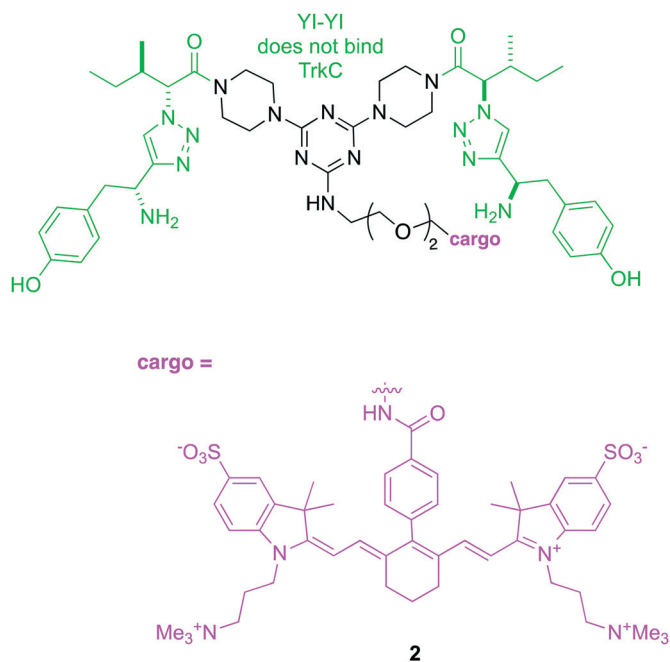


**Scheme 1** Retrosynthetic route to probe **1** illustrating an improved route to the IY-IY fragment.

been added to the triazine, but that step did not scale well. Instead, the current route involves an  $S_NAr$  reaction of a tyrosine-derived azide, then a click reaction to build up the IY-IY fragment in layers.

The following electronic spectral data summarize the key points from the full analysis shown in the ESI.† Probe **1** had an extinction coefficient of  $140\,000\text{ L mol}^{-1}\text{ cm}^{-1}$  and a quantum yield of 5.6% (in 7.4 PBS buffer); these data are typical of the strong absorption from the cyanine fragment and indicate excellent overall brightness. Maximal absorption and emission were observed at 760 and 780 nm (in 7.4 PBS buffer), ideal for optical imaging.

Compound **2** is an isomer of **1** with the targeting amino acids inverted (YI-YI); this was a useful control in the cellular studies that are now described.



### Probe behavior in live cell and tissue studies

Probe **1** was first tested for binding cells stably transfected with TrkC; the data obtained (Fig. 1a, horizontal row) show that the cells did, in fact, bind the probe, whereas the parent NIH3T3 cells that do not express this receptor, did not (Fig. 1b). Control experiments (Fig. S1–S3†), demonstrated that the control probe **2** did not stain TrkC<sup>+</sup> or wild type (TrkC<sup>−</sup>) NIH3T3 cells, and neither did the parent cyanine dye without the targeting group. Confocal studies at a higher magnification revealed that **1** tends to localize in the lysosomes (Fig. 1c and d), just as natural neurotrophins do when they are imported *via* the TrkC receptor.<sup>26</sup> In the histology studies with commercial samples from breast cancer patients, the metastatic breast cancer tissue was stained but not the normal tissue (Fig. 1e and f).

### In vivo imaging with probe 1

Mouse 4T1 breast tumor is a well-established animal model for the study of human metastatic breast cancer.<sup>27</sup> In this study, murine 4T1 tumor cells were subcutaneously injected into BALB/c nu/nu mice to create 8–10 mm diameter metastatic breast tumor xenografts. After intravenous injection of the imaging probe, NIR fluorescence images of the tumor-bearing mice were captured at various time points after injection of **1** (Fig. 2). The 4T1 tumors were clearly visualized through the fluorescence differences displayed from the tumor to muscle background as early as 15 min post injection of the targeting agent. Moreover, the agent **1** rapidly cleared from the body; fluorescence intensities of the tumor dropped from 15 min to 1 h, and further at 3 h, and almost to background at 24 h.

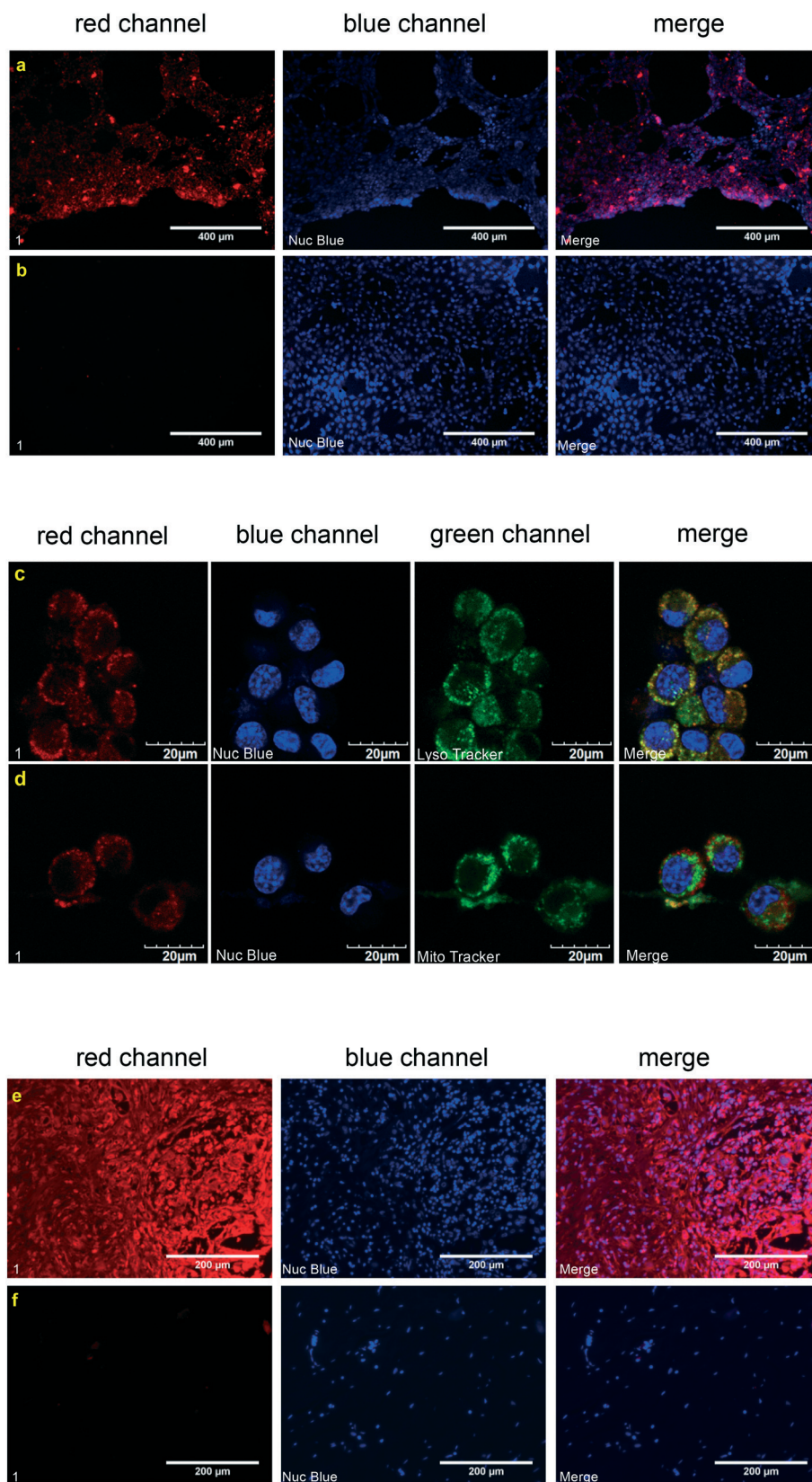


**Fig. 1** a: Probe 1 binds to NIH3T3 TrkC<sup>+</sup> cells, but not to NIH3T3 WT cells (b). Confocal experiments revealed that 1 colocalizes c: with the LysoTracker green, and d: not with the MitoTracker green. Histology studies of 1 with e: metastatic breast cancer tissue (invasive ductal carcinoma), and f: normal breast tissue (adjacent normal breast tissue). Throughout the blue channel, the nucleus is detected by nuclear staining with Nuc Blue.

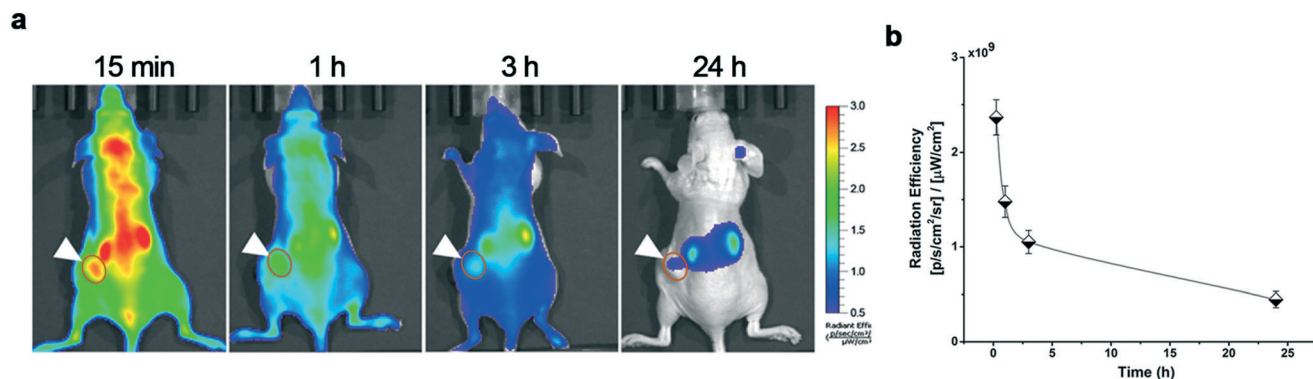


Fig. 2 a: *In vivo* NIR fluorescence images of 4T1 tumor-bearing mice at 15 min, 1 h, 3 h, and 24 h post-injection of the targeting agent. White arrows indicate the tumors, and the circles mark the ROI study of the tumor for the quantification analysis in b. b: Quantification of fluorescence in the tumors. Data shown represent mean  $\pm$  SD ( $n = 3$  per group).

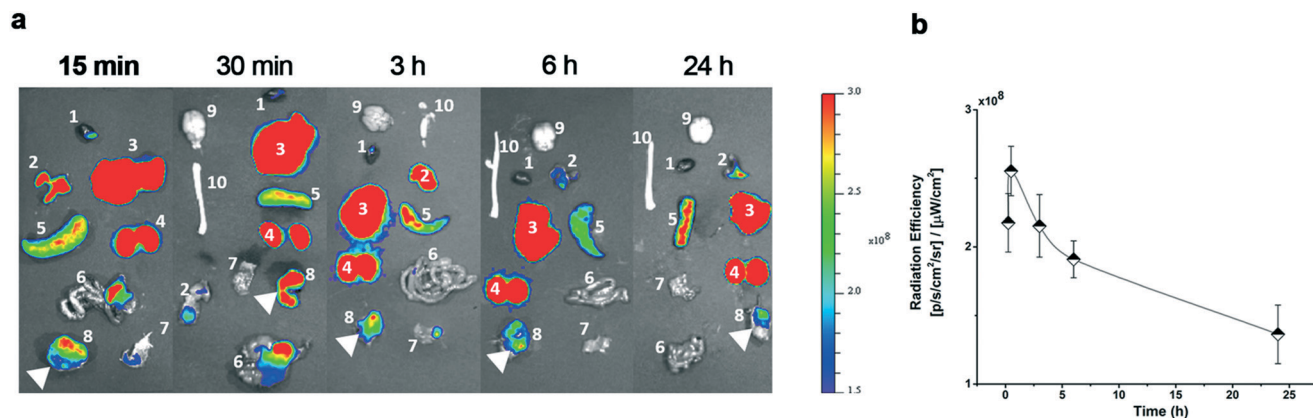


Fig. 3 a: Representative *ex vivo* fluorescence images of: 1 heart, 2 lungs, 3 liver, 4 kidney, 5 spleen, 6 gastrointestinal, 7 muscle, 8 tumor, 9 brain, and 10 spinal cord, collected from mice at 15 min, 30 min, 3 h, 6 h and 24 h post-injection of the targeting agent. White arrows mark the tumors. b: Quantification of fluorescence in the tumors. Data shown represent mean  $\pm$  SD ( $n = 3$  per group).

Compared to TrkC targeting agent B, the retention time of 1 was much shorter, presumably because of the more hydrophilic nature of the zwitterionic dye.

To further validate the tumor uptake of the targeting agent, the internal organs of the imaged mice were collected for *ex vivo* imaging. The relatively higher fluorescence intensities in tumors, compared to the muscle background, indicated the selective uptake (Fig. 3a). Trk receptors play important roles in the mammalian nervous system, and tend to exhibit high expression of the TrkC receptor;<sup>28,29</sup> however, we did not observe uptake in the mice brain and spinal cord, and hence it appears that the size and charge of the probe suppress its penetration into the central nervous system. A kinetic curve of the tumor uptake extracted from the *ex vivo* imaging data corresponded to that from the *in vivo* imaging (Fig. 3b). The uptake of the targeting agent in the tumor reached its peak half an hour after the injection, then, clearance from the body dominated.

Probe 1 localized in the TrkC expressing tumors, as anticipated, providing a way to stain them with NIR fluorescence.

In retrospect, the observation that the probe was washed out of the system relatively rapidly can be attributed to the polarity of the cyanine dye. However, the observation of the rapid washout from tumors *in vivo* surprised us, for two reasons. First, the cell imaging data in this paper prove that probe 1 is selectively imported into the TrkC<sup>+</sup> cells. Secondly, at least some members of the parent dye system E (particularly where R<sup>1</sup> and R<sup>2</sup> contain carboxylate or sulfonate functionalities) tend to localize in many types of solid tumors.<sup>2,30–32</sup> Further experiments are in progress to try to understand these apparent inconsistencies.

## Conclusions

In this work, an imaging probe that incorporated with the TrkC targeting agent and zwitterionic NIR dye was reported for imaging metastatic breast cancer. *In vitro* and *in vivo* imaging studies showed the specific association of the TrkC targeting probe with 4T1 tumors. This study is helpful for further development of a TrkC targeting agent for theranostics of metastatic breast cancer.

## Materials and methods

### Probe synthesis

All reactions were carried out under an inert atmosphere (nitrogen or argon where stated) with dry solvents under anhydrous conditions. Glassware for the anhydrous reactions was dried in an oven at 140 °C for a minimum of 6 h prior to use. Dry solvents were obtained by passing the previously degassed solvents through activated alumina columns. The yields refer to chromatographically and spectroscopically (<sup>1</sup>H-NMR) homogeneous materials, unless otherwise stated. The reagents were purchased at high commercial quality (typically 97% or higher) and used without further purification, unless otherwise stated. Analytical thin layer chromatography (TLC) was carried out on Merck silica gel plates with a QF-254 indicator and visualized by UV. Flash column chromatography was performed using silica gel 60 (SiliCycle, 230–400 mesh). <sup>1</sup>H and <sup>13</sup>C spectra were recorded on a 400 MHz spectrometer and were calibrated using a residual non-deuterated solvent as an internal reference. The detailed synthesis information is provided in the ESI†. The abbreviations or combinations in the ESI† thereof were used to explain the multiplicities: s = singlet, d = doublet, t = triplet, q = quartet, m = multiplet, dd = doublet of doublet, ddd = doublet of doublet of doublets.

### In vitro assays

NIH3T3-WT cells (from the American Type Culture Collection) were cultured on 75 cm<sup>2</sup> culture flasks in Dulbecco's Modified Eagle's Medium/nutrient mixture F-12 (DMEM/F12, Sigma-Aldrich, St. Louis, MO) supplemented with 10% FBS. NIH3T3-TrkC cells were obtained and cultured according to previous procedures.<sup>11</sup> The cells were cultured in a humidified incubator at 37 °C with 5% CO<sub>2</sub> and 95% air.

### Fluorescence microscopy

Intracellular localization of the NIH3T3 cells was measured using an Olympus Fluoview FV1000. The images were taken using a 60×/1.20 water immersed objective. Lysosome staining LysoTracker Green DND 26 (ThermoFisher), mitochondria staining MitoTracker Green FM (ThermoFisher) and for the nucleus, Nuc Blue (ThermoFisher) was used. A 488 nm laser was used for the green channel dyes, a 205 nm laser was used for the nucleus and a 633 nm laser was used for 1 and 2. The rest of the fluorescence images were taken using an Evos FL Imaging System (ThermoFisher).

### Intracellular localization

The NIH3T3 cells were incubated with 20 μM of compound 1 for 2 h at 37 °C. After 2 h, the cells were washed with PBS, and LysoTracker and MitoTracker were added for 40 min. The cells were washed again with PBS and the nucleus was stained using Nuc Blue.

### Histology on patient's tissues

The slide of the human malignant melanoma tissue microarray (BR243w) was purchased from US Biomax, Inc.; the array includes 13 cases of malignant melanoma and 12 cases of adjacent normal cells. The slide was transferred to a xylene bath for 10 min and then rehydrated in two changes of fresh absolute ethanol for 7 min each. Excess liquid was shaken off and the slide was incubated in fresh 90% and 70% ethanol and then water for 7 min each. The slide was washed in two changes of PBS for 5 min each, then incubated with PBS containing 4% BSA for 30 min. The tissues were rinsed with PBS and incubated twice in PBS for 5 min each. The compound 1 solution in 4% PBS/BSA was added to the slide and incubated overnight at 4 °C. The slide was rinsed twice in PBS, then in water (10 min each). Then the slide containing 1 was mounted on permanent mounting media with DAPI (Vector) and incubated at 4 °C for 4 h. The tissues were imaged with an Evos FL Imaging System. Throughout, digital images were captured with a 20×/0.45 excitation at 730 nm for 1 and 405 nm for DAPI.

### Animal model

Murine breast cancer 4T1 cells were obtained from the American Type Culture Collection and cultured as protocol suggested, *i.e.* in Dulbecco's modified Eagle's medium (DMEM) supplemented with 10% fetal bovine serum (FBS) at 37 °C in a humidified atmosphere with 5% CO<sub>2</sub>. Upon 80% confluence, the cells were collected and suspended in PBS, and then subcutaneously injected into 6 week old BALB/c nu/nu mice (Charles River) at 2 × 10<sup>6</sup> cells per 100 μL per mouse. Then the mice were fed for two weeks to allow the tumor growth to reach 8–10 mm for the imaging study. The animal procedures were performed according to a protocol approved by the Animal Care and Use Committee of Houston Methodist Research Institute and in accordance with the NIH guidelines for the care and use of laboratory animals (NIH Publication No. 85–23 Rev. 1985).

### In vivo and ex vivo fluorescence imaging

The fluorescence imaging was performed using an IVIS200 imaging system, and the ROI study was quantified using Living Imaging software (Xenogen, CA). Excitation and emission filters were set at 745 nm and 800 nm, respectively, for image acquisition. For injection, the synthesized agent was firstly prepared as a 1 mM stock solution in DMSO, and then diluted into 10 nmol per 100 μL in PBS for each mouse. Upon intravenous injection *via* the tail vein, the mice (3 per group) were anesthetized to accomplish the imaging acquisition. As to *ex vivo* imaging, the mice (3 per group) were euthanized as animal protocol described at various time points after injection of the targeting agent, and the internal organs (*i.e.* heart, lungs, liver, kidney, spleen, gastrointestinal, tumor, muscle, brain, and spinal cord) were collected for *ex vivo* image acquisition. Upon image acquisition, ROI analysis and

quantification of the fluorescence signals were performed using Living Imaging software.

## Definitions

BODIPY	4,4-Difluoro-4-bora-3a,4a-diaza-s-indacene
NT3	Neurotrophin-3
PET	Positron emission tomography
Trk	Tropomyosin receptor kinases

## Conflicts of interest

The authors declare no competing financial interests.

## Acknowledgements

We acknowledge the DoD BCRP Breakthrough Award (BC141561 and BC141561P1), CPRIT (RP150559 and RP170144), the Robert A. Welch Foundation (A-1121) and the George and Angelina Kostas Research award for financial support. The NMR instrumentation at Texas A&M University was supported by a grant from the National Science Foundation (DBI-9970232) and the Texas A&M University System. The Olympus FV1000 confocal microscope acquisition was supported by the Office of the Vice President for Research at Texas A&M University. We thank the preclinical imaging core facility of Houston Methodist Research Institute for imaging support. Procedures for animal housing, maintenance, and euthanization were performed according to the American Veterinary Medical Association guidelines, and the IACUC approval from Methodist Hospital.

## References

- 1 C. S. Kue, A. Kamkaew, K. Burgess, L. V. Kiew, L. Y. Chung and H. B. Lee, *Med. Res. Rev.*, 2016, **36**, 494–575.
- 2 M. Gao, F. Yu, C. Lv, J. Choo and L. Chen, *Chem. Soc. Rev.*, 2017, **46**, 2237–2271.
- 3 C. Cedolini, S. Bertozzi, A. P. Londero, S. Bernardi, L. Seriau, S. Concina, F. Cattin and A. Risaliti, *Clin. Breast Cancer*, 2014, **14**, 235–240.
- 4 H. G. Welch, D. H. Gorski and P. C. Albertsen, *N. Engl. J. Med.*, 2015, **373**, 1685–1687.
- 5 W. Jin, G. M. Kim, M. S. Kim, M. H. Lim, C. Yun, J. Jeong, J.-S. Nam and S.-J. Kim, *Carcinogenesis*, 2010, **31**, 1939–1947.
- 6 A. Vaishnavi, A. T. Le and R. C. Doebele, *Cancer Discovery*, 2015, **5**, 25.
- 7 D. J. Slamon, B. Leyland-Jones, S. Shak, H. Fuchs, V. Paton, A. Bajamonde, T. Fleming, W. Eiermann, J. Wolter, M. Pegram, J. Baselga and L. Norton, *N. Engl. J. Med.*, 2001, **344**, 783–792.
- 8 M. Ogawa, N. Kosaka, P. L. Choyke and H. Kobayashi, *Cancer Res.*, 2009, **69**, 1268.
- 9 K. Imai and A. Takaoka, *Nat. Rev. Cancer*, 2006, **6**, 714.
- 10 A. Kamkaew, F. Li, Z. Li and K. Burgess, *MedChemComm*, 2017, **8**, 1946–1952.
- 11 C. S. Kue, A. Kamkaew, H. B. Lee, L. Y. Chung, L. V. Kiew and K. Burgess, *Mol. Pharmaceutics*, 2015, **12**, 212–222.
- 12 A. Kamkaew and K. Burgess, *J. Med. Chem.*, 2013, **56**, 7608–7614.
- 13 H. S. Choi, K. Nasr, S. Alyabyev, D. Feith, J. H. Lee, S. H. Kim, Y. Ashitate, H. Hyun, G. Patonay, L. Strekowski, M. Henary and J. V. Frangioni, *Angew. Chem., Int. Ed.*, 2011, **50**, 6258–6263.
- 14 S. C. Kue, A. Kamkaew, H. B. Lee, L. L. Chung, L. V. Kiew and K. Burgess, *Mol. Pharmaceutics*, 2015, **12**, 212–222.
- 15 A. Kamkaew and K. Burgess, *Chem. Commun.*, 2015, **51**, 10664–10667.
- 16 M. A. Pysz, S. S. Gambhir and J. K. Willmann, *Clin. Radiol.*, 2010, **65**, 500–516.
- 17 J. V. Frangioni, *Curr. Opin. Chem. Biol.*, 2003, **7**, 626–634.
- 18 A. Kamkaew, N. Fu, W. Cai and K. Burgess, *ACS Med. Chem. Lett.*, 2017, **8**, 179–184.
- 19 H.-S. Choi, K. Nasr, S. Alyabyev, D. Feith, J.-H. Lee, S.-H. Kim, Y. Ashitate, H. Hyun, G. Patonay, L. Strekowski, M. Henary and J. V. Frangioni, *Angew. Chem., Int. Ed.*, 2011, **50**, 6258–6263.
- 20 G. Beckford, E. Owens, M. Henary and G. Patonay, *Talanta*, 2012, **92**, 45–52.
- 21 H. S. Choi, S. L. Gibbs, J. H. Lee, S. H. Kim, Y. Ashitate, F. Liu, H. Hyun, G. L. Park, Y. Xie, S. Bae, M. Henary and J. V. Frangioni, *Nat. Biotechnol.*, 2013, **31**, 148–153.
- 22 N. S. James, Y. Chen, P. Joshi, T. Y. Ohulchanskyy, M. Ethirajan, M. Henary, L. Strekowski and R. K. Pandey, *Theranostics*, 2013, **3**, 692–702, p. 611.
- 23 E. A. Owens, H. Hyun, J. G. Tawney, H. S. Choi and M. Henary, *J. Med. Chem.*, 2015, **58**, 4348–4356.
- 24 C. N. Njiojob, E. A. Owens, L. Narayana, H. Hyun, H. S. Choi and M. Henary, *J. Med. Chem.*, 2015, **58**, 2845–2854.
- 25 D. Su, C. L. Teoh, A. Samanta, N.-Y. Kang, S.-J. Park and Y.-T. Chang, *Chem. Commun.*, 2015, **51**, 3989–3992.
- 26 R. Butowt and C. S. von Bartheld, *J. Neurosci.*, 2001, **21**, 8915–8930.
- 27 B. A. Pulaski and S. Ostrand-Rosenberg, in *Current Protocols in Immunology*, John Wiley & Sons, Inc., 2001, DOI: 10.1002/0471142735.im2002s39.
- 28 B. Stoleru, A. M. Popescu, D. E. Tache, O. M. Neamtu, G. Emami, L. G. Tataranu, A. S. Buteica, A. Dricu and S. O. Purcaru, *Mædica*, 2013, **8**, 43–48.
- 29 Y. Muragaki, N. Timothy, S. Leight, B. L. Hempstead, M. V. Chao, J. Q. Trojanowski and V. M. Y. Lee, *J. Comp. Neurol.*, 1995, **356**, 387–397.
- 30 X. Tan, S. F. Luo, D. F. Wang, Y. F. Su, T. F. Cheng and C. Shi, *Biomaterials*, 2012, **33**, 2230–2239.
- 31 S. Luo, X. Yang and C. Shi, *Curr. Med. Chem.*, 2016, **23**, 483–497.
- 32 C. Zhang, T. Liu, Y. Su, Y. Zhu, X. Tan, S. Fan, L. Zhang, Y. Zhou, T. Cheng and C. Shi, *Biomaterials*, 2010, **31**, 6612–6617.

# Optimized Heptamethine Cyanines for Photodynamic Therapy

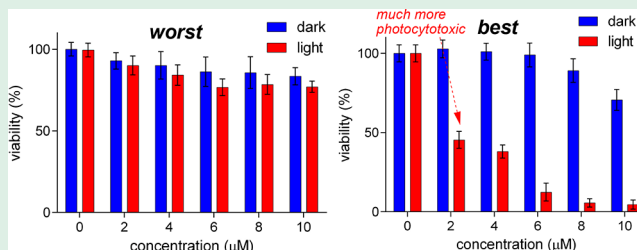
Syed Muhammad Usama,<sup>ID</sup> Sopida Thavornpradit,<sup>ID</sup> and Kevin Burgess<sup>\*ID</sup>

Department of Chemistry, Texas A&amp;M University, PO Box 30012, College Station, Texas 77842, United States

## S Supporting Information

**ABSTRACT:** Over 10 near-IR fluorescent sensitizers were prepared to explore their properties relevant to potential applications in photodynamic therapy (PDT). Key properties of these compounds are that they can be excited around 800 nm, (i) are hydrophilic, (ii) generate singlet oxygen with acceptable quantum yields, and (iii) are imported into cancer cells via the organic anion transporter proteins (OATPs). (This is crucial to tumor localization.) The *N*-substituents of these cyanines were varied to adjust their charges and polarities and to accommodate conjugation to other entities (e.g., biomolecules or fragments to expand their theranostic modalities). Thus, it was possible to optimize their photocytotoxicities without compromising their other desirable characteristics for PDT. Overall, sensitizers like this have superior characteristics relative to clinically approved sensitizers for PDT insofar as they can be excited at greater depths in tissue.

**KEYWORDS:** photodynamic therapy, cyanine, singlet oxygen, photocytotoxicity, cancer, near-infrared



## INTRODUCTION

Photodynamic therapy, PDT, relies on illumination of sensitizers absorbed in tissue.<sup>1–3</sup> Appropriate sensitizers populate triplet excited states with long half-lives (relative to singlet states), which therefore have time to react with endogenous oxygen. That interaction transforms ubiquitous <sup>3</sup>O<sub>2</sub> into its extremely reactive singlet state. Singlet oxygen destroys tissues via several oxidative mechanisms, and this effect can be used in various ways, including for cancer therapy.<sup>4–6</sup>

A significant attribute of PDT is that it is spatially targeted. This is because the areas to be illuminated can be controlled, singlet oxygen can only be generated there, and <sup>1</sup>O<sub>2</sub> is so reactive that tissue damage is effectively confined in those regions. (The half-life of singlet oxygen in tissue has been estimated to be 3.5 μs;<sup>7,8</sup> hence, its effects in PDT are localized within about 155 nm of the illuminated area.)<sup>9,10</sup> Overall, these combined effects widen the therapeutic window of PDT relative to agents that are not targeted.

The main weakness of PDT is that light must permeate through tissue to excite the sensitizers. At best, light only traverses through about 1 cm of tissue, so PDT is only viable for the destruction of cells on or near tissues accessible to surface illumination or via fiber-optic devices delivered through needles into deep tissue. In both cases, it is necessary to treat around the area targeted in case there are outbreaks, e.g., tumor growths, that were undetectable, in other words, to maintain a “negative margin” around the lesion. The optimal wavelength range for excitation of sensitizers in PDT is from approximately 750 to around 850 nm. Tissue is relatively opaque to light of <750 nm than to longer wavelengths (penetration of light wavelength 800

nm is twice that of light 630 nm),<sup>11</sup> whereas above 850 nm the quanta do not have enough energy to form singlet oxygen.<sup>12</sup>

Characteristics of ideal PDT sensitizers include: (i) strong absorption in the 750–850 nm range; (ii) high quantum yield for singlet oxygen generation; (iii) low dark cytotoxicity for the agent and its metabolites; (iv) photostability; (v) solubility in aqueous media; and (vi) an intrinsic tendency to localize in cancer cells over healthy ones. In our view, and in the opinions of others,<sup>12–14</sup> the most limiting restriction on the available hydrophilic PDT sensitizers is (i) strong absorbance in the 750–850 nm range combined with (ii) efficient generation of singlet oxygen. This assertion is supported by the review of sensitizers for PDT that are FDA-approved (i.e., in the U.S.; five total, porfimer sodium, ALA, MAL, HAL, and BPD-MA) and/or those approved in other countries (three total, mTHPC, NPe6, and AlPcS4; Figure 1), all of which have absorption maxima well below the desired 750–850 nm range. [The aminovulinate derivatives (ALA, MAL, and HAL) are transformed into porphyrins in situ, which have absorption maxima below the desired range.] Studies that feature hydrophilic sensitizers that do not absorb strongly in the 750–850 nm range are unlikely to improve upon the clinically approved substances, despite the fact that the greatest potential for improvements in the area are associated with facilitating PDT for nonsuperficial tissue. There is some interest in modified bacteriochlorins, a few of which do absorb above 750 nm.<sup>1,11,15</sup> However, the efficiency of PDT sensitizers is directly related to the product of their extinction coefficient and quantum yield for singlet oxygen production, and

Received: August 10, 2018

Accepted: September 5, 2018

Published: September 17, 2018

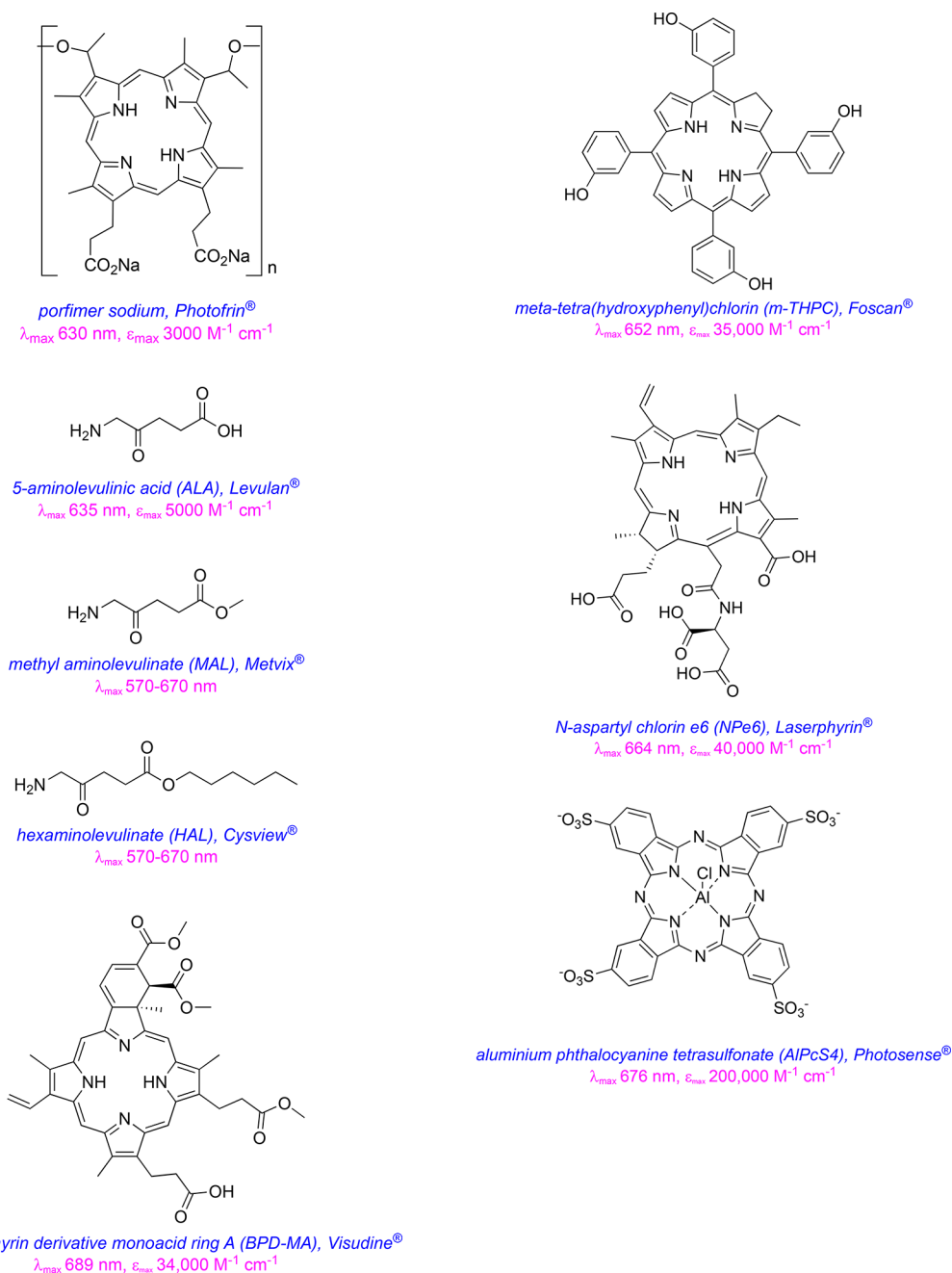


**Figure 1.** Photosensitizers clinically approved for PDT treatment.

even the most promising bacteriochlorins have lesser values for both of these parameters relative to the heptamethine cyanine dyes considered here.

Heptamethine cyanine (Cy7) dyes (Figure 2, A) tend to absorb in the 750–850 nm range, but there has been relatively a few reported attempts to modify them for use in PDT.<sup>1,16–23</sup> Indocyanine green (ICG) is particularly relevant because it is FDA-approved for optical imaging, but typical of cyanines for PDT, it has an extremely low quantum yield for singlet oxygen production (0.077).<sup>24</sup> Heptamethine cyanines B, with a six-membered carbocyclic ring, have an increased rigidity, leading to an increase in fluorescence quantum yield and decrease in aggregation relative to the parent systems A. Some systems containing framework B (without heavy atoms) can be photosensitizers, but their quantum yields for singlet oxygen

production are also low.<sup>25–28</sup> In a patent, iodinated systems B for PDT have been described, with no evidence that they were actually made. Another patent covered diiodinated indozalines specifically for conversion into class A cyanine dyes for PDT, but no examples with type B systems were reported. While this work was in progress, Callan and co-workers published on a diiodinated Cy7 derivative that has a significantly higher efficiency for <sup>1</sup>O<sub>2</sub> production than those mentioned previously. (This compound is later numbered 2bb; see Figure 3 below for the structure and explanation of numbering scheme in this work.<sup>29</sup>)

Cyanines with different N-alkyl substituents are desirable because they facilitate optimization for PDT effects. (It is known that the N-alkyl substituents can have an influence.<sup>25–28</sup>) However, unsymmetrical Cy7 analogues are significantly harder

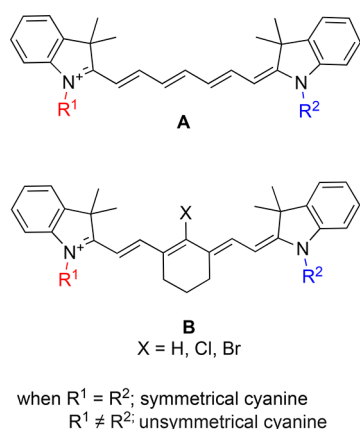
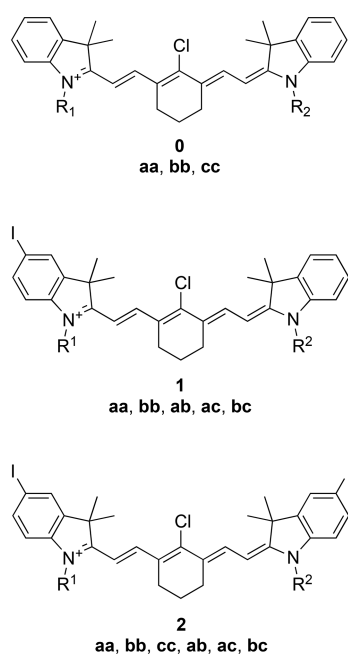


**Figure 2.** Basic structures of heptamethine cyanine dyes. **A** does not have a cyclohexyl ring, where as **B** has it.



where  $R^1$  and  $R^2$  are

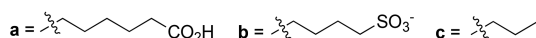


**Figure 3.** Cyanines prepared in this work with zero, one, or two iodines with different side chains are notated **0**, **1**, and **2**, respectively. The synthesis of these compounds is described in Figures S2–S4.

to make than symmetrical ones. In fact, there are only a few experimental procedures for making unsymmetrical cyanine dyes, and they are all small-scale, low-yielding procedures.<sup>30,31</sup> It is therefore unsurprising that unsymmetrical Cy7 analogues for PDT are at least rare and indeed may not have been reported to date.

This article reports the syntheses of 10 new cyanine dyes to test for PDT. Throughout, they retain some near-IR fluorescence properties (emission maxima around 780 nm); hence, they are dual mode theranostics (for fluorescence detection of tumor tissue locations and for therapy). We show that these sensitizers also have properties that are conducive to import into cancer cells. They include compounds that are symmetrical and unsymmetrical, containing zero, one, or two

iodine atoms (hereafter labeled with the numbers **0**, **1**, and **2**). Photophysical properties of these compounds, including quantum yields of singlet oxygen generation, have been measured and compared to the literature standard mentioned above (**2bb**). Two Cy7 derivatives were shown to be significantly more photocytotoxic than the others. These two particular compounds were tracked via confocal microscopy to determine sites of localization in cells, particularly in mitochondria since compounds that accumulate there can be especially effective in cancer therapy.<sup>32</sup> Preferred cell uptake mechanisms for one of these compounds were also established.

## RESULTS AND DISCUSSION

**Syntheses.** Symmetrical cyanine dyes are typically prepared by double condensation reactions (Scheme S1a), while the few protocols for unsymmetrical ones available describe stepwise, different, conjugation processes (Scheme S1b). The problem with the stepwise route is that the products tend to be contaminated by symmetrical impurities; hence, the yields of the isolated, pure unsymmetrical products tend to be low. Others have noted that this difficulty is accentuated for type **B** cyanine dyes.<sup>33</sup> In this work, it was found to be a considerable advantage to perform the first condensation to give the hemicyanines at 50 °C (a significantly lower temperature than used in published procedures) and then to purify via flash chromatography on silica. Using this modification, it was possible to obtain gram amounts of pure (usually >95% by analytical HPLC) materials after preparative HPLC or MPLC on C18 reversed-phase supports. The products prepared are shown in Figure 3, where the numbers **0–2** denote the number of iodines on the scaffold and the suffixes describe the *N*-substituents. Of these, the iodinated compounds are new except our “literature standard” **2bb**.<sup>29</sup>

**Photophysical Properties.** Rates of singlet oxygen production for the compounds **0–2** are shown in Figure S1a–c, respectively. There appears to be no correlation between the polarities or acidities of the side-chain (**a**, **b**, and **c**) combinations and the amounts of singlet oxygen produced. Figure S2a–c indicates there is a similar lack of correlation for the photostabilities of these dyes, and in any event, photostabilities did not vary much with *N*-substitution ( $t_{1/2}$  between around 12 and 32 min), except compound **2bc** was somewhat more resilient to excitation, especially over the early stages.

Singlet oxygen production and photostability data described above is summarized with other photophysical data in Table 1. All of the dyes absorb maximally between 794 and 812 nm and fluoresce with maxima in the range from 811 to 827 nm. Their fluorescence quantum yields are low (0.044–0.095), but their high extinction coefficients (ca. 100000–340000) mean these dyes are bright (brightness = quantum yield  $\times$  extinction coefficient, Table S2), as expected for Cy7 dyes. The data indicates that compounds with a sulfonic acid in the *N*-substituent tend to have higher extinction coefficients, presumably due to increased water solubility and less aggregation in aqueous media. Broadly speaking, compounds **2** tend to have higher quantum yields for singlet oxygen production than **1** and **0**; i.e., the most iodinated fluors produce the most singlet oxygen, again as expected from heavy atom effects. The presence of two iodines facilitates transitions between singlet and triplet states that would be forbidden in simpler systems and less facile in monoiodo-compounds. Singlet oxygen generation increased by approximately 4-fold with the addition of the first iodine atom and 2-fold with the addition of

**Table 1. Spectroscopic Properties of Compounds 0, 1, and 2 Dissolved in PBS Buffer (pH 7.4)**

compound	R <sup>1</sup>	R <sup>2</sup>	$\lambda_{\text{abs}}$ (nm)	$\lambda_{\text{em}}$ (nm)	$\epsilon_{\text{max}}$ (M <sup>-1</sup> cm <sup>-1</sup> )	$\Phi^a$	$\Phi$ ( <sup>1</sup> O <sub>2</sub> ) <sup>b</sup>
0	a	a	796	815	235120	0.076	0.058
	b	b	812	827	340920	0.095	0.070
	c	c	803	818	100080	0.077	0.144
1	a	a	803	819	209480	0.071	0.379
	b	b	796	812	208600	0.072	0.347
	a	b	812	823	211800	0.069	0.272
	a	c	803	819	199960	0.077	0.403
	b	c	812	827	200240	0.071	0.449
2	a	a	794	811	229200	0.044	0.627
	b	b	812	825	252000	0.065	0.686
	c	c	813	827	148360	0.047	0.591
	a	b	812	825	268560	0.063	0.790
	a	c	803	816	180680	0.069	0.675
	b	c	803	819	248960	0.062	0.767

<sup>a</sup>Fluorescence quantum yields vs ICG ( $\Phi = 0.13$  in DMSO) as a standard. <sup>b</sup><sup>1</sup>O<sub>2</sub> quantum yield measured using ICG ( $\Phi = 0.077$ ) as a reference.

the second iodine atom (average for compounds: 0, 0.091; 1, 0.370; 2, 0.689).<sup>34</sup>

**Cell Studies. Light and Dark Toxicities.** Throughout, the photocytotoxicity experiments described below were performed using inexpensive LEDs that generate a light flux of only 2.28 J/cm<sup>2</sup>. A choice of low-flux light sources was deliberate to emphasize the effectiveness of the featured photosensitizers.

Compounds 2, i.e., the ones that afforded the most singlet oxygen when illuminated, were incubated with HepG2 cells in the absence of light for 48 h to examine viability under those conditions. In the event, there was a little difference; all of the compounds had IC<sub>50</sub> values in the 7–23  $\mu$ M range (Figure S3). However, differences in the characteristics of the compounds became more prevalent in photocytotoxicity experiments. Thus, HepG2 cells were incubated with compounds 2 for 1 h, washed, then illuminated in fresh medium at 780 nm (3.8 mW/cm<sup>2</sup> LED) for 10 min, incubated for 24 h, and then tested for viability (AlamarBlue). Throughout this article, the Thor Lab LED780E used has a maximum absorbance around 780  $\pm$  10 nm, which covers the maximum wavelengths for most of the synthesized compounds. Figure 4 shows data for compounds 2 organized from least to most photocytotoxic. All of the compounds were significantly more photocytotoxic (red bars) than dark controls (blue bars), in which the illumination step was omitted. The di-*n*-propyl compound 2cc was less photocytotoxic than the known, disulfonic acid, sensitizer 2bb, but all of the others were more so. The following observation is to compare the best (2ac) with the standard (2bb): more than 50% of the cells remained in the experiments featuring treatment with 2bb at 10  $\mu$ M, but under the same conditions, 2ac (sulfonic acid and propyl *N*-substituents) killed almost all of the cells. At 6  $\mu$ M, 2ac killed more than half of the cells in this assay.

**Localization of the Sensitizers in Cancer Cells.** Confocal microscopy experiments were undertaken to visualize favored organelles for accumulation of the two most photocytotoxic of the featured sensitizers: i.e., 2ac and 2bc. Both dyes readily permeated into HepG2 cells. Both 2ac and 2bc colocalized to some degree with LysoTracker green and much more with MitoTracker green (Figures 5 and 6, respectively). In fact, similar localization studies were performed for all of the series 2

compounds reported in this article. All of them accumulated mostly in the mitochondrion and less in the lysosome, with the exception of the control 2bb, which was found mostly in lysosomes and less in mitochondria (Figure S4). This observation is consistent with the greater positive charges of these particular sensitizers in the series.

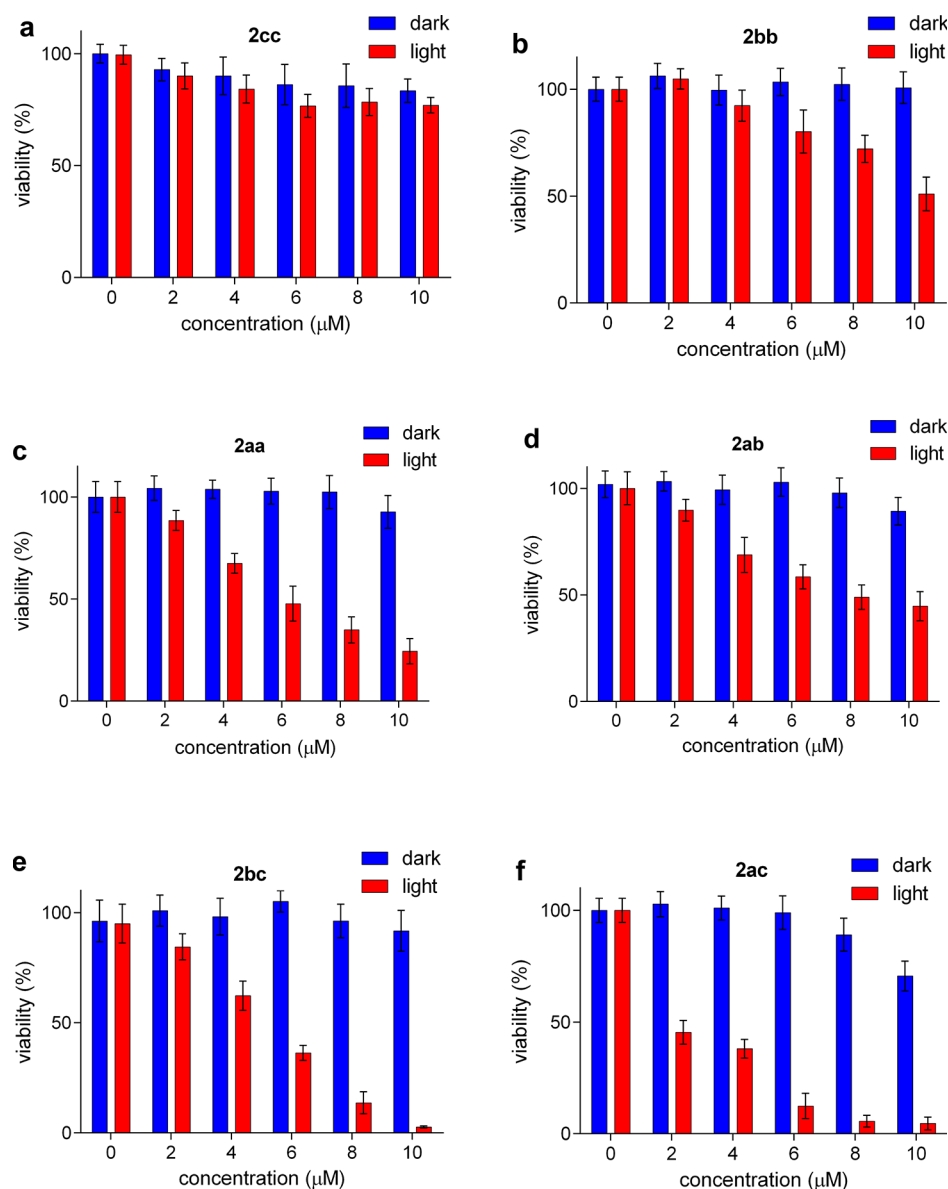
Some class B dyes are known to localize in solid tumor tissue (e.g., prostate,<sup>35</sup> gastric,<sup>36</sup> kidney,<sup>37</sup> lung,<sup>26</sup> glioblastoma,<sup>38,39</sup> and liver tumor tissues<sup>40</sup>) but not in normal cells and tissue.<sup>25,41–44</sup> Evidence from several studies suggests this is because those particular fluors are taken up by the organic anion transporter proteins (OATPs).<sup>45,46</sup> These OATP cell surface receptors are overexpressed on solid tumors; their natural function is to influx organic anions (and some neutral materials), which are important to cells (e.g., bile salts, steroids, bilirubin, and thyroid hormones), and to balance this ion influx. OATP receptors efflux intracellular bicarbonate, glutathione, and glutathione adducts. We inferred that OATP-mediated uptake of the iodinated dyes in series 2 imparts the potential for enhanced tumor uptake over healthy tissues that do not express these receptors. Consequently, a series of fluorescence studies were undertaken to establish a mechanism of uptake of 2ac into HepG2 cells (Figure 7).

Figure 7 compares the fluorescence uptake by HepG2 cells treated with 2ac alone (i.e., no blocking, Figure 7a), with the fluorescence when the same cell type but treated first with pan-inhibitor OATPs (which there are several subtypes within this category, but the inhibitor is believed to inhibit all; Figure 7b),<sup>45,46</sup> and finally (Figure 7c) with HepG2 cells treated with an agent to induce hypoxia and therefore to promote expression of HIF1 $\alpha$ , leading to an enhance expression of OATPs.<sup>36,47</sup> Data in Figure 7 shows there is less uptake of 2ac when the OATPs are inhibited and more when their overexpression is enhanced. (Quantification is provided in Figure S5.)

Derivatives of the parent cyanine dyes that are too lipo- or hydrophilic tend not to localize in tumor tissue. Calculations of physiochemical properties were performed using Marvin (17.21.0, ChemAxon; Table S1) to examine if the substitution of iodine atoms on to the cyanine framework impacts these types of properties. Relative to the noniodinated cyanines 0, the mono- and di-iodinated ones 1 and 2 had insignificant differences in calculated polar surface areas. The addition of one then another iodine (from 0 to 1 to 2) somewhat increased the calculated LogP and LogD values for the compounds, but only by around one or two log units, i.e., probably not enough to cause significant changes in their pharmacokinetic properties. LogD (and LogP) data are important because others have singled this out as important for biodistribution of Cy7 derivatives.<sup>48</sup>

Callan's sensitizer, 2bb, has no convenient function groups to facilitate its conjugation to biomolecules or other fragments to expand theranostic modalities, except displacement of the *meso*-chloride via S<sub>RN</sub>1 or S<sub>N</sub>Ar mechanisms. Consequently, we were curious to probe the effects of substituting that same chloride with nitrogen, oxygen, and sulfur nucleophiles; hence, three test compounds were made (Supporting Information) giving compounds 3bb, 4bb, and 5bb (Table 2).

Table 2 shows that the absorption and emission maxima of the *N*-substituted compound 4bb is blue-shifted relative to 2bb by 145 nm, whereas the *O*- and *S*-substituted ones were much less affected by this change. These observations are consistent with literature reports on the structurally similar, but noniodinated, cyanines.<sup>48,49</sup> Unfortunately, we were not able to make a true



**Figure 4.** Light and dark cytotoxicity of compounds (a) **2cc**, (b) **2bb**, (c) **2aa**, (d) **2ab**, (e) **2bc**, and (f) **2ac** determined after irradiation under a 780 nm LED or kept in dark as a control. (See text for details.)

comparison of quantum yields for singlet oxygen production because the LED we used (780 nm) was appropriate for excitation of **2bb** and the *O*- and *S*-substituted compounds **3bb** and **5bb**, but gave effectively no excitation of the “blue-shifted sensitizer” **4bb**. However, these experiments do show that the quantum yields of singlet oxygen production for *O*- and *S*-substituted compounds **3bb** and **5bb** were approximately half that of **2bb**.

## CONCLUSIONS

Callan et al. reported the first near-IR cyanine sensitizer in the open literature; this was a milestone in the area, and the work reported here builds on those studies. Thus, a slight refinement of literature syntheses of unsymmetrical cyanines facilitated preparation and studies of the series **0**, **1**, and **2** molecules, some of which might not have been conveniently accessible otherwise. The only iodinated compound in series **1** and **2** that has been reported in the open literature prior to this work was **2bb**.

Most of the new compounds featured here in series **2** (specifically, **2aa**, **2ab**, **2ac**, and **2bc**) were more photocytotoxic than the literature control **2bb**. Moreover, unlike **2bb**, the novel sensitizers accumulated in mitochondria. Mitochondrion targeting is particularly important for PDT in cancer because where sensitizers accumulate is of comparable importance to the number of reactive oxygen species it produces. Targeting mitochondria makes cells particularly sensitive to PDT,<sup>6,32</sup> so this tends to explain why most of the compounds in series **2** were more photocytotoxic than **2bb**. The observation that **2bb** localized in the lysosome, in preference to the mitochondrion, might correlate with the observation that this compound is uniquely has two sulfonates, making it the most hydrophilic member of series **2**. Consistent with this, the parent disulfonate dye with no iodines, **0bb**, also accumulates mostly in the lysosomes. However, mitochondrion targeting is not the only factor involved. Compound **2cc** also localized at mitochondria, but it was one of the least potent photosensitizers in series **2**. We suggest the explanation for this is that more of this relatively

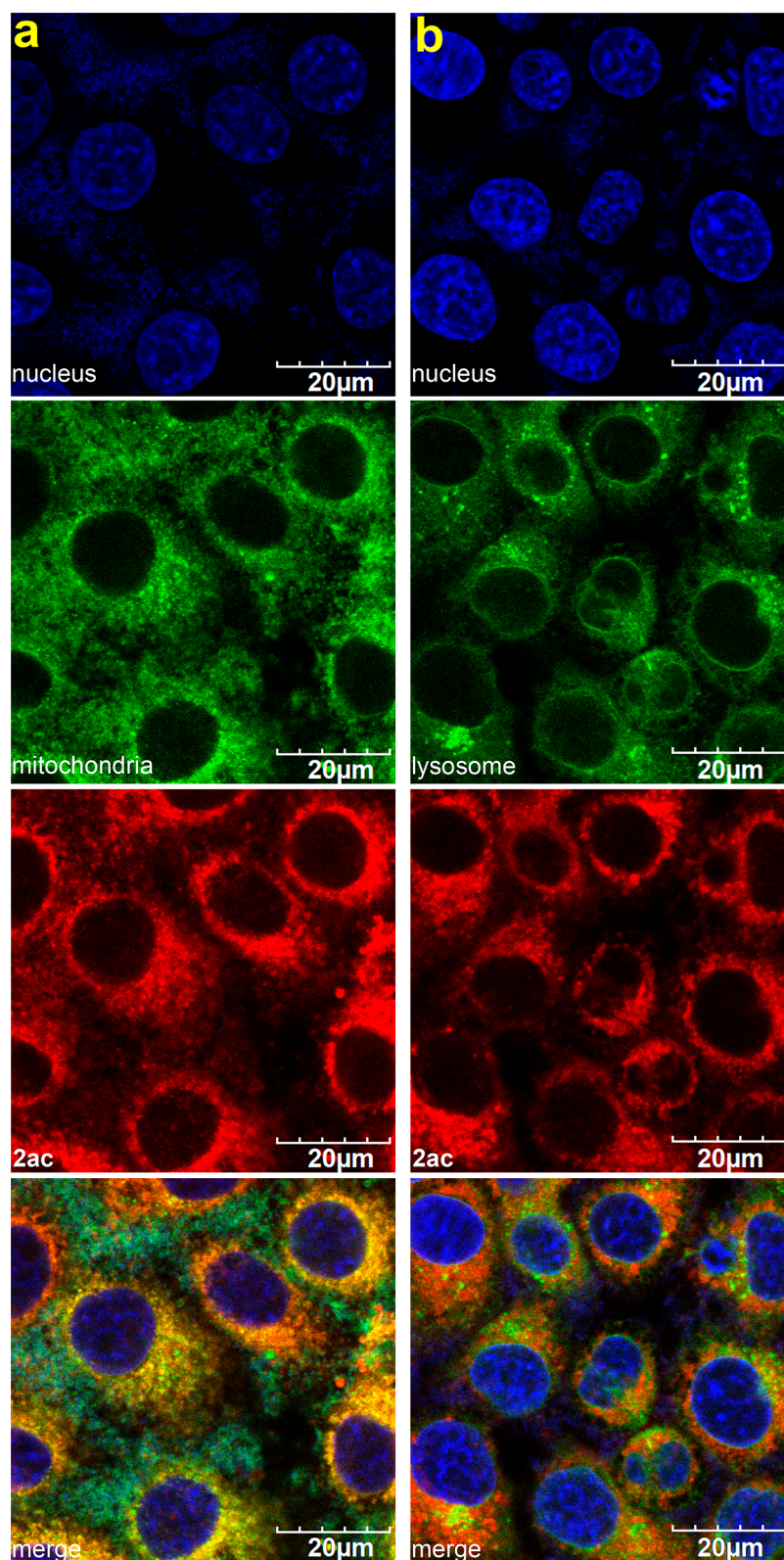


**Figure 5.** Confocal imaging of **2ac** with (a) MitoTracker Green (Pearson's  $R$  value = 0.70) and (b) LysoTracker Green (Pearson's  $R$  value = 0.68). **2ac** internalized more in mitochondria than lysosomes.

hydrophilic dye is retained in the membrane, and this is not accounted for in relative colocalization studies that only consider the dye inside the cell.

Finally, uptake of photosensitizers via overexpressed OATPs is potentially useful for targeting PDT agents, most of which

have a dual function; i.e., they are theranostics for imaging and therapy. Parenthetically, we note that **2bb** is less suitable for conjugation to other agents than the novel member of series **2** that has carboxylic acid side chains (denoted **a**). In other words, **2bb** is not amenable to the typical mode of conjugation of

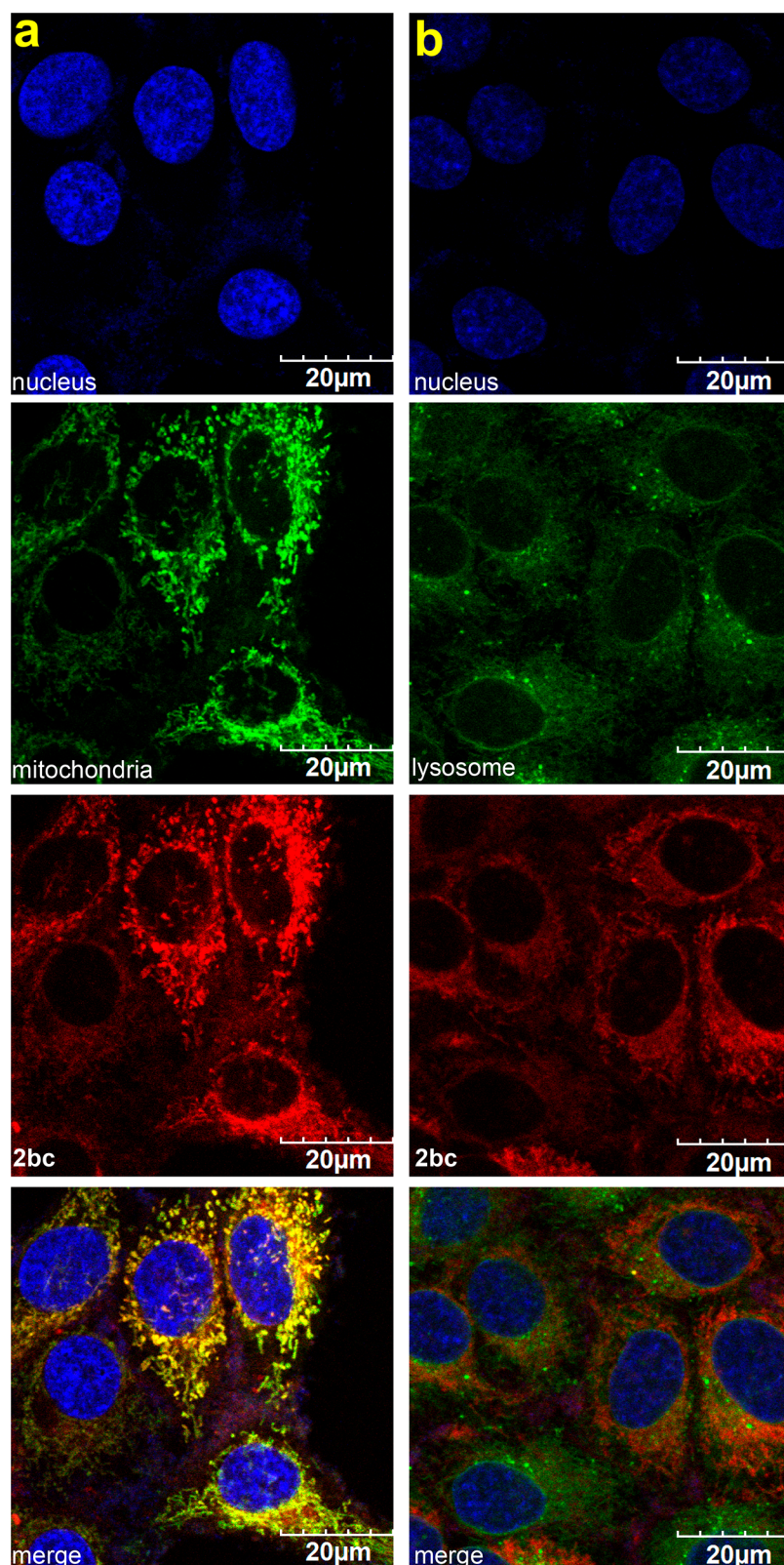


**Figure 6.** Confocal imaging of **2bc** with (a) MitoTracker Green (Pearson's  $R$  value = 0.89) and (b) LysoTracker Green (Pearson's  $R$  value = 0.54). **2bc** internalized more in mitochondria than lysosomes.

fluorescent dyes to biomolecules (e.g., mAbs) via amide bond coupling, but the compounds developed here are. Data in Table 2 shows that conjugation by *meso*-substitution would be possible, but the absorption maxima would be blue-shifted for secondary amine nucleophiles (cf. **4bb**), and if *S*- and *O*-

nucleophiles were used (cf. **3bb** and **5bb**), researchers could anticipate that singlet oxygen production would be cut by around 50%.

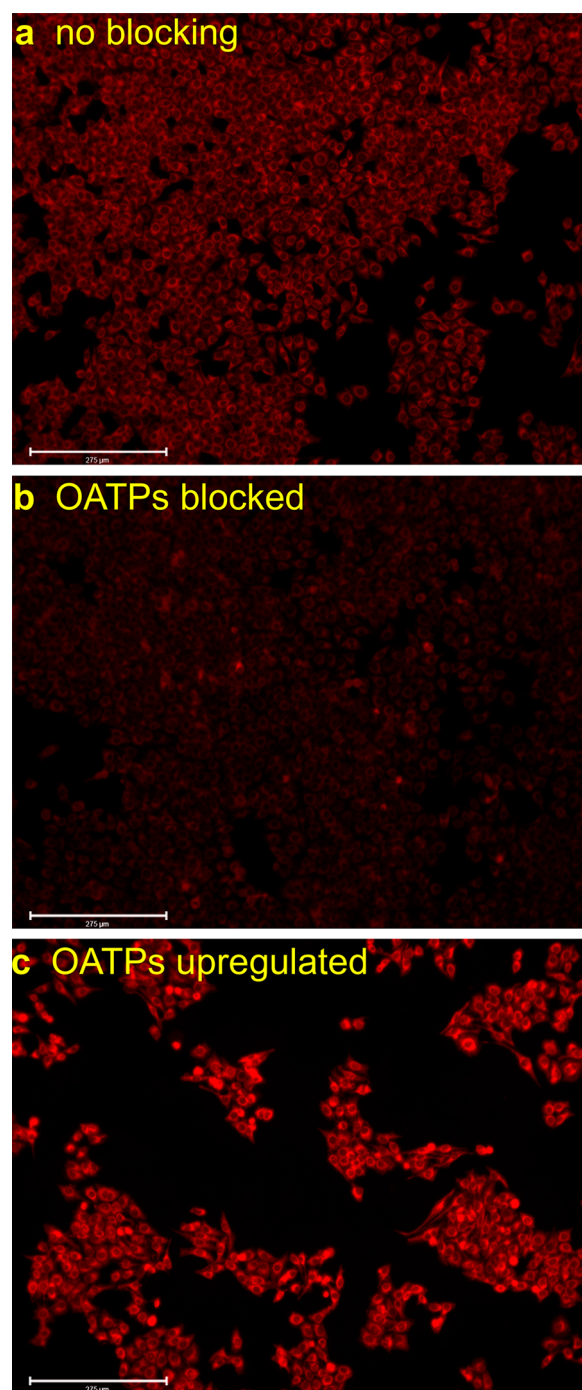


**Figure 7.** Uptake of **2ac** under (a) normal conditions, (b) blocked by a pan-OATP inhibitor BSP (bromosulphophthalein), and (c) under hypoxia conditions induced by DMOG (dimethyloxallylglycine). Scale bar is 275  $\mu\text{m}$ .

## EXPERIMENTAL SECTION

**General Synthesis Procedure.** The reagents were purchased at a high commercial quality (typically 97% or higher) and used without further purification, unless otherwise stated. Compounds **0bb** and **0cc** were purchased from Sigma-Aldrich and abcr GmbH, respectively. The general synthesis of compounds **3a–d** and **1–2** is described below. Detailed synthesis and characterization are described in the [Supporting Information](#).

**Hemicyanine Synthesis (3a–d).** Compound **A** (1 equiv), compound **4a–b** or **5a–b** (1 equiv), and NaOAc (1 equiv) were dissolved in 100 mL of absolute ethanol in a 250 mL round-bottom

**Table 2.** Absorption and Emission Maxima of the *meso*-Substituted Compounds **3bb–5bb**<sup>a</sup> and Quantum Yields for Singlet Oxygen Generation

compound	$\lambda_{\text{abs}}$ (nm)	$\lambda_{\text{em}}$ (nm)	$\Phi(^1\text{O}_2)^b$
<b>2bb</b>	812	825	0.686
<b>3bb</b>	793	816	0.382
<b>4bb</b>	667	800	
<b>5bb</b>	820	832	0.298

<sup>a</sup>Synthesis described in [Figure S5](#). <sup>b</sup> $^1\text{O}_2$  quantum yield measured using ICG ( $\Phi = 0.077$ ) as a reference.

flask. The mixture was heated at 50  $^{\circ}\text{C}$  for 2 h. The solvent was removed, and the crude material was purified by normal phase flash chromatography with  $\text{MeOH}-\text{CH}_2\text{Cl}_2$  (1:25 v/v) for **3a,c** and  $\text{MeOH}-\text{CHCl}_3$  (1:3) for **3b,d** to afford a blue solid.

**Unsymmetric and Symmetric Cyanine Synthesis (1–2).** Compound **3a–d** (1 equiv), compound **4a–c** or **5a–b** (1 equiv), and NaOAc (1 equiv) were dissolved in 50 mL of absolute ethanol in a 100 mL round-bottom flask. The mixture was refluxed for 3 h. The solvent was removed, and the crude was purified by reversed-phase prep HPLC.

HepG2 cells were grown in Dulbecco's modified Eagle's medium (DMEM) containing 10% fetal bovine serum (FBS). Cells were grown in an incubator at 37  $^{\circ}\text{C}$  with a humidified atmosphere containing 5%  $\text{CO}_2$ . Cells were grown in a T-75 culture flask until 70% confluency before splitting into the next passage.

**Fluorescence Quantum Yield Measurements.** Fluorescence quantum yield was determined according to a previous literature procedure.<sup>50</sup> The fluorescence emission spectra of compounds **0–2** were determined in PBS 7.4 (0.1% CrEL) using a Cary-Varian 100 UV–vis NIR spectrophotometer. Samples in PBS were excited in 1 cm path length cuvettes at 750 nm, and integrated emission (760–900) was quantified, keeping the maximum absorbance below 0.1. ICG in DMSO (QY 0.13) was used as the internal standard to do the calculations. Briefly, the integrated fluorescence intensity was plotted against absorbance at different concentrations to generate a gradient, which is proportional to the quantum yield of the samples.

$$\Phi_x = \Phi_{\text{st}}(\text{grad}_x / \text{grad}_{\text{st}})(\eta_x^2 / \eta_{\text{st}}^2) \quad (1)$$

$\Phi_{\text{st}}$  represents the quantum yield of the standard;  $\Phi_x$  represents the quantum yield of the unknown, and grad is the slope of the best linear fit.  $\eta$  is the refractive index of the solvent used, and subscripts x and st denote the unknown and the standard, respectively.

**Singlet Oxygen Detection.**<sup>51</sup> Singlet oxygen generation of compounds **0–2** was determined using 780 nm LEDs (Thor Lab, LED780E) embedded on a 24-well plate holder. Sample solutions were prepared in PBS 7.4 (0.1% CrEL) at a concentration of 5  $\mu\text{M}$  in a 24-well plate. DPBP (1 mM) was prepared in DMSO and diluted to 80  $\mu\text{M}$  in PBS 7.4 (0.1% CrEL). The decrease in absorbance was measured at 418 nm every 1 min for 10 min by a BioTek Synergy 4 microplate reader. The rate of change of absorbance is plotted against irradiation time.

$$\Phi_x = \Phi_{\text{st}}(\text{grad}_x/\text{grad}_{\text{st}})(F_{\text{st}}/F_x) \quad (2)$$

$\Phi_{\text{st}}$  represents the quantum yield of the standard;  $\Phi_x$  represents the quantum yield of the unknown, and grad is the slope of the best linear fit.  $F$  stands for the absorption correction factor ( $F = 1 - 10^{-\text{abs}}$ ; abs represents absorbance), and subscripts x and st denote the unknown and the standard, respectively.

**Photostability.** The photostability of compounds **0–2** was compared by irradiating samples under 780 nm LEDs (Thor Lab, LED780E). The compounds were dissolved in PBS 7.4 (0.1% CrEL) to give a concentration of 10  $\mu\text{M}$ . The decrease in absorbance at 780 nm was measured every 2 min for 10 min and then every 10 min interval for 60 min by a BioTek Synergy 4 microplate reader. The decrease in absorbance was plotted against time.

**Live Cell Staining.** Intracellular localization of dyes with the HepG2 cells was measured using an Olympus Fluoview FV1000 microscope. The images were taken at  $60\times/1.20$  water immersed objective. The lysosome, mitochondrion, and nucleus were stained using LysoTracker Green DND 26, Mitotracker Green FM, and NucBlue, respectively, bought from Life Technologies. A 488 nm laser was used for the green channel; a 405 nm laser was used for the nucleus, and a 633 nm laser was used for compound **2**.

Briefly, 50000 cells were seeded on 4-well chambers (Nunc Lab-Tek) and allowed to adhere overnight. The cells were incubated with 20  $\mu\text{M}$  compound **2** for 30 min, washed twice with PBS, and incubated with organelle stains according to the manufacturer's instructions. The cells were washed twice again and stained with NucBlue for 10 min. The localization of **2ac** and **2bc** in organelles was quantified using ImageJ (coloc2 plug in).

**Blocking Study.** The mode of uptake of **2ac** was determined on an Evos FL Imaging System (ThermoFisher). The images were taken at  $10\times/0.4$ . Briefly, cells were either preblocked with 250  $\mu\text{M}$  BSP for 10 min or treated with 1 mM DMOG for 24 h before treating with the dye. After 30 min of incubation, cells were washed twice with PBS and stained with NucBlue for 10 min and taken for imaging. The amount of uptake was quantified by using Image Studio Lite (version 5.2).

**Cytotoxicity Assays.** Approximately 5000 HepG2 cells/well were seeded on a 96-well plate containing 10% fetal bovine serum. Cells were allowed to adhere overnight before test compounds were added. Stock solutions of **2** (0.02 M in DMSO) were diluted with a protein-free medium (PFHM-II) to make the desired final concentrations varying from 0.01 to 80  $\mu\text{M}$ . The cells were incubated with the desired concentration for 48 h. The cell viabilities were calculated using an AlamarBlue assay. Briefly, 10  $\mu\text{L}$  of AlamarBlue Reagent was incubated for an additional 2 h, and the fluorescence was measured with an excitation at 560 nm and emission wavelength at 590 nm with a BioTek Synergy 4 microplate reader. The viability of each cell line in response to the treatment with tested compounds was calculated as % dead cells =  $100 - (\text{OD treated}/\text{OD control}) \times 100$ .

**Photocytotoxicity Assays.** Approximately 5000 cells in DMEM/F12 containing 10% FBS were seeded in a 96-well plate. Cells were allowed to adhere overnight before test compounds were added. Stock solutions of **2** (0.02 M in DMSO) were diluted with a protein-free medium (PFHM-II) to make the desired final concentrations varying from 1 to 10  $\mu\text{M}$ . The cells were treated with desired concentrations of compound for 1 h. Afterward, cells were washed with PBS twice, and the culture medium was changed to ACAS. LED light (3.8 mW/cm<sup>2</sup>) was irradiated on the cells for 10 min, and the cells were incubated in darkness for 24 h. Cell viabilities were determined by an AlamarBlue assay as mentioned above.

## ■ ASSOCIATED CONTENT

### Supporting Information

The Supporting Information is available free of charge on the ACS Publications website at DOI: 10.1021/acsabm.8b00414.

Synthesis and NMR spectra, HRMS for compounds **3a–d** and series of compounds **1–5**, structural and photophysical properties (brightness, UV/vis), <sup>1</sup>O<sub>2</sub> production, photostability, and cytotoxicity for compounds **0–2**, and

organelle localization and blocking study of compound **2** (PDF)

## ■ AUTHOR INFORMATION

### Corresponding Author

\*E-mail: [burgess@tamu.edu](mailto:burgess@tamu.edu).

### ORCID

Syed Muhammad Usama: 0000-0002-7487-1568

Sopida Thavornpradit: 0000-0002-4654-5116

Kevin Burgess: 0000-0001-6597-1842

### Notes

The authors declare no competing financial interest.

## ■ ACKNOWLEDGMENTS

We thank the DoD BCRP Breakthrough Award (BC141561), CPRIT (RP150559 and RP170144), Robert A. Welch Foundation (A-1121), Texas A&M University (RP180875), and NSF (M1603497) for financial support. The NMR instrumentation at Texas A&M University was supported by a grant from the National Science Foundation (DBI-9970232) and the Texas A&M University System. The use of the Microscopy and Imaging Center facility at Texas A&M University is acknowledged. The Olympus FV1000 confocal microscope acquisition was supported by the Office of the Vice President for Research at Texas A&M University. The use of Chemistry Mass Spectrometry Facility is acknowledged. Marvin was used for drawing, displaying, and characterizing chemical structures, substructures, and reactions, Marvin 17.21.0, ChemAxon.

## ■ REFERENCES

- (1) Ormond, A. B.; Freeman, H. S. Dye Sensitizers for Photodynamic Therapy. *Materials* **2013**, *6*, 817–840.
- (2) Celli, J. P.; Spring, B. Q.; Rizvi, I.; Evans, C. L.; Samkoe, K. S.; Verma, S.; Pogue, B. W.; Hasan, T. Imaging and Photodynamic Therapy: Mechanisms, Monitoring, and Optimization. *Chem. Rev.* **2010**, *110*, 2795–2838.
- (3) Agostinis, P.; Berg, K.; Cengel Keith, A.; Foster Thomas, H.; Girotti Albert, W.; Gollnick Sandra, O.; Hahn Stephen, M.; Hamblin Michael, R.; Juzeniene, A.; Kessel, D.; Korbelik, M.; Moan, J.; Mroz, P.; Nowis, D.; Piette, J.; Wilson Brian, C.; Golab, J. Photodynamic Therapy of Cancer: An Update. *Ca-Cancer J. Clin.* **2011**, *61*, 250–281.
- (4) Foote, C. S. Definition of Type I and Type II Photosensitized Oxidation. *Photochem. Photobiol.* **1991**, *54*, 659.
- (5) Plaetzer, K.; Krammer, B.; Berlanda, J.; Berr, F.; Kiesslich, T. Photophysics and Photochemistry of photodynamic Therapy: Fundamental Aspects. *Lasers Med. Sci.* **2009**, *24*, 259–268.
- (6) Mehraban, N.; Freeman, H. S. Developments in PDT Sensitizers for Increased Selectivity and Singlet Oxygen Production. *Materials* **2015**, *8*, 4421–4456.
- (7) Pedersen, B. W.; Sinks, L. E.; Breitenbach, T.; Schack, N. B.; Vinogradov, S. A.; Ogilby, P. R. Single Cell Responses to Spatially Controlled Photosensitized Production of Extracellular Singlet Oxygen. *Photochem. Photobiol.* **2011**, *87*, 1077–1091.
- (8) Ogilby, P. R. Singlet Oxygen: There is Indeed Something New Under the Sun. *Chem. Soc. Rev.* **2010**, *39*, 3181–3209.
- (9) Schweitzer, C.; Schmidt, R. Physical Mechanisms of Generation and Deactivation of Singlet Oxygen. *Chem. Rev.* **2003**, *103*, 1685–1757.
- (10) da Silva, E. F. F.; Pedersen, B. W.; Breitenbach, T.; Toftegaard, R.; Kuimova, M. K.; Arnaut, L. G.; Ogilby, P. R. Irradiation- and Sensitizer-Dependent Changes in the Lifetime of Intracellular Singlet Oxygen Produced in a Photosensitized Process. *J. Phys. Chem. B* **2012**, *116*, 445–461.

- (11) Ethirajan, M.; Chen, Y.; Joshi, P.; Pandey, R. K. The Role of Porphyrin Chemistry in Tumor Imaging and Photodynamic Therapy. *Chem. Soc. Rev.* **2011**, *40*, 340–362.
- (12) Castano, A. P.; Demidova, T. N.; Hamblin, M. R. Mechanisms in Photodynamic Therapy: Part One - Photosensitizers, Photochemistry and Cellular Localization. *Photodiagn. Photodyn. Ther.* **2004**, *1*, 279–293.
- (13) Zhu, T. C.; Finlay, J. C. The Role of Photodynamic Therapy (PDT) Physics. *Med. Phys.* **2008**, *35*, 3127–3136.
- (14) Yoon, I.; Li Jia, Z.; Shim Young, K. Advance in Photosensitizers and Light delivery for Photodynamic Therapy. *Clin Endosc* **2013**, *46*, 7–23.
- (15) Patel, N.; Pera, P.; Joshi, P.; Dukh, M.; Tabaczynski, W. A.; Sifers, K. E.; Kryman, M.; Cheruku, R. R.; Durrani, F.; Missert, J. R.; Watson, R.; Ohulchanskyy, T. Y.; Tracy, E. C.; Baumann, H.; Pandey, R. K. Highly Effective Dual-Function Near-Infrared (NIR) Photosensitizer for Fluorescence Imaging and Photodynamic Therapy (PDT) of Cancer. *J. Med. Chem.* **2016**, *59*, 9774–9787.
- (16) Santos, P. F.; Reis, L. V.; Almeida, P.; Oliveira, A. S.; Vieira Ferreira, L. F. Singlet Oxygen Generation Ability of Squarylium Cyanine Dyes. *J. Photochem. Photobiol., A* **2003**, *160*, 159–161.
- (17) Wezgowiec, J.; Kotulska, M.; Saczko, J.; Derylo, M. B.; Teissie, J.; Rols, M.-P.; Orio, J.; Garbiec, A.; Kulbacka, J. Cyanines in Photodynamic Reaction Assisted by Reversible Electroporation-In Vitro Study on Human Breast Carcinoma Cells. *Photodiagn. Photodyn. Ther.* **2013**, *10*, 490–502.
- (18) Murakami, L. S.; Ferreira, L. P.; Santos, J. S.; da Silva, R. S.; Nomizo, A.; Kuz'min, V. A.; Borissevitch, I. E. Photocytotoxicity of a Cyanine Dye With Two Chromophores Toward Melanoma and Normal Cells. *Biochim. Biophys. Acta, Gen. Subj.* **2015**, *1850*, 1150–1157.
- (19) James, N. S.; Ohulchanskyy, T. Y.; Chen, Y.; Joshi, P.; Zheng, X.; Goswami, L. N.; Pandey, R. K. Comparative Tumor Imaging and PDT Efficacy of HPPH Conjugated in the Mono- and Di-Forms to Various Polymethine Cyanine Dyes: Part - 2. *Theranostics* **2013**, *3*, 703–718.
- (20) Camerin, M.; Jori, G.; Della Ciana, L.; Fabbioni, S.; Bonacchi, S.; Montalti, M.; Prodi, L. Photothermal Sensitisation and Therapeutic Properties of a Novel Far-Red Absorbing Cyanine. *Photochem. Photobiol. Sci.* **2009**, *8*, 1422–1431.
- (21) Santos, P. F.; Reis, L. V.; Almeida, P.; Serrano, J. P.; Oliveira, A. S.; Vieira Ferreira, L. F. Efficiency of Singlet Oxygen Generation of Aminosquarylium Cyanines. *J. Photochem. Photobiol., A* **2004**, *163*, 267–269.
- (22) Santos, P. F.; Reis, L. V.; Duarte, I.; Serrano, J. P.; Almeida, P.; Oliveira, A. S.; Ferreira, L. F. V. Synthesis and Photochemical Evaluation of Iodinated Squarylium Cyanine Dyes. *Helv. Chim. Acta* **2005**, *88*, 1135–1143.
- (23) Pandey, R. K.; James, N.; Chen, Y.; Dobhal, M. P. Cyanine Dye-Based Compounds for Tumor Imaging With and Without Photodynamic Therapy. *Top. Heterocycl. Chem.* **2008**, *14*, 41–74.
- (24) Cardillo, J. A.; Jorge, R.; Costa, R. A.; Nunes, S. M. T.; Lavinsky, D.; Kuppermann, B. D.; Tedesco, A. C.; Farah, M. E. Experimental Selective Choriocapillaris Photothrombosis Using a Modified Indocyanine Green Formulation. *Br. J. Ophthalmol.* **2008**, *92*, 276–280.
- (25) Tan, X.; Luo, S.; Wang, D.; Su, Y.; Cheng, T.; Shi, C. A NIR Heptamethine Dye With Intrinsic Cancer Targeting, Imaging and Photosensitizing Properties. *Biomaterials* **2012**, *33*, 2230–2239.
- (26) Luo, S.; Tan, X.; Qi, Q.; Guo, Q.; Ran, X.; Zhang, L.; Zhang, E.; Liang, Y.; Weng, L.; Zheng, H.; Cheng, T.; Su, Y.; Shi, C. A Multifunctional Heptamethine Near-Infrared Dye for Cancer Therapy. *Biomaterials* **2013**, *34*, 2244–2251.
- (27) Luo, S.; Tan, X.; Fang, S.; Wang, Y.; Liu, T.; Wang, X.; Yuan, Y.; Sun, H.; Qi, Q.; Shi, C. Mitochondria-Targeted Small-Molecule Fluorophores for Dual Modal Cancer Phototherapy. *Adv. Funct. Mater.* **2016**, *26*, 2826–2835.
- (28) Tan, X.; Luo, S.; Long, L.; Wang, Y.; Wang, D.; Fang, S.; Ouyang, Q.; Su, Y.; Cheng, T.; Shi, C. Structure-Guided Design and Synthesis of a Mitochondria-Targeting Near-Infrared Fluorophore with Multimodal Therapeutic Activities. *Adv. Mater.* **2017**, *29*, 817–840.
- (29) Atchison, J.; Kamila, S.; Nesbitt, H.; Logan, K. A.; Nicholas, D. M.; Fowley, C.; Davis, J.; Callan, B.; McHale, A. P.; Callan, J. F. Iodinated Cyanine Dyes: A New Class of Sensitisers for use in NIR Activated Photodynamic Therapy (PDT). *Chem. Commun.* **2017**, *53*, 2009–2012.
- (30) Guan, Y.; Zhang, Y.; Xiao, L.; Li, J.; Wang, J.-p.; Chordia, M. D.; Liu, Z.-Q.; Chung, L. W. K.; Yue, W.; Pan, D. Improving Therapeutic Potential of Farnesylthiosalicylic Acid: Tumor Specific Delivery via Conjugation with Heptamethine Cyanine Dye. *Mol. Pharmaceutics* **2017**, *14*, 1–13.
- (31) Xi, R.; Zhang, J.; Zhang, Y.; Li, S.; Li, Y.; Li, X.; Chen, L.; Li, C. Near-Infrared Asymmetrical Heptamethine Cyanines Specifically Imaging Cancer Cells by Sensing Their Acidic Lysosomal Lumen. *RSC Adv.* **2016**, *6*, 68220–68226.
- (32) van Straten, D.; Mashayekhi, V.; Oliveira, S.; de Bruijn, H.; Robinson, D.; Oliveira, S. Oncologic Photodynamic Therapy: Basic Principles, Current Clinical Status and Future Directions. *Cancers* **2017**, *9*, 19–63.
- (33) Henary, M.; Levitz, A. Synthesis and Applications of Unsymmetrical Carbocyanine Dyes. *Dyes Pigm.* **2013**, *99*, 1107–1116.
- (34) Gorman, A.; Killoran, J.; O'Shea, C.; Kenna, T.; Gallagher, W. M.; O'Shea, D. F. In Vitro Demonstration of the Heavy-Atom Effect for Photodynamic Therapy. *J. Am. Chem. Soc.* **2004**, *126*, 10619–10631.
- (35) Yuan, J.; Yi, X.; Yan, F.; Wang, F.; Qin, W.; Wu, G.; Yang, X.; Shao, C.; Chung, L. W. K. Near-Infrared Fluorescence Imaging of Prostate Cancer Using Heptamethine Carbocyanine Dyes. *Mol. Med. Rep.* **2015**, *11*, 821–828.
- (36) Zhao, N.; Zhang, C.; Zhao, Y.; Bai, B.; An, J.; Zhang, H.; Shi, C.; Wu Jason, B. Optical Imaging of Gastric Cancer With Near-Infrared Heptamethine Carbocyanine Fluorescence Dyes. *Oncotarget* **2016**, *7*, 57277–57289.
- (37) Yang, X.; Shao, C.; Wang, R.; Chu, C.-Y.; Hu, P.; Master, V.; Osunkoya, A. O.; Kim, H. L.; Zhau, H. E.; Chung, L. W. K. Optical Imaging of Kidney Cancer with Novel Near Infrared Heptamethine Carbocyanine Fluorescent Dyes. *J. Urol.* **2013**, *189*, 702–710.
- (38) Wu, J. B.; Shi, C.; Chu, G. C.-Y.; Xu, Q.; Zhang, Y.; Li, Q.; Yu, J. S.; Zhau, H. E.; Chung, L. W. K. Near-Infrared Fluorescence Heptamethine Carbocyanine Dyes Mediate Imaging and Targeted Drug Delivery for Human Brain Tumor. *Biomaterials* **2015**, *67*, 1–10.
- (39) Kushal, S.; Wang, W.; Vaikari, V. P.; Kota, R.; Chen, K.; Yeh, T.-S.; Jhaveri, N.; Groshen, S. L.; Olenyuk, B. Z.; Chen, T. C.; Hofman, F. M.; Shih, J. C. Monoamine oxidase A (MAO A) Inhibitors Decrease Glioma Progression. *Oncotarget* **2016**, *7*, 13842–13853.
- (40) An, J.; Zhao, N.; Zhang, C.; Zhao, Y.; Tan, D.; Zhao, Y.; Bai, B.; Zhang, H.; Shi, C.; An, J.; Wu Boyang, J. Heptamethine Carbocyanine DZ-1 Dye for Near-Infrared Fluorescence Imaging of Hepatocellular Carcinoma. *Oncotarget* **2017**, *8*, 56880–56892.
- (41) Yang, X.; Shi, C.; Tong, R.; Qian, W.; Zhau, H. E.; Wang, R.; Zhu, G.; Cheng, J.; Yang, V. W.; Cheng, T.; Henary, M.; Strekowski, L.; Chung, L. W. K. Near IR Heptamethine Cyanine Dye-Mediated Cancer Imaging. *Clin. Cancer Res.* **2010**, *16*, 2833–2844.
- (42) Zhang, C.; Liu, T.; Su, Y.; Luo, S.; Zhu, Y.; Tan, X.; Fan, S.; Zhang, L.; Zhou, Y.; Cheng, T.; Shi, C. A Near-Infrared Fluorescent Heptamethine Indocyanine Dye with Preferential Tumor Accumulation for In Vivo Imaging. *Biomaterials* **2010**, *31*, 6612–6617.
- (43) Luo, S.; Yang, X.; Shi, C. Newly Emerging Theranostic Agents for Simultaneous Cancer targeted Imaging and Therapy. *Curr. Med. Chem.* **2016**, *23*, 483–497.
- (44) Gao, M.; Yu, F.; Lv, C.; Choo, J.; Chen, L. Fluorescent Chemical Probes for Accurate Tumor Diagnosis and Targeting Therapy. *Chem. Soc. Rev.* **2017**, *46*, 2237–2271.
- (45) Thakkar, N.; Lockhart, A. C.; Lee, W. Role of Organic Anion-Transporting Polypeptides (OATPs) in Cancer Therapy. *AAPS J.* **2015**, *17*, 535–545.
- (46) Kotsampasakou, E.; Ecker, G. F. Organic Anion Transporting Polypeptides as Drug Targets, in Transporters as Drug Targets. In *Transporters as Drug Targets*; Sitte, H. H., Ecker, G. F., Mannhold, R., Buschmann, H., Clausen, R. P., Eds.; Wiley-VCH Verlag GmbH & Co. KGaA: Hoboken, NJ, 2017; pp 271–324.

(47) Wu, J. B.; Shao, C.; Li, X.; Shi, C.; Li, Q.; Hu, P.; Chen, Y.-T.; Dou, X.; Sahu, D.; Li, W.; Harada, H.; Zhang, Y.; Wang, R.; Zhau, H. E.; Chung, L. W. K. Near-Infrared Fluorescence Imaging of Cancer Mediated by Tumor Hypoxia and HIF1 $\alpha$ /OATPs Signaling Axis. *Biomaterials* **2014**, *35*, 8175–8185.

(48) Njiojob, C. N.; Owens, E. A.; Narayana, L.; Hyun, H.; Choi, H. S.; Henary, M. Tailored Near-Infrared Contrast Agents for Image Guided Surgery. *J. Med. Chem.* **2015**, *58*, 2845–2854.

(49) James, N. S.; Chen, Y.; Joshi, P.; Ohulchanskyy, T. Y.; Ethirajan, M.; Henary, M.; Strekowski, L.; Pandey, R. K. Evaluation of Polymethine Dyes as Potential Probes for Near Infrared Fluorescence Imaging of Tumors: part - 1. *Theranostics* **2013**, *3*, 692–702.

(50) Mottram, L. F.; Boonyarattanakalin, S.; Kovel, R. E.; Peterson, B. R. The Pennsylvania Green Fluorophore: A Hybrid of Oregon Green and Tokyo Green for the Construction of Hydrophobic and pH-Insensitive Molecular Probes. *Org. Lett.* **2006**, *8*, 581–584.

(51) Tian, J.; Zhou, J.; Shen, Z.; Ding, L.; Yu, J.-S.; Ju, H. A pH-Activatable and Aniline-Substituted Photosensitizer for Near-Infrared Cancer Theranostics. *Chem. Sci.* **2015**, *6*, 5969–5977.

# Targeted Maytansinoid Conjugate Improves Therapeutic Index for Metastatic Breast Cancer Cells

Zhengyang Jiang,<sup>†</sup> Zhen Yang,<sup>‡</sup> Feng Li,<sup>‡</sup> Zheng Li,<sup>\*,‡</sup> Nathan Fishkin,<sup>§,||</sup> and Kevin Burgess<sup>\*,†,||</sup>

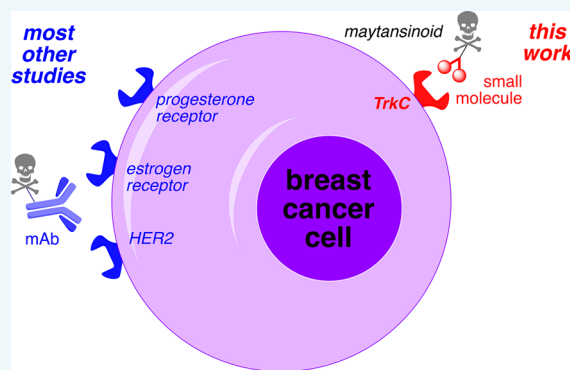
<sup>†</sup>Department of Chemistry, Texas A & M University, Box 30012, College Station, Texas 77842, United States

<sup>‡</sup>Center for Bioenergetics, Houston Methodist Research Institute, 6670 Bertner Avenue, Houston, Texas 77030, United States

<sup>§</sup>ImmunoGen, 830 Winter Street, Waltham, Massachusetts 02451, United States

## S Supporting Information

**ABSTRACT:** This study was undertaken to target cell surface receptors other than the ones typically associated with breast cancer {estrogen receptor (ER), progesterone receptor (PR), and human epidermal growth factor receptor 2 (HER2)}. It was also launched to use small molecules other than those most widely used for active targeting in general (e.g. folate and carbonic anhydrase IX ligands). Specifically, the focus of this study was on unique small molecules that bind the TrkC receptor, which is overexpressed in metastatic breast cancer. A conjugate (**1**) of a TrkC-targeting small molecule and the highly cytotoxic warhead, DM4 (a maytansinoid), was prepared. Cellular studies featuring TrkC<sup>+</sup> and TrkC<sup>−</sup> human breast cells indicated this conjugate might have a better therapeutic effect than DM4 alone. It emerged that the conjugate **1** was very efficacious *in vivo*, completely ablating orthotopic 4T1 breast tumor in one case and dramatically reducing the tumor size in four other mice. Throughout, no significant weight loss or obvious neurotoxic effects were observed in the animals tested.



## INTRODUCTION

Cancer is not a single disease. Primary tumors originating from the same organ but in different individuals express different profiles of cell-surface receptors, and those fingerprints indicate prognoses and treatment strategies for personalized care.<sup>1</sup> Breast cancer, for instance, can be classified in terms of expression of the ER, PR, and HER2.<sup>2,3</sup> If all three of these receptors are *not* expressed (*triple negative*), the tumor has a high tendency for metastatic spread, and the prognoses is relatively poor. It is unlikely that profiling for just these three receptors, however, is optimal for all breast cancer types.

Cell surface receptors overexpressed on breast (and other) types of cancers can be used to favorably skew the pharmacokinetics of drug binding, to increase the local concentration of chemotherapeutics around the tumor, minimize damage to surrounding healthy tissues, and thereby increase therapeutic index (Figure 1). This is important because therapeutic windows for

that can be administered to patients without serious side effects. Directing cytotoxic drugs to cancer cells via cell surface receptors is “active targeting”, which in this article we abbreviate to “targeting”.

Humanized monoclonal antibodies (humAb) raised to receptors expressed on the surface of cancer cells have proven therapeutic value. For instance, one of the first FDA approved humAb's for breast cancer, trastuzumab (Herceptin), binds HER2 extracellular domain and downregulates cell signaling pathways that lead to proliferation.<sup>4,5</sup> This development paved the way to the first mAb–drug conjugates to be FDA approved for solid tumors: ado-trastuzumab emtansine (Kadcyla) which is typical of a now-broader class of antibody drug conjugates (ADCs) that are used to treat patients today for various forms of cancer.<sup>6</sup> Ado-trastuzumab emtansine has a dual function: the mAb part binds HER2 and inhibits proliferation, while the emtansine cargo (emtansine is a highly cytotoxic derivative of the macrolide maytansine,<sup>7</sup> i.e. a maytansinoid<sup>8,9</sup>) is preferentially delivered to tumors over healthy tissue.<sup>10,11</sup> Thus, ado-trastuzumab emtansine localizes the maytansinoid in tumors, decreasing the therapeutic dose of that cargo relative to the free macrolide, increasing the maximum tolerated dose by suppressing the cytotoxicity of the cargo until it is liberated, thus raising the therapeutic index of the ADC relative to the parent maytansinoid.

$$\text{therapeutic index} = \frac{\text{tolerated dose}_{50}}{\text{effective dose}_{50} \text{ in humans}}$$

increases with decreased toxicity

decreases with increased potency

**Figure 1.** Active targeting can increase therapeutic indices by increasing the potency and decreasing the toxicity of a warhead in a conjugate.

cytotoxic substances that are not directly targeted to tumor cells are notoriously narrow, and this severely limits dose levels

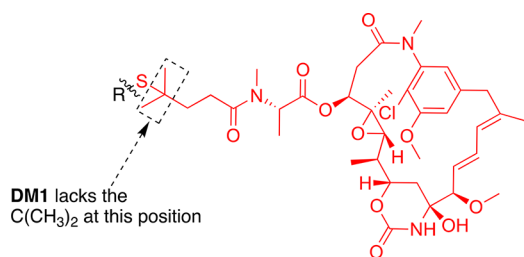
**Received:** May 16, 2018

**Revised:** July 16, 2018

**Published:** August 13, 2018

There are intrinsic advantages and disadvantages to ADCs. One major attribute is that methods to generate mAbs to cell surface receptors, and others to humanize them, have high success rates.<sup>12</sup> A second advantage is that mAbs have high affinities for the targeted receptors. Paradoxically, those high affinities (and the size of Abs) mean that mAbs tend to accumulate around the surface of tumor cells where they first encountered receptor antigens and compressed vascular structure prevents permeation to the tumor core.<sup>13</sup> Thus, solid tumors are said to possess “antigen barriers”.<sup>14–16</sup> Second, relatively slow *in vivo* clearances of mAbs mean that ADCs tend to remain in circulation outside tumors where they can damage healthy tissues, decreasing their therapeutic indices.<sup>17–19</sup> A third major limitation originates in the difficulties encountered when attempting to obtain batch-to-batch reproducibility with the same Ab to cargo payload.

Maytansine alkaloids (like that in ado-trastuzumab maytansine) are one of the extremely cytotoxic cargoes favored in development of ADCs.<sup>6</sup> In cells, they interact with tubulin preventing its assembly into microtubule fibers, thus inhibiting cell division.<sup>20</sup> Free maytansinoids tend to be too toxic for chemotherapy; in clinical trials from 1977 to 1984, they were evaluated in 35 different types of tumor in over 800 patients, but complete response was only found in one case and partial response in a few others.<sup>8</sup> Maytansinoids are too destructive to



DM4  
R = H

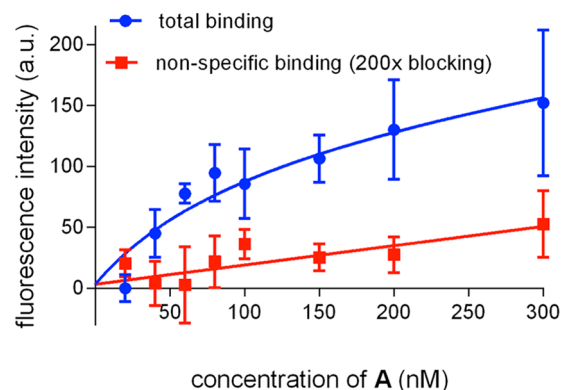
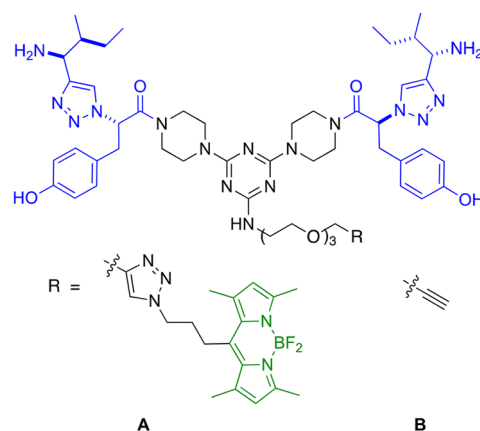
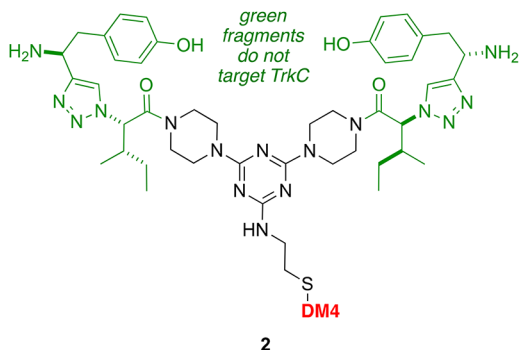
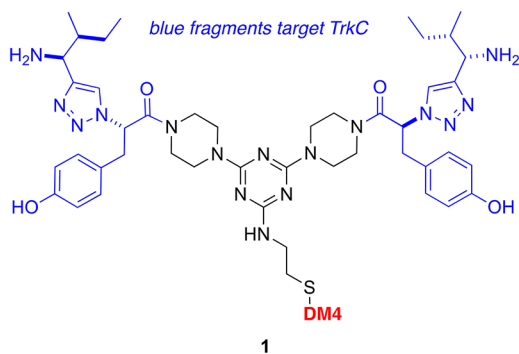


**Figure 2.** Cell-based compound dissociation constant measurements indicated  $K_d = 112 \pm 74$  nM, based on 3 parallel experiments, calculated using GraphPad Prism 6.

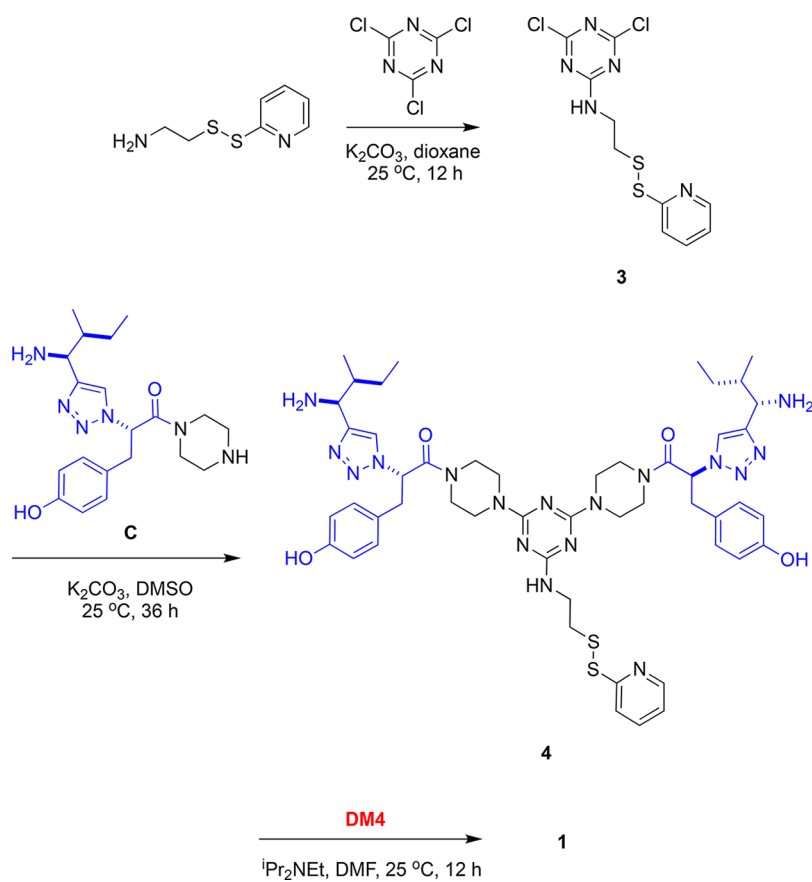
healthy tissue to be used safely without conjugation, but they are ideal for targeted approaches.

Small molecule targeting agents have entirely different, and complementary, disadvantages and advantages relative to ADCs.<sup>21</sup> First, the pool of molecules that bind appropriate cell surface receptors is relatively small, hence the number of appropriate targets is limited.<sup>22,23</sup> Affinities of small molecules for cell surface receptors tend to be lower than mAbs binding the same targets, but this, and the fact that their lower molecular masses lead to more rapid and extensive distribution *in vivo*, and allow them to cross antigen barriers and permeate throughout tumor interiors.<sup>24</sup> Moreover, small molecules having targeting and cytotoxic fragments tend to be more rapidly cleared *in vivo* than ADCs hence minimizing their relative damage to healthy tissues. Other factors that also favor use of small molecule targeting groups include cost, shelf life, batch-to-batch reproducibility, lack of ambiguity when conjugating cytotoxic cargoes,<sup>25</sup> and the fact that even Abs can cause side effects related to residual immunogenicity.

Folate,<sup>26</sup> carbonic anhydrase IX,<sup>27,28</sup> and prostate-specific antigen ligands are commonly used for targeting conjugates,<sup>29</sup> and these have been tested with maytansinoid derivatives. However, for breast cancer, prostate-specific antigen ligands are not applicable, the levels of folate receptor expression tend to be low,<sup>30</sup> and small molecules that target other receptor types may have useful complementary properties.

Some work from our laboratories has focused on using the tropomyosin kinase receptor-C (TrkC) to target breast cancer (and melanoma).<sup>31,32</sup> More particularly, there is a good

Scheme 1. Synthesis of the Cleavable Targeted DM4 Conjugate



correlation between overexpression of TrkC and *metastatic* breast cancer.<sup>36–42</sup> Throughout we have used a bivalent dipeptide mimic designed in these laboratories to bind TrkC; these are the blue parts of structure 1.<sup>43</sup> An isomer of 1 that has the Ile- and Tyr-like side chains reversed (green fragments in 2) does *not* bind TrkC and is therefore a useful control for nonspecific binding. All our previous work features photodynamic therapy (PDT).<sup>44,45</sup> Active targeting in PDT involves accumulation of the ligand in tumors *and* illumination of those regions; areas that are not illuminated incur less tissue damage, hence there is overall a double targeting effect<sup>35</sup> that increases the therapeutic index.

Research reported in this paper describes, for the first time, use of the TrkC-targeting ligands to deliver a conventional cytotoxic compound *in vivo*, *i.e.* without PDT. Specifically, the cargo used is the maytansinoid DM4 (DM1 and DM4 differ only in that the thiol is connected directly to a methylene, or an extended CMe<sub>2</sub> group, where disulfides from the latter have more favorable rates of cleavage in lysosomes).<sup>46</sup> We hesitated to initiate this work because (i) TrkC receptors are found on healthy tissues in the nervous system; (ii) maytansinoids are extremely toxic as discussed above; and (iii) there would be no double targeting effect (unlike our work on active targeting in PDT). In the worse possible case, TrkC-targeted maytansinoids might negotiate the blood brain barrier and cause catastrophic neurotoxicity issues. In the event, however, the data collected here reveals that was not the case, and a significant reduction in the size of orthotopic TrkC<sup>+</sup> tumors was observed in mice treated with agent 1.

## RESULTS AND DISCUSSION

Initial experiments were performed to establish the affinity of the TrkC targeting fragment of compound 1. This was most

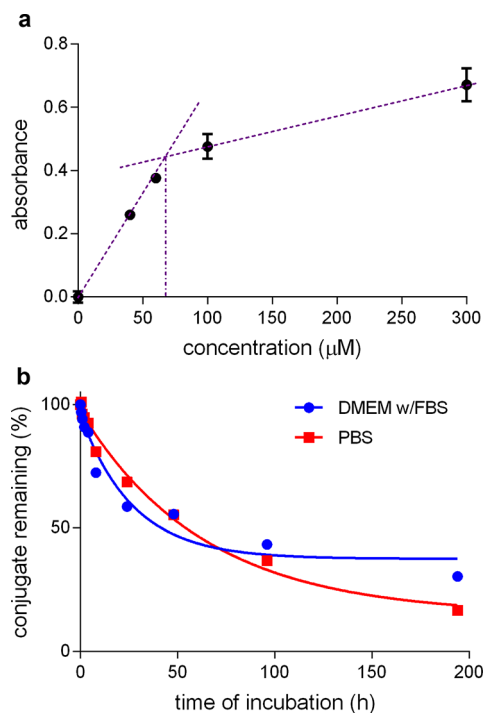


**Figure 3.** a. Solubility of 1 in pH 7.40 PBS with 9% ethanol, 1% DMSO, and 0.5% CrEL. b. Stability of 1 in either DMEM culture medium or pH 7.40 PBS at 37 °C as evidenced by analytical HPLC (initial concentration 20 μM).

conveniently achieved using the fluorescently labeled derivative A<sup>31</sup> on live NIH3T3 cells stably transfected with TrkC (Figure 2).

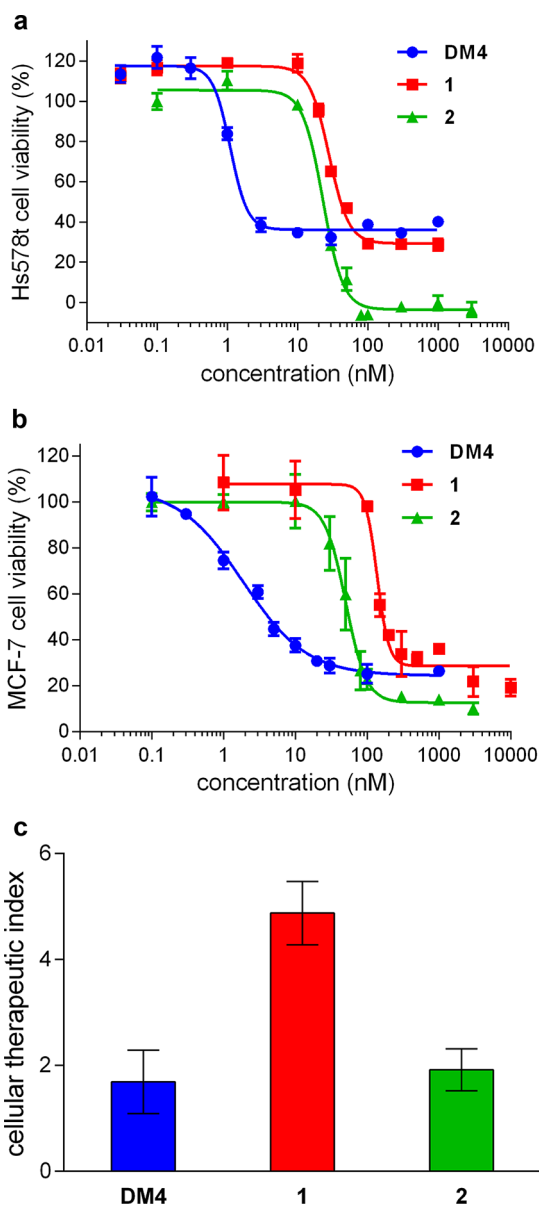


**Figure 4.** Cytotoxicity and cellular therapeutic index comparison. a. and b. Dose responses of DM4, 1, and 2 on human breast cancer cell lines Hs578t (TrkC<sup>+</sup>) and MCF7 (TrkC<sup>-</sup>). Calculated IC<sub>50</sub> values are listed in Supporting Material. c. Calculated *in vitro* therapeutic index based on IC<sub>50</sub> values {IC<sub>50</sub> (MCF-7)/IC<sub>50</sub> (Hs578t)}.

Fluorescence labeling of the cells was measured in the absence (blue line) and presence (red) of a large excess of the unlabeled TrkC-targeting group B.<sup>43,47,48</sup> The extent of specific binding in these experiments is revealed by subtraction of fluorescence with the blocking group B from the corresponding data without it. Analysis of the data revealed a  $K_d$  value of  $112 \pm 74$  nM. A lower  $K_d$  value would have been preferable for active targeting, but we decided this affinity was sufficient to justify synthesis of the key compound.

Scheme 1 outlines how a known amino disulfide<sup>49</sup> was added to cyanuric chloride in the first of three S<sub>N</sub>Ar displacements, wherein the last two involved coupling of the TrkC targeting groups C.<sup>48</sup> Comparison of NMR data for DM4 and the conjugate 1 indicated the coupling step had proceeded without perturbation of the DM4 fragment, as desired (Figure S1).

Experiments were then performed to assess the solubility and stability of the conjugate 1 in pertinent aqueous media. Maytansinoid DM4 is hydrophobic, hence it was impossible to dissolve 1 in buffer at the required concentrations. Consequently, following literature precedent<sup>50</sup> the solubility of the maytansinoid derivative 1 was measured in pH 7.40 phosphate-buffered saline (PBS) with 9% ethanol, 1% DMSO, and 0.5% CrEL (cremophor EL). Thus, using a UV-plate reader assay<sup>51</sup> gave data (Figure 3a) indicating a solubility of 67  $\mu$ M. Figure 3b indicates that conjugate 1 has a half-life of over 40 h in DMEM culture medium or pH 7.40 PBS at 37 °C.

Cell assays were performed on 1 and 2, to determine if *in vivo* studies were clearly justified. Data collected for these experiments are shown in Figure 4a for TrkC<sup>+</sup> cells and in Figure 4b for TrkC<sup>-</sup> cells (Hs578t and MCF-7, respectively). Throughout, DM4 was the most toxic compound, hence the types of conjugates featured here (1 and 2) have reduced cytotoxicity relative to DM4. To our surprise, the isomeric control 2 was marginally more toxic, even for TrkC<sup>+</sup> cells (IC<sub>50</sub> values for 1,  $28.1 \pm 1.9$  nM and 2,  $23.0 \pm 2.5$  nM). However, Figure 4c shows that the reduction of cytotoxicities for conjugate 1 was sufficient to outweigh its less absolute cytotoxicity affording it a superior therapeutic index in cell assays. After binding to TrkC proteins on a cell surface, the conjugate 1 is uptaken into lysosomes via endocytosis,<sup>35</sup> and then free DM4 can be released via intracellular reduction of the disulfide bond.<sup>10</sup> Released maytansinoid DM4 inhibits microtubule function in targeted tumor cells, causes cell cycle arrest, and eventually causes cell death by apoptosis.<sup>52</sup> In any event, cellular therapeutic indices are determined in static systems, whereas pharmacokinetic effects involve dynamic flow of fluids around tumors. In other words, cellular therapeutic indices do not reflect the positive effects active targeting has on pharmacokinetics *in vivo*. For these reasons, an *in vivo* study was initiated.

An *in vivo* toxicity study was carried out using Balb/C mice to compare maytansinoid DM4 and TrkC targeted maytansinoid conjugate 1 at a dose of 30 nmol and 100 nmol per mouse ( $n = 3$ ) via a single intravenous (*i.v.*) injection. We found that mice lost about 10% of body weight at 30 nmol and over 20% of body weight at 100 nmol in the DM4 group, whereas no significant weight loss in the 1 group at both doses was observed (Figure 5). This result demonstrated that TrkC targeted

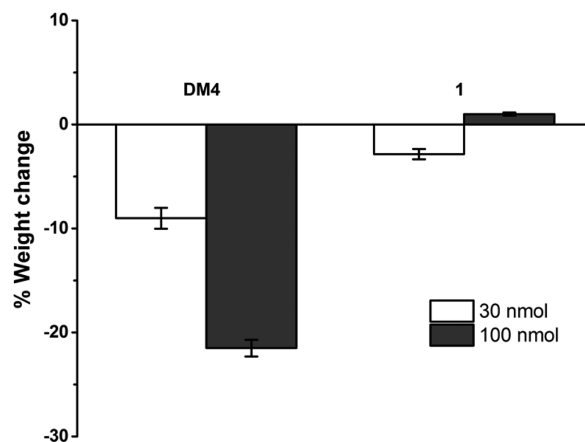


**Figure 5.** Body weight changes after single *i.v.* injection of DM4 and 1 ( $n = 3$ ).

delivery of toxic compound DM4 dramatically reduced systemic toxicity as we expected.

Therapeutic efficacy of targeted maytansinoid conjugate **1** was investigated using 4T1 tumor bearing mice. A scrambled nontargeted maytansinoid conjugate **2**, which does not bind to TrkC, was synthesized and used as a control comparison. As shown in Figure 6a, the administration of **1** efficiently

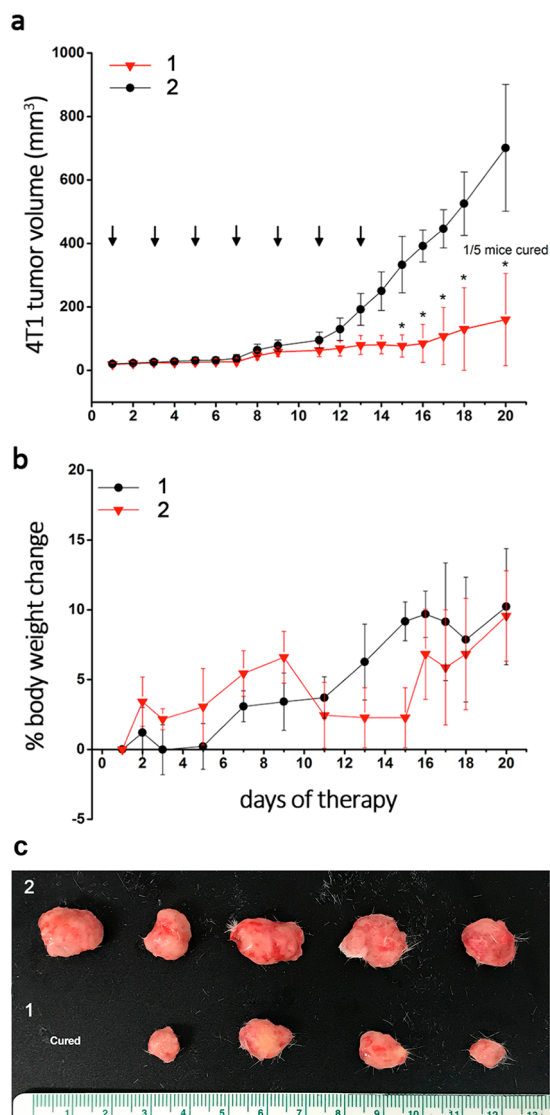


**Figure 6.** *In vivo* therapy study of maytansinoid conjugates **1** and **2**. **a.** Tumor growth curves of 4T1 xenograft bearing mice injected with  $7 \times 30$  nmol **1** as therapy group and **2** as control group. Data represent mean  $\pm$  SD ( $n = 5$  per group). \* indicates one mice of the five tested was cured of tumor in the therapy group. **b.** Weight change of mice shown in **a**. No animals were observed with weight loss  $>15\%$  throughout the therapy study. **c.** Tumors collected from *in vivo* therapeutic studied mice. (Arrows in **a** mark the injection days of therapy. On each arrow marked injection day, the compounds were reconstituted into PBS buffer and injected into mice via tail vein.)

suppressed tumor growth comparing to the control conjugate **2**, which was evidenced by the outcomes that one tumor out of five was cured and the other four were significantly decreased compared with the control group. It strongly supported our hypothesis that conjugating toxic agent such as **DM4** with targeting agent IY significantly promoted therapeutic efficacy in tumor targeting therapy. Meanwhile, animal body weight was also monitored throughout the study (Figure 6b). No

animal was observed with weight loss larger than 15% of its initial weight throughout the study. It suggests that the administration of the therapeutic conjugate **1** was well-tolerated by the animals.

## CONCLUSIONS

Expression of ER, PR, and HER2 is usually applied to classify breast cancers. This is convenient for predicting prognoses and guiding some treatment strategies. However, that does not mean active targeting of other cell surface receptors in breast cancers is not viable. This work establishes that a TrkC ligand with a modest receptor affinity ( $\sim 112$  nM) can be used to deliver a cytotoxic cargo. Unlike our previous studies featuring PDT, this strategy does not have the advantages of double targeting, but nevertheless it is effective against orthotopic 4T1 tumors in mice. The approach outlined here is complementary to active targeting of ER, PR, and/or HER2 and, based on the literature outlined here, probably also to mAb approaches in terms of tumor penetration and residence time *in vivo*.

## ASSOCIATED CONTENT

### Supporting Information

The Supporting Information is available free of charge on the ACS Publications website at DOI: 10.1021/acs.bioconjchem.8b00340.

Detailed syntheses and characterization of the compounds, protocol of biological assays, evidence of TrkC expression on cells applied (PDF)

## AUTHOR INFORMATION

### Corresponding Authors

\*E-mail: [burgess@tamu.edu](mailto:burgess@tamu.edu) (K.B.).

\*E-mail: [zli@HoustonMethodist.org](mailto:zli@HoustonMethodist.org) (Z.L.)

### ORCID

Kevin Burgess: 0000-0001-6597-1842

### Present Address

<sup>||</sup>H3 Biomedicine, 300 Technology Square, Cambridge, MA 02139, USA.

### Notes

The authors declare no competing financial interest.

## ACKNOWLEDGMENTS

Financial support for this project was provided by the National Science Foundation (M1603497), The Robert A. Welch Foundation (A-1121), DoD BCRP Breakthrough Award (BC141561), CPRIT (RP150559 and RP170144), and George and Angelina Kostas Fund at Houston Methodist Research Institute. NMR instrumentation at Texas A&M University was supported by a grant from the National Science Foundation (DBI-9970232) and the Texas A&M University System. DM4 was supplied by ImmunoGen (Waltham, MA).

## REFERENCES

- (1) van 't Veer, L. J., and Bernards, R. (2008) Enabling personalized cancer medicine through analysis of gene-expression patterns. *Nature* 452, 564–570.
- (2) Reis-Filho, J. S., and Tutt, A. N. J. (2008) Triple negative tumours: a critical review. *Histopathology* 52, 108–18.
- (3) Vici, P., Pizzuti, L., Natoli, C., Gamucci, T., Di Lauro, L., Barba, M., Sergi, D., Botti, C., Michelotti, A., Moscetti, L., et al. (2015) Triple positive breast cancer: A distinct subtype? *Cancer Treat. Rev.* 41, 69–76.

- (4) Goldenberg, M. M. (1999) Trastuzumab, a recombinant DNA-derived humanized monoclonal antibody, a novel agent for the treatment of metastatic breast cancer. *Clin. Ther.* 21, 309–318.
- (5) Hudis, C. A. (2007) Trastuzumab - mechanism of action and use in clinical practice. *N. Engl. J. Med.* 357, 39–51.
- (6) Chari, R. V. J., Miller, M. L., and Widdison, W. C. (2014) Antibody-Drug Conjugates: An Emerging Concept in Cancer Therapy. *Angew. Chem., Int. Ed.* 53, 3796–3827.
- (7) Kupchan, S. M., Komoda, Y., Court, W. A., Thomas, G. J., Smith, R. M., Karim, A., Gilmore, C. J., Haltiwanger, R. C., and Bryan, R. F. (1972) Tumor inhibitors. LXXIII. Maytansine, a novel antileukemic ansa macrolide from *Maytenus ovatus*. *J. Am. Chem. Soc.* 94, 1354–6.
- (8) Cassady, J. M., Chan, K. K., Floss, H. G., and Leistner, E. (2004) Recent developments in the maytansinoid antitumor agents. *Chem. Pharm. Bull.* 52, 1–26.
- (9) Widdison, W. C., Wilhelm, S. D., Cavanagh, E. E., Whiteman, K. R., Leece, B. A., Kovtun, Y., Goldmacher, V. S., Xie, H., Steeves, R. M., Lutz, R. J., et al. (2006) Semisynthetic Maytansine Analogs for the Targeted Treatment of Cancer. *J. Med. Chem.* 49, 4392–4408.
- (10) Lewis Phillips, G. D., Li, G., Dugger, D. L., Crocker, L. M., Parsons, K. L., Mai, E., Blaettler, W. A., Lambert, J. M., Chari, R. V. J., Lutz, R. J., et al. (2008) Targeting HER2-Positive Breast Cancer with Trastuzumab-DM1, an Antibody-Cytotoxic Drug Conjugate. *Cancer Res.* 68, 9280–9290.
- (11) Lambert, J. M., and Chari, R. V. J. (2014) Ado-trastuzumab Emtansine (T-DM1): An Antibody-Drug Conjugate (ADC) for HER2-Positive Breast Cancer. *J. Med. Chem.* 57, 6949–6964.
- (12) Li, J., Chen, F., Cona Marlein, M., Feng, Y., Himmelreich, U., Oyen, R., Verbruggen, A., and Ni, Y. (2012) A review on various targeted anticancer therapies. *Target Oncol.* 7, 69–85.
- (13) Dennis, M. S., Jin, H., Dugger, D., Yang, R., McFarland, L., Ogasawara, A., Williams, S., Cole, M. J., Ross, S., and Schwall, R. (2007) Imaging Tumors with an Albumin-Binding Fab, a Novel Tumor-Targeting Agent. *Cancer Res.* 67, 254–261.
- (14) Saga, T., Neumann, R. D., Heya, T., Sato, J., Kinuya, S., Le, N., Paik, C. H., and Weinstein, J. N. (1995) Targeting cancer micrometastases with monoclonal antibodies: a binding-site barrier. *Proc. Natl. Acad. Sci. U. S. A.* 92, 8999–9003.
- (15) Adams, G. P., Schier, R., McCall, A. M., Simmons, H. H., Horak, E. M., Alpaugh, R. K., Marks, J. D., and Weiner, L. M. (2001) High affinity restricts the localization and tumor penetration of single-chain Fv antibody molecules. *Cancer Res.* 61, 4750–4755.
- (16) Rudnick, S. I., Lou, J., Shaller, C. C., Tang, Y., Klein-Szanto, A. J. P., Weiner, L. M., Marks, J. D., and Adams, G. P. (2011) Influence of Affinity and Antigen Internalization on the Uptake and Penetration of Anti-HER2 Antibodies in Solid Tumors. *Cancer Res.* 71, 2250–2259.
- (17) Baluk, P., Morikawa, S., Haskell, A., Mancuso, M., and McDonald, D. M. (2003) Abnormalities of basement membrane on blood vessels and endothelial sprouts in tumors. *Am. J. Pathol.* 163, 1801–1815.
- (18) di Tomaso, E., Capen, D., Haskell, A., Hart, J., Logie, J. J., Jain, R. K., McDonald, D. M., Jones, R., and Munn, L. L. (2005) Mosaic Tumor Vessels: Cellular Basis and Ultrastructure of Focal Regions Lacking Endothelial Cell Markers. *Cancer Res.* 65, 5740–5749.
- (19) O'Connor, R. (2007) The pharmacology of cancer resistance. *Anticancer Res.* 27, 1267–1272.
- (20) Fellous, A., Luduena, R. F., Prasad, V., Jordan, M. A., Anderson, W., Ohayon, R., and Smith, P. T. (1985) Effects of Tau and MAP2 on the interaction of maytansine with tubulin: inhibitory effect of maytansine on vinblastine-induced aggregation of tubulin. *Cancer Res.* 45, 5004–10.
- (21) Srinivasarao, M., Galliford, C. V., and Low, P. S. (2015) Principles in the design of ligand-targeted cancer therapeutics and imaging agents. *Nat. Rev. Drug Discovery* 14, 203–219.
- (22) Srinivasarao, M., and Low, P. S. (2017) Ligand-Targeted Drug Delivery. *Chem. Rev.* 117, 12133–12164.
- (23) Kue, C. S., Kamkaew, A., Burgess, K., Kiew, L. V., Chung, L. Y., and Lee, H. B. (2016) Small Molecules for Active Targeting in Cancer. *Med. Res. Rev.* 36, 494–575.
- (24) Vlashi, E., Sturgis, J. E., Thomas, M., and Low, P. S. (2009) Real Time, Noninvasive Imaging and Quantitation of the Accumulation of Ligand-Targeted Drugs into Receptor-Expressing Solid Tumors. *Mol. Pharmaceutics* 6, 1868–1875.
- (25) Firer, M. A., and Gellerman, G. (2012) Targeted drug delivery for cancer therapy: the other side of antibodies. *J. Hematol. Oncol.* 5, 70.
- (26) Reddy, J. A., Westrick, E., Santhapuram, H. K. R., Howard, S. J., Miller, M. L., Vetzal, M., Vlahov, I., Chari, R. V. J., Goldmacher, V. S., and Leamon, C. P. (2007) Folate Receptor-Specific Antitumor Activity of EC131, a Folate-Maytansinoid Conjugate. *Cancer Res.* 67, 6376–6382.
- (27) Krall, N., Pretto, F., Decurtins, W., Bernardes, G. J. L., Supuran, C. T., and Neri, D. (2014) A small-molecule drug conjugate for the treatment of carbonic anhydrase IX expressing tumors. *Angew. Chem., Int. Ed.* 53, 4231–4235.
- (28) Krall, N., Pretto, F., and Neri, D. (2014) A bivalent small molecule-drug conjugate directed against carbonic anhydrase IX can elicit complete tumour regression in mice. *Chem. Sci.* 5, 3640–3644.
- (29) Kumar, A., Mastren, T., Wang, B., Hsieh, J.-T., Hao, G., and Sun, X. (2016) Design of a Small-Molecule Drug Conjugate for Prostate Cancer Targeted Theranostics. *Bioconjugate Chem.* 27, 1681–1689.
- (30) Necela, B. M., Crozier, J. A., Andorfer, C. A., Lewis-Tuffin, L., Kachergus, J. M., Geiger, X. J., Kalari, K. R., Serie, D. J., Sun, Z., Moreno-Aspitia, A., et al. (2015) Folate receptor- $\alpha$  (FOLR1) expression and function in triple negative tumors. *PLoS One* 10, e0122209.
- (31) Kue, S. C., Kamkaew, A., Lee, H. B., Chung, L. Y., Kiew, L. V., and Burgess, K. (2015) Targeted PDT Agent Eradicates TrkC Expressing Tumors Via Photodynamic Therapy (PDT). *Mol. Pharmaceutics* 12, 212–222.
- (32) Kamkaew, A., Li, F., Li, Z., and Burgess, K. (2017) An agent for optical imaging of TrkC-expressing, breast cancer. *MedChemComm* 8, 1946–1952.
- (33) Kamkaew, A., Fu, N., Cai, W., and Burgess, K. (2017) Novel Small Molecule Probes for Metastatic Melanoma. *ACS Med. Chem. Lett.* 8, 179–184.
- (34) Ko, E., Kamkaew, A., and Burgess, K. (2012) Small Molecules Ligands for Active Targeting of TrkC-expressing Tumor Cells. *ACS Med. Chem. Lett.* 3, 1008–1012.
- (35) Kamkaew, A., and Burgess, K. (2013) Double-targeting Using a TrkC-Ligand Conjugated to Dipyrrometheneboron Difluoride (BODIPY) Based Photodynamic Therapy (PDT) Agent. *J. Med. Chem.* 56, 7608–7614.
- (36) Jin, W., Kim, G.-M., Kim, M.-S., Lim, M.-H., Yun, C.-H., Jeong, J., Nam, J.-S., and Kim, S.-J. (2010) TrkC plays an essential role in breast tumor growth and metastasis. *Carcinogenesis* 31, 1939–1947.
- (37) Jin, W., Yun, C., Jeong, J., Park, Y., Lee, H.-D., and Kim, S.-J. (2008) c-Src Is Required for Tropomyosin Receptor Kinase C (TrkC)-induced Activation of the Phosphatidylinositol 3-Kinase (PI3K)-AKT Pathway. *J. Biol. Chem.* 283, 1391–1400.
- (38) Jin, W., Yun, C., Kwak, M. K., Kim, T. A., and Kim, S. J. (2007) TrkC binds to the type II TGF- $\beta$  receptor to suppress TGF- $\beta$  signaling. *Oncogene* 26, 7684–7691.
- (39) Blasco-Gutierrez, M. J., San Jose-Crespo, I. J., Zozaya-Alvarez, E., Ramos-Sanchez, R., and Garcia-Atares, N. (2007) TrkC: a new predictive marker in breast cancer? *Cancer Invest.* 25, 405–410.
- (40) Louie, E., Chen, X. F., Coomes, A., Ji, K., Tsirka, S., and Chen, E. I. (2013) Neurotrophin-3 modulates breast cancer cells and the microenvironment to promote the growth of breast cancer brain metastasis. *Oncogene* 32, 4064–4077.
- (41) Stephens, P., Edkins, S., Davies, H., Greenman, C., Cox, C., Hunter, C., Bignell, G., Teague, J., Smith, R., Stevens, C., et al. (2005) A screen of the complete protein kinase gene family identifies diverse

patterns of somatic mutations in human breast cancer. *Nat. Genet.* 37, 590–592.

(42) Kim, M. S., Jeong, J., Seo, J., Kim, H.-S., Kim, S.-J., and Jin, W. (2016) Dysregulated JAK2 expression by TrkC promotes metastasis potential, and EMT program of metastatic breast cancer. *Sci. Rep.* 6, 33899.

(43) Angell, Y., Chen, D., Brahimi, F., Saragovi, H. U., and Burgess, K. (2008) A Combinatorial Method for Solution-Phase Synthesis of Labeled Bivalent  $\beta$ -Turn Mimics. *J. Am. Chem. Soc.* 130, 556–565.

(44) van Straten, D., Mashayekhi, V., Oliveira, S., de Bruijn, H., and Robinson, D. (2017) Oncologic Photodynamic Therapy: Basic Principles, Current Clinical Status and Future Directions. *Cancers* 9, 19.

(45) Fan, W., Huang, P., and Chen, X. (2016) Overcoming the Achilles' heel of photodynamic therapy. *Chem. Soc. Rev.* 45, 6488–6519.

(46) Erickson, H. K., Park, P. U., Widdison, W. C., Kovtun, Y. V., Garrett, L. M., Hoffman, K., Lutz, R. J., Goldmacher, V. S., and Blaettler, W. A. (2006) Antibody-Maytansinoid Conjugates Are Activated in Targeted Cancer Cells by Lysosomal Degradation and Linker-Dependent Intracellular Processing. *Cancer Res.* 66, 4426–4433.

(47) Wayua, C., and Low, P. S. (2014) Evaluation of a Cholecystokinin 2 Receptor-Targeted Near-Infrared Dye for Fluorescence-Guided Surgery of Cancer. *Mol. Pharmaceutics* 11, 468–476.

(48) Chen, D., Brahimi, F., Angell, Y., Li, Y.-C., Moscowicz, J., Saragovi, H. U., and Burgess, K. (2009) Bivalent Peptidomimetic Ligands of TrkC are Biased Agonists, Selectively Induce Neuritegenesis, or Potentiate Neurotrophin-3 Trophic Signals. *ACS Chem. Biol.* 4, 769–781.

(49) Johnson, R. J., and Chenoweth, D. E. (1985) Labeling the granulocyte CSa receptor with a unique photoreactive probe. *J. Biol. Chem.* 260, 7161–7164.

(50) Kalepu, S., and Nekkanti, V. (2015) Insoluble drug delivery strategies: review of recent advances and business prospects. *Acta Pharm. Sin. B* 5, 442–453.

(51) Bharate, S. S., and Vishwakarma, R. A. (2015) Thermodynamic equilibrium solubility measurements in simulated fluids by 96-well plate method in early drug discovery. *Bioorg. Med. Chem. Lett.* 25, 1561–1567.

(52) Blanc, V., Bousseau, A., Caron, A., Carrez, C., Lutz, R. J., and Lambert, J. M. (2011) SAR3419: An Anti-CD19-Maytansinoid Immunoconjugate for the Treatment of B-Cell Malignancies. *Clin. Cancer Res.* 17, 6448–6458.